

Degree in Industrial Technologies Engineering

Bachelor's Final Project

Analysis of transient stability phenomenon in grid-forming power converters

Author:
Nicolás Hervías García

Supervised by:
Dr. Francisco Javier Renedo Anglada
Dr. Régulo Enrique Ávila Martínez

Madrid
July 2026

Declaration of originality

I declare under my responsibility that the Project presented with the title **Analysis of transient stability phenomenon in grid-forming power converters** at the ICAI School of Engineering of the Comillas Pontifical University in the academic year **2025/2026** is of my authorship and has not been presented previously for other purposes. The Project is not plagiarised from any other, either totally or partially, and the information that has been taken from other documents is duly referenced.

Use of Artificial Intelligence[1]

I declare under my responsibility that (indicate the correct option):

☐ I have not used Artificial Intelligence in the preparation of this document.

☒ I have used Artificial Intelligence in the preparation of this document and/or Annex B under the conditions allowed by Comillas Pontifical University, i.e. applying Level 2 of the Perkins et al. (2024) Assessment Scale: "AI can be used for pre-task activities such as brainstorming, description and initial research. This level focuses on the use of AI for planning, synthesising and generating ideas, but assessments should emphasise the ability to develop and refine these ideas independently". Specifically, Artificial Intelligence has been used to:

(indicate here the concrete use that has been made of Artificial Intelligence)

I have used Artificial Intelligence for the practical tasks of the project, such as study of different aspects of the topic, revision of Matlab Scripts for development of new ones, and for the search of functions for LaTex writing. I must add that all of the figures included in my memory are of my own making or used with permission. No figure has been generated using Artificial Intelligence.
I have not used Artificial Intelligence for the complete writing of the Memory or Annex B, but I have used it for the translation of the English summary into Spanish, and for translation of specific words and sentences, and in search of synonyms.

[1] This declaration refers to the use of generative Artificial Intelligence to carry out the Project documents (Annex B and Memory). It does not apply to Projects where, by their nature, artificial intelligence must be used as part of them (application of machine learning techniques, neural networks, data analysis...).

Figure 1: Annex I page no. 1

NHG
Signature (student): Nicolás Hervías García
Date: 06/07/2026

Authorisation for Project delivery

Thesis supervisor	Thesis deputy supervisor (if any)
Francisco Javier Rondo Anguita	
Signature:	Signature:
Date: Madrid, España, 6-7-2026	Date: 06/07/2026

Figure 2: Annex I page no.2

Project summaries

0.1 Resumen en Español

Los sistemas de potencia actuales y futuros en todo el mundo se están planificando para la incorporación de fuentes de energía renovable. Los generadores renovables no convencionales, como los aerogeneradores y los generadores solares fotovoltaicos, están parcial o totalmente acoplados a la red a través de convertidores de electrónica de potencia, en particular mediante convertidores de fuente de tensión (VSC, por sus siglas en inglés). El enfoque de control más común utilizado en los convertidores VSC es el llamado control "seguidor de red" (grid-following, GFL-VSC), donde el VSC requiere de una red con cierta robustez para poder conectarse. Otro enfoque de control podría ser el de los convertidores VSC con control "formador de red" (grid-forming, GFM-VSC). Este ha sido identificado como uno de los habilitadores tecnológicos clave para garantizar la estabilidad de los sistemas de potencia con grandes cantidades, o incluso un 100%, de generación basada en convertidores. El comportamiento transitorio en los convertidores de potencia GFM-VSC es un fenómeno que aún no se comprende por completo, y los métodos convencionales utilizados en las máquinas síncronas, como el Criterio de las Áreas, no son directamente aplicables a los convertidores de potencia GFM-VSC. El análisis de las diferentes variables importantes para este fenómeno y el estudio de la aplicabilidad del Criterio de las Áreas es importante para la futura implementación de los convertidores de potencia GFM-VSC en los sistemas de potencia.

0.2 English summary

Current and future power systems all over the world are being planned for the incorporation of renewable energy sources. Non-conventional renewable generators such as wind turbines and solar photovoltaic generators, are partially or totally coupled to the grid through power-electronic converters, in particular by voltage source converters (VSC). The most common control approach used in VSC

converters is the so-called “grid-following” control (GFL-VSC), where the VSC requires a grid with a certain strength to be connected to. Another control approach could be VSC converters with “grid-forming” control (GFM-VSC). This has been identified as one of the key technology enablers to guarantee the stability of power systems with large amounts or even 100% converter-based generation. The transitory behaviour in GFM-VSC power converters is a phenomenon that is still not fully understood, and conventional methods used in synchronous machines, such as the Equal Area Criterion, are not directly applicable to GFM-VSC power converters. The analysis of the different important variables for this phenomenon, and the study of the applicability of the Equal Area Criterion is important for the implementation of GFM-VSC power converters into power systems in the future.

Abstract

Current and future power systems all over the world are being planned for the incorporation of renewable energy sources. Non-conventional renewable generators such as wind turbines and solar photovoltaic generators, are partially or totally coupled to the grid through power-electronic converters, in particular by voltage source converters (VSC). The most common control approach used in VSC converters is the so-called "grid-following" control (GFL-VSC), where the VSC requires a grid with a certain strength to be connected to. Another control approach could be VSC converters with "grid-forming" control (GFM-VSC). This has been identified as one of the key technology enablers to guarantee the stability of power systems with large amounts or even 100% converter-based generation. Since GFM-VSC technology is relatively new, it is essential to fully understand the dynamic behaviour of GFM-VSC power converters and the stability of power systems with large amounts of power-electronic converters. One of the power system stability phenomena that is not fully understood yet when considering GFM-VSC's is transient stability (angle stability under large disturbances). In this bachelor thesis, to understand the transient stability phenomenon, various examples of GFM-VSC power converter model examples connected to infinite grids will be used. With these models, important variables such as the angle difference between the GFM-VSC power converter and the grid, frequency of the GFM-VSC power converter, active and reactive power injection, grid and modulated voltage and current injection will be analysed via fault simulation for faults with different clearing times. Also, using simulation and the Equal Area Criterion, various Critical Clearing Times will be obtained to compare transient stability between the models. In the different chapters of the bachelor thesis, an initial model will be introduced, a model to improve understanding of the phenomenon will be added and the effect of damping will be assessed for the GFM-VSC power converter connected to an infinite grid. From this, conclusions will be obtained on transient stability of GFM-VSC power converters compared to Synchronous Machines, and whether the EAC is applicable or not.

Acknowledgements

I would like to express my gratitude to all the people that have directly and indirectly helped the completion of this project.

Firstly, I would like to thank my supervisors, Francisco Javier Renedo Anglada and Régulo Enrique Ávila Mártinez, and my partner, who made a similar project, Álvaro Millán García.

In particular:

I appreciate Javier for his patience when teaching me about the topic, when designing the outline with me, and finally when discussing the final results.

I appreciate Enrique for his mastery of the models used and their development, and the countless hours trying to find the reason for which something might not work.

I also appreciate Álvaro for the time dedicated to discuss our projects and the support given when memory writing was crucial.

I would like to add that all of them have been very available when needed, and that they have made the duration of this project quite enjoyable and enriching until the end

I would also like to thank the university Universidad Pontificia Comillas and the IIT for having used their installations during the full 9 months of duration of the project.

To Fernando de Cuadra García, the coordinator of electrical projects for being available for any doubts I could have for the completion of the project.

To my parents and siblings, Marta, Josete, Yago and Valentina for their unshakeable support, and the use of my father's office for the last few weekends and study sessions with Yago and Valentina.

To my 4 grandparents, José Luis, Annunziata, Carmen and the late José Antonio (the first ICAI of the family) for helping me know what is important with unconditional care.

To my friends, Ana and Carlos for their guidance and their shared experiences of their own projects.

Finally, to my classmates and teachers, as this has been a tough but very pleasant chapter in my life that I will forever remember dearly.

Contents

Project summaries **v**
0.1 Resumen en Español v
0.2 English summary v

Acknowledgements **ix**

1 Introduction **1**
1.1 Introduction and motivation 1
1.2 Transient stability in GFM-VSCs 1
1.3 Example of a synchronous generator connected to an infinite grid . 2
1.4 Equal Area Criterion for Synchronous Machines 3
1.5 Objectives of the bachelor thesis 5
1.6 Project outline 5
1.6.1 Phase I 6
1.6.2 Phase II 6
1.6.3 Phase III 7
1.6.4 Appendixes 7

2 Modelling and control of GFM-VSCs **9**
2.1 Introduction 9
2.2 Model of a GFM-VSC power converter connected to an infinite grid 9
2.3 Summary 12

3 Transient Stability of GFM-VSCs **15**
3.1 Introduction 15
3.2 Simulation model 15
3.3 Analysis and representation of important variables 15
3.4 P-δ curves and EAC in GFM-VSC power converters 18
3.5 Fault simulation and results 20
3.6 CCT calculation and comparison 30
3.7 Summary & Conclusions 31

4 Analysis of the PLL of GFM-VSCs on Transient Stability **33**
4.1 Introduction . . . 33
4.2 Frozen PLL model design . . . 33
4.3 P-δ curves and EAC for Frozen PLL . . . 34
4.4 Fault simulation and results . . . 34
4.5 CCT calculation and comparison . . . 43
4.6 Summary & Conclusions . . . 46

5 Effect of Damping in GFM-VSCs on Transient Stability **49**
5.1 Introduction . . . 49
5.2 P-δ curves and EAC . . . 49
5.3 Fault simulation and results . . . 50
5.3.1 Effect of damping with CL & CSA . . . 51
5.3.2 Effect of damping with No CL . . . 59
5.4 CCT calculation and comparison . . . 69
5.5 Summary & Conclusions . . . 70

6 Conclusions **73**
6.1 General conclusions . . . 73
6.1.1 Model without the frozen PLL . . . 73
6.1.2 Effect of the frozen PLL . . . 74
6.1.3 Effect of damping . . . 74
6.1.4 Final conclusions . . . 75
6.2 Future work . . . 76

A Economic analysis **79**

B Budget for the replication of the project **81**
B.1 Material costs . . . 81
B.2 Labour costs . . . 82
B.3 Total costs . . . 82

C Bisection Method Algorithm **85**

D P-δ script **87**

E Alignment with the Sustainable Development Goals **93**
E.1 SDG $n°7$: Affordable & Clean Energy . . . 94
E.2 SDG $n°9$: Industry, Innovation & Infrastructure . . . 94
E.3 SDG $n°13$: Climate Action . . . 94

Bibliography **95**

List of Figures

1 Annex I page no. 1 ii
2 Annex I page no.2 iii

1.1 Classification of power system stability of IEEE Transactions on Power Systems 2
1.2 Equal Area Criterion diagram for a general clearing angle 3
1.3 Equal Area Criterion diagram for the critical clearing angle 5

2.1 Equivalent model of a GFM-VSC power converter connected to an infinite grid. 10
2.2 General scheme of the control system of a GFM-VSC power converter. 10
2.3 GFM-VSC power converter self-synchronisation strategy. 11

3.1 GFM-VSC power converter connected to an infinite grid single-line scheme 16
3.2 GFM-VSC power converter simulink model 16
3.3 GFM-VSC WITH CL-CSA: P-δ curve 19
3.4 EAC WITH CL-CSA: generic angle 19
3.5 EAC WITH CL-CSA: critical angle 19
3.6 δ-t curve for a clearing time of 300ms 20
3.7 P-t curve for a clearing time of 300ms 21
3.8 P-δ curve for a clearing time of 300ms 21
3.9 δ-t curve for a clearing time of 800ms 22
3.10 P-t curve for a clearing time of 800ms 22
3.11 P-δ curve for a clearing time of 800ms 23
3.12 δ-t curve for a clearing time of 1600ms 23
3.13 P-t curve for a clearing time of 1600ms 24
3.14 P-δ curve for a clearing time of 1600ms 24
3.15 δ-t curve for a clearing time of 2000ms 25
3.16 P-t curve for a clearing time of 2000ms 25
3.17 P-δ curve for a clearing time of 2000ms 26

3.18 δ-t curves for previous fault clearing times 27
3.19 P_g & Q_g-t curves for previous fault clearing times 28
3.20 ω-t curves for previous fault clearing times 28
3.21 v_g & e_m-t curves for previous fault clearing times 29
3.22 v_g & i_g-t curves for previous fault clearing times 29
3.23 i_s-t curves for previous fault clearing times 30

4.1 PLL block diagram equipped with an anti-windup 34
4.2 PLL estimated frequency compared to GFM-VSC frequency before fault clears (No Freeze) 35
4.3 PLL estimated frequency compared to GFM-VSC frequency before fault clears (Freeze) 35
4.4 δ-t curve for a clearing time of 300ms 36
4.5 P-t curve for a clearing time of 300ms 37
4.6 P-δ curve for a clearing time of 300ms 37
4.7 δ-t curve for a clearing time of 800ms 38
4.8 P-t curve for a clearing time of 800ms 38
4.9 P-δ curve for a clearing time of 800ms 39
4.10 δ-t curve for a clearing time of 950ms 39
4.11 P-t curve for a clearing time of 950ms 40
4.12 P-δ curve for a clearing time of 950ms 40
4.13 δ-t curve for a clearing time of 1500ms 41
4.14 P-t curve for a clearing time of 1500ms 41
4.15 P-δ curve for a clearing time of 1500ms 42
4.16 δ-t curves for PLL-Freeze vs PLL-NoFreeze 43
4.17 P_g & Q_g-t curves for PLL-Freeze vs PLL-NoFreeze 44
4.18 ω-t curves for PLL-Freeze vs PLL-NoFreeze 44
4.19 v_g & e_m-t curves for PLL-Freeze vs PLL-NoFreeze 45
4.20 v_g & i_g-t curves for PLL-Freeze vs PLL-NoFreeze 45
4.21 i_s-t curves for PLL-Freeze vs PLL-NoFreeze 46

5.1 GFM-VSC VSM-PLL No CL: P-δ curve 50
5.2 δ-t curve for a clearing time of 100ms with $D_{GFM} = 20pu$ and CL-CSA 51
5.3 P-t curve for a clearing time of 100ms with $D_{GFM} = 20pu$ and CL-CSA 52
5.4 P-δ curve for a clearing time of 100ms with $D_{GFM} = 20pu$ and CL-CSA 52
5.5 δ-t curve for a clearing time of 300ms with $D_{GFM} = 20pu$ and CL-CSA 53
5.6 P-t curve for a clearing time of 300ms with $D_{GFM} = 20pu$ and CL-CSA 53

5.7 P-δ curve for a clearing time of 300ms with $D_{GFM} = 20pu$ and CL-CSA 54
5.8 δ-t curves for $D_{GFM} = 20pu$ vs $D_{GFM} = 202,61pu$ with CL-CSA . . 55
5.9 P_g & Q_g-t curves for $D_{GFM} = 20pu$ vs $D_{GFM} = 202,61pu$ with CL-CSA 55
5.10 ω-t curves for $D_{GFM} = 20pu$ vs $D_{GFM} = 202,61pu$ with CL-CSA . . 56
5.11 v_g & e_m-t curves for $D_{GFM} = 20pu$ vs $D_{GFM} = 202,61pu$ with CL-CSA 56
5.12 v_g & i_g-t curves for $D_{GFM} = 20pu$ vs $D_{GFM} = 202,61pu$ with CL-CSA 57
5.13 i_s-t curves for $D_{GFM} = 20pu$ vs $D_{GFM} = 202,61pu$ with CL-CSA . 58
5.14 δ-t curve for a clearing time of 800ms with $D_{GFM} = 202,61pu$ and No CL 60
5.15 P-t curve for a clearing time of 800ms with $D_{GFM} = 202,61pu$ and No CL 60
5.16 P-δ curve for a clearing time of 800ms with $D_{GFM} = 202,61pu$ and No CL 61
5.17 δ-t curve for a clearing time of 3000ms with $D_{GFM} = 202,61pu$ and No CL 61
5.18 P-t curve for a clearing time of 3000ms with $D_{GFM} = 202,61pu$ and No CL 62
5.19 P-δ curve for a clearing time of 3000ms with $D_{GFM} = 202,61pu$ and No CL 62
5.20 δ-t curve for a clearing time of 500ms with $D_{GFM} = 20pu$ and No CL 63
5.21 P-t curve for a clearing time of 500ms with $D_{GFM} = 20pu$ and No CL 64
5.22 P-δ curve for a clearing time of 500ms with $D_{GFM} = 20pu$ and No CL 64
5.23 δ-t curve for a clearing time of 600ms with $D_{GFM} = 20pu$ and No CL 65
5.24 P-t curve for a clearing time of 600ms with $D_{GFM} = 20pu$ and No CL 65
5.25 P-δ curve for a clearing time of 600ms with $D_{GFM} = 20pu$ and No CL 66
5.26 δ-t curves for $D_{GFM} = 20pu$ vs $D_{GFM} = 202,61pu$ No CL 66
5.27 P_g & Q_g-t curves for $D_{GFM} = 20pu$ vs $D_{GFM} = 202,61pu$ No CL . 67
5.28 ω-t curves for $D_{GFM} = 20pu$ vs $D_{GFM} = 202,61pu$ No CL 67
5.29 v_g & e_m-t curves for $D_{GFM} = 20pu$ vs $D_{GFM} = 202,61pu$ No CL . 68
5.30 v_g & i_g-t curves for $D_{GFM} = 20pu$ vs $D_{GFM} = 202,61pu$ No CL . . 68
5.31 i_s-t curves for $D_{GFM} = 20pu$ vs $D_{GFM} = 202,61pu$ No CL 69

D.1 Matlab script for producing P-δ curves page no. 1 88
D.2 Matlab script for producing P-δ curves page no. 2 89
D.3 Matlab script for producing P-δ curves page no. 3 90
D.4 Matlab script for producing P-δ curves page no. 4 91
D.5 Matlab script for producing P-δ curves page no. 5 92

E.1 Sustainable Development Goals 93

List of Tables

2.1 Parameters of the GFM-VSC power converter 12

3.1 Transitory variables analysed 17
3.2 CCT table GFM-VSC VSM-PLL-CL-CSA 31

4.1 CCT table GFM-VSC VSM-PLL-Freeze-CL-CSA 46

5.1 CCT table GFM-VSC VSM-PLL-Freeze effect of damping coefficient 70

B.1 Material Costs 82
B.2 Labour Costs 82
B.3 Labour Costs 83

C.1 Bisection Method Algorithm 86

Chapter 1

Introduction

1.1 Introduction and motivation

Current and future power systems all over the world are being planned for the incorporation of renewable energy sources. Non-conventional renewable generators such as wind turbines and solar photovoltaic generators, are partially or totally coupled to the grid through power-electronic converters, in particular by voltage source converters (VSC). The most common control approach used in VSC converters is the so-called "grid-following" control (GFL-VSC), where the VSC requires a grid with a certain strength to be connected to. Another control approach could be VSC converters with "grid-forming" control (GFM-VSC). This has been identified as one of the key technology enablers to guarantee the stability of power systems with large amounts or even 100% converter-based generation.

Since GFM-VSC technology is relatively new, it is essential to fully understand the dynamic behaviour of GFM-VSC power converters and the stability of power systems with large amounts of power-electronic converters. One of the power system stability phenomena that is not fully understood yet when considering GFM-VSC's is transient stability (angle stability under large disturbances).

1.2 Transient stability in GFM-VSCs

The concept of transient stability refers to the angle stability under large disturbances. In this case, the equations that define the problem are complex differential equations, but methods to resolve these have been used in the past mostly for synchronous machines (SM), but some could be applicable to GFM-VSC power converters. The classification designed in [1], is shown in figure 1.1. For SM, when talking about transient stability, this clearly falls in the subdivision of rotor angle stability. Note that, for GFM-VSC power converters, there is no rotor an-

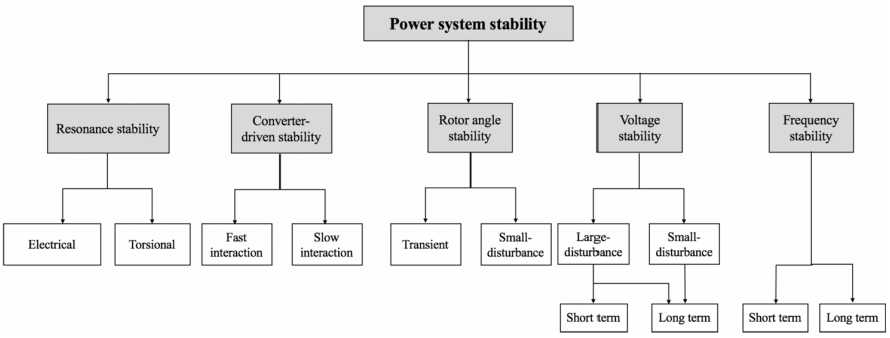

Figure 1.1: Classification of power system stability of IEEE Transactions on Power Systems

gle, as there is no rotor, and therefore, it would not be completely true to speak about transient stability in GFM-VSC power converters in rotor angle stability, but still, angle stability applies. This phenomenon could also be classified as a slow interaction, inside converter-driven stability.

Transient stability in GFM-VSC power converters does not apply to the rest of classifications, as resonance, voltage and frequency stability are not directly related to this phenomenon. That is why [2], proposes, in order to improve IEEE's definition of Transient Stability, to join the boxes of transient stability within rotor angle stability (but take out the term rotor), and slow interaction within converter-driven stability into a single box called converter angle stability, which better defines the completeness of the phenomenon.

1.3 Example of a synchronous generator connected to an infinite grid

Consider the case of a generator connected to an infinite grid. When a three-phase fault appears in the generator's terminals, the line between is disconnected on both ends, until the fault is cleared, where the line is reconnected. In this sequence, a transitory appears. The analysis of transient stability consists in observing what is the limit time to clear the fault before the reconnection of the line causes loss of synchronism. This loss of synchronism in a SM is caused by the acceleration of the generator's rotor during the time the line is open (it accelerates because the mechanical power remains, whilst, there is no electrical power injected into the grid). If the rotor accelerates too much, this acceleration cannot be absorbed by the grid, and synchronism is lost once the line is closed. The balance between acceleration and deceleration can be analysed by the Equal Area Criterion (EAC)

using the P-δ curve. The power-angle curve, known otherwise as P-δ, represents the active power injected by the generator with respect to the angle difference between the generator's and the grid's tension ($\delta - \delta_e$). The expression of this power injected is:

$$P_e = \frac{e_m^0 U_\infty}{X_e} sin(\delta - \delta_e) \tag{1.1}$$

When a three-phase fault occurs occurs in the PCC, as mentioned before, the generator goes from an initial pre-fault stable state where it is in coordinates (δ_0,Pg_0) to a point where it ceases to inject power (as the equivalent impedance of an open circuit tends to infinity, $X_e = \infty$), and instantly drops to coordinates (δ_0,0). Then, the generator accelerates until the fault is cleared in the coordinates (δ_{cl},0). Then, the point goes back to the initial P-delta curve to coordinates (δ_{cl},Pg_{cl}). Here, if the fault has been cleared fast enough, the generator starts to decelerate and the angle reaches a maximum (δ_{max},Pg_{max}), before returning to the initial coordinate (δ_0,Pg_0). Otherwise, synchronism is lost, and the generator continues to accelerate indefinitely.

1.4 Equal Area Criterion for Synchronous Machines

With the sequence in the P-δ curve shown previously, the EAC method consists in comparing the accelerating and decelerating areas as shown in figure 1.2. If the decelerating area is able to equal the accelerating area, the machine is able to regain synchronism with the grid. A_1 represents the accelerating area and A_2 represents the decelerating area.

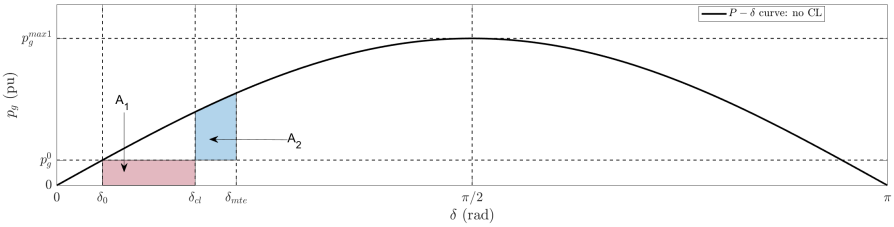

Figure 1.2: Equal Area Criterion diagram for a general clearing angle

This method is derived from the swing equation, which can be obtained as shown in [3]:

$$\frac{2H}{\omega_{0,pu}} \frac{d\omega}{dt} = P_m - P_e - D(\omega - \omega_{0,pu}) \tag{1.2}$$

Being H the inertia of the generator, ω the angular velocity of the generator, ω_0 the angular velocity of synchronism, P_m the mechanical power developed, P_e the electrical power generated, and finally D is the damping coefficient. It assumes the damping coefficient D is negligible in comparison to the other terms of the equation (as it is usually in an order of magnitude of 1 pu in SM, and does not cause a great effect when not taken into account, but otherwise, if taken into consideration, the equation becomes complex). The resulting equation is:

$$\frac{2H}{\omega_{0,pu}}\frac{d\omega}{dt} = P_m - P_e = P_{acc} \tag{1.3}$$

The demonstration of the EAC is as follows: If the equation is multiplied by $d\delta$, it becomes:

$$\frac{d\delta}{dt}d\omega = \frac{\omega_{0,pu}}{2H}P_{acc}d\delta \tag{1.4}$$

Which can then be shown as:

$$(\omega - \omega_{0,pu})d\omega = \frac{\omega_{0,pu}}{2H}P_{acc}d\delta \tag{1.5}$$

This equation is integrated between δ and δ_0, as shown below:

$$\int_0^{\Delta\omega} \Delta\omega d\Delta\omega = \frac{\omega_{0,pu}}{2H}\int_{\delta_0}^{\delta} P_{acc}d\delta \tag{1.6}$$

Which results in:

$$\frac{1}{2}\Delta\omega^2 = \frac{\omega_{0,pu}}{2H}\int_{\delta_0}^{\delta} P_{acc}d\delta \tag{1.7}$$

If, after the fault, the variation of angular velocity becomes zero, the generator will be able to regain synchronism. In this case, the previous equation can be expressed as in 1.8, which then completes the formulation of the EAC as shown in 1.9:

$$\int_{\delta_0}^{\delta_{cl}} P_{acc}d\delta = \int_{\delta_{cl}}^{\delta_{max}} P_{dec}d\delta \tag{1.8}$$

$$A_1 = A_2 \tag{1.9}$$

δ_{cl} and δ_{max} represent the angle in which the fault is cleared, and the maximum angle reached, respectively. In the instant in which the angle is δ_{max}, the variation of angular velocity is zero. P_{dec} is the decelerating power. In the P-δ curve, the

previous equation can be analysed qualitatively by observing the accelerating and decelerating areas:

There is an angle where for any angle greater than this one, the generator is not able to regain synchronism with the grid. This is called the critical angle (δ_{cl}^{crit}), and can be observed graphically in the figure 1.3, where the decelerating area is maximum and equal to the accelerating area. Once the critical angle is obtained,

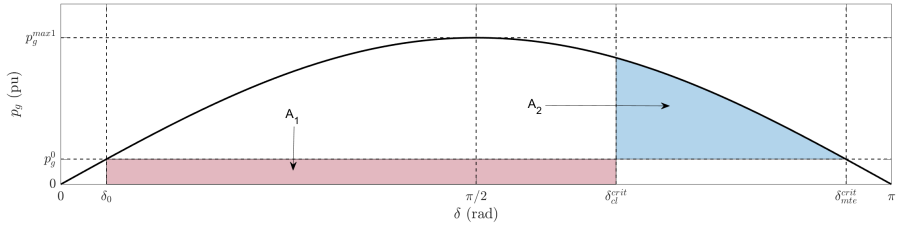

Figure 1.3: Equal Area Criterion diagram for the critical clearing angle

the CCT can be calculated with the expression 1.10:

$$t_{cl}^{crit} = \sqrt{\frac{4H(\delta_{cl}^{crit} - \delta_0)}{P_a \omega_{0,pu}}} \tag{1.10}$$

1.5 Objectives of the bachelor thesis

In this bachelor thesis, the following objectives will be tackled:

- Modelling, control and simulation of GFM-VSC power converters
- A thorough analysis of transient stability phenomenon in GFM-VSC power converters
- Detailed analysis of the active-power/angle (P-δ) curve of GFM-VSC when a fault occurs and loss of synchronism phenomenon
- Analysis of the limitations of the application of EAC when analysing transient stability of GFM-VSC power converters
- Verification by non-linear time-domain simulation

1.6 Project outline

The outline of the thesis is divided into three phases and is as follows:

1.6.1 Phase I

- Chapter 1: Introduction
  - Introduction
  - Context of GFM-VSC power converters
  - Transient stability definition & Equal Area Criterion
- Chapter 2: Modelling and control of GFM-VSCs
  - Modelling & control of GFM-VSC power converters

1.6.2 Phase II

- Chapter 3: Transient stability of GFM-VSCs
  - Example of a GFM-VSC power converter connected to infinite grid
  - GFM-VSC VSM-PLL-CL-CSA model
  - Simulation and representation of faults with different clearing times
  - CCT calculation: simulation vs EAC
- Chapter 4: Analysis of the PLL of GFM-VSCs on transient stability
  - GFM-VSC VSM-PLL-Freeze-CL-CSA
  - Simulation and representation of faults with different clearing times
  - CCT calculation: simulation vs EAC & previous GFM-VSC VSM-PLL-CL-CSA model
- Chapter 5: Effect of damping in GFM-VSCs on transient stability
  - GFM-VSC VSM-PLL-Freeze-CL-CSA with $D_{GFM} = 20pu$ vs $D_{GFM} = 202,61pu$
  - Simulation and representation of faults with different clearing times
  - CCT calculation: simulation vs EAC & previous models
  - GFM-VSC VSM-PLL-Freeze-NoCL with $D_{GFM} = 20pu$ vs $D_{GFM} = 202,61pu$
  - Simulation and representation of faults with different clearing times
  - CCT calculation: simulation vs EAC

1.6.3 Phase III

- Conclusions:
  - Conclusions per chapter & general conclusions
  - Applicability of EAC for GFM-VSC power converters
  - Future work

1.6.4 Appendixes

- Economic analysis
- Budget of the project
- Bisection method algorithm
- P-δ script
- Alignment with SDG's

Chapter 2

Modelling and control of GFM-VSCs

2.1 Introduction

The goal of this chapter is to introduce the model of the GFM-VSC power converter connected to the infinite grid and the control scheme of the GFM-VSC power converter, together with the parameters of the models. Also the strategy selected for the GFM-VSC power converter will be presented, and some of the control features for the GFM-VSC power converter will be designed.

2.2 Model of a GFM-VSC power converter connected to an infinite grid

Fig. 2.1 represents the diagram of a GFM-VSC power converter connected to an infinite grid. $\bar{e}_m$ is the modulated voltage of the GFM-VSC power converter, and $\bar{z}_c = r_c + jx_c$ ($x_c = L_c\omega$) is its series connection impedance. This includes its equivalent series reactor and the impedance of the connection transformer. The infinite grid has a voltage $\bar{v}_{e,i}$ and an equivalent impedance $\bar{z}_g = r_g + jx_g$. The voltage seen at the Point of Common Coupling (PCC) of the GFM-VSC power converter is $\bar{v}_g$ and the current and power injections of the GFM-VSC power converter at the PCC are $\bar{i}_g$ and $\bar{s}_g = p_g + jq_g$, respectively.

The GFM-VSC has a constant set point for the magnitude of the modulated voltage (e_m^0), and it uses a quasi-static model to calculate the current set points (marked with (a) in Fig. 2.2), following the approach of [4, 5, 6]:

$$i_{g,q}^{ref'} = \frac{v_{g,d} - e_{m,d}^0}{x_{cv}},\ i_{g,d}^{ref'} = \frac{e_{m,q}^0 - v_{g,q}}{x_{cv}}. \tag{2.1}$$

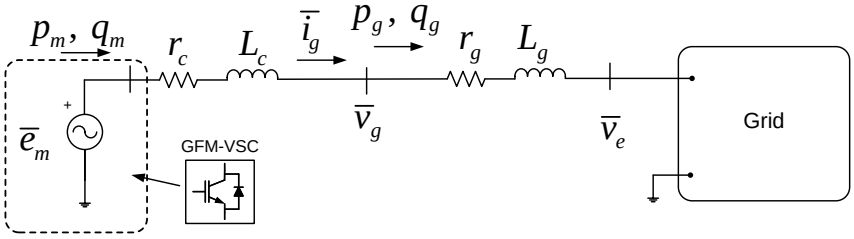

Figure 2.1: Equivalent model of a GFM-VSC power converter connected to an infinite grid.

This approach intends to align the modulated voltage with the d axis in a d-q mobile reference frame. In this way, $e^0_{m,d} = e^0_m$ and $e^0_{m,q} = 0$. The model uses an equivalent virtual reactance $x_{cv} = x_c + x_v$ composed by the true (or estimated) series reactance (x_c) and an additional virtual reactance (x_v). It is used for the current-setpoint calculation. Notice that $x_v = 0$ pu could be used, but $x_v > 0$ pu is also available if required to limit active-power variation in case of a phase shift.

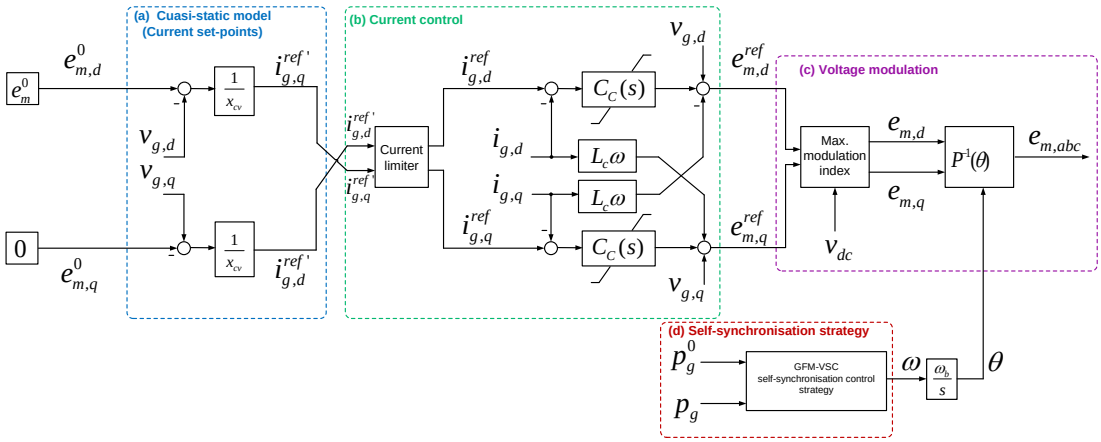

Figure 2.2: General scheme of the control system of a GFM-VSC power converter.

There are various self-synchronisation strategies for the GFM-VSC power converter, as seen in [7]. For this bachelor thesis, in order to reach a deeper analysis of the phenomena, the control scheme used will be of the type Virtual Synchronous Machine (VSM) with frequency estimation at the PCC. This is the strategy known as GFM-VSC power converter with a phase locked loop (PLL), or GFM-VSC VSM-PLL in short. The model also implements a current controller and a current limiter

based on current-saturation algorithm (CSA). The general scheme of a GFM-VSC power converter is shown in Fig. 2.2 and the self-synchronisation strategy is shown in Fig. 2.3.

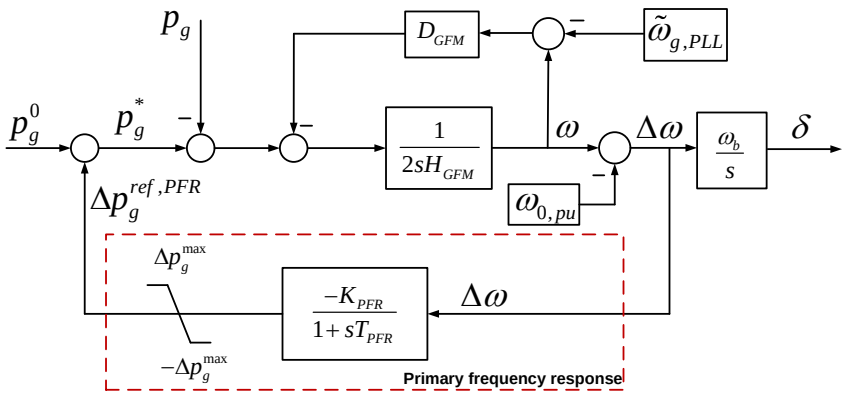

Figure 2.3: GFM-VSC power converter self-synchronisation strategy.

In this chosen strategy; equipped with Primary Frequency Response (PFR) control, the GFM-VSC power converter imposes its frequency according to the swing equation. This is later compared to the frequency estimated by the PLL in the PCC. The difference is multiplied by the damping factor D_{GFM} and then used to obtain the frequency of the GFM-VSC power converter and therefore, the angle. The use of the PLL permits the PFR to be decoupled from the power control. This means that the PFR can be as slow as required (time constant T_{PFR}) without affecting the synchronising properties of the strategy.

Table 2.1 shows the parameters of the GFM-VSC power converter.

Table 2.1: Parameters of the GFM-VSC power converter

Parameters VSC's rating are base values for pu	**Values**
Rating VSC, DC voltage, AC voltage	100 MVA, 640 kV, 400 kV
Max. current	1.20 pu (equal priority for $d-q$ axes)
Series resistance (r_c) / reactance (x_c)	0.005 pu / 0.15 pu
(series reactor + transformer)	
(transformer: 100 MVA 400/320 kV)	
Current control bandwidth ($\omega_{n,CC}$)	1500 rad/s
Current control prop. / int. gains ($K_{C,P}$ / $K_{C,I}$)	1.0027 pu / 1074.3 pu/s
Quasi-static model, virt. reactance (x_v / x_{ev})	0 pu / 0.15 pu
Emulated inertia (H_{GFM})	5 s
Primary freq. controller ($K_{PFR,i}$ / T_{PFR})	20 pu / 1 s
Primary freq. controller limit (Δp_g^{max})	1 pu
PLL control bandwidth ($\omega_{n,PLL}$)	500 rad/s
PLL control prop. / int. gains ($K_{P,PLL}/K_{I,PLL}$)	3.1831 pu / 795.7747 pu/s
PLL frequency saturation ($\Delta\omega_{PLL}^{max}$)	$\pm$ 0.1 pu

For the scheme of the GFM-VSC VSM-PLL, to calculate the damping factor D_{GFM} and the natural frequency ω_n, the inertia H_{GFM}, the damping ratio ζ and the PFR parameters (time constant T_{PFR} & proportional gain K_{PFR}) must be specified. With these values stated, the relationships used to obtain the damping factor D_{GFM} and the natural frequency w_n are the following:

$$\zeta = \frac{D_{GFM}}{4H_{GFM}}\frac{1}{\omega_n},\ \omega_n = \sqrt{\frac{\omega_b}{2H_{GFM}x_c}}. \tag{2.2}$$

The result of the parameters obtained using the values of the table 2.1 and by using a design of $\zeta = 0,7$ & $H_{GFM} = 5s$ is:

$$\omega_n = 14,472 rad/s,\ D_{GFM} = 202,61 pu. \tag{2.3}$$

2.3 Summary

In this chapter, the following points have been tackled:

- Introduction of a GFM-VSC power converter connected to an infinite grid with its equivalent model
- Introduction of the different control schemes and strategies with models based in the d-q axis with blocks for the current set-points, current control, and voltage modulation controlled by the previous blocks and a self-synchronisation strategy

- Use of the strategy of the GFM-VSC VSM-PLL
- Table of parameters of the model used for design
- Design of the natural frequency (ω_n) and the damping coefficient (D_{GFM}) by using a design by selecting the virtual inertia (H_{GFM}) and the damping ratio (ζ)

Chapter 3

Transient Stability of GFM-VSCs

3.1 Introduction

The goal of this chapter is to introduce the scheme and model of the GFM-VSC power converter, introduce the important variables which will be analysed and the way they will be represented. Then, for the first model used in this bachelor thesis, a series of fault durations will be simulated and the important variables represented, and finally, some results will be obtained.

3.2 Simulation model

To enable a good analysis of transient stability of GFM-VSC power converters, a 100 MVA GFM-VSC-based generator connected to an infinite grid is considered. Simulations were carried out with VSCLib tool, an open-source tool based on Matlab + Simulink + SimPowerSystems developed by L2EP-LILLE in Migrate project [8],[9],[10].

An image of the single-line scheme is shown in figure 3.1 and the Simulink model is shown in figure 3.2.

3.3 Analysis and representation of important variables

With this model, three-phase short circuits will be simulated on the PCC to observe how the GFM-VSC power converter reacts. Some faults may cause the GFM-VSC power converter to lose synchronism with the infinite-grid, so therefore it is important to distinguish cases where there is and where there is not loss of synchronism. The difference between a case where synchronism is lost and another

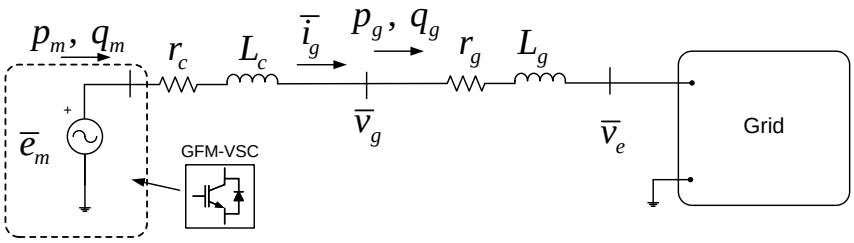

Figure 3.1: GFM-VSC power converter connected to an infinite grid single-line scheme

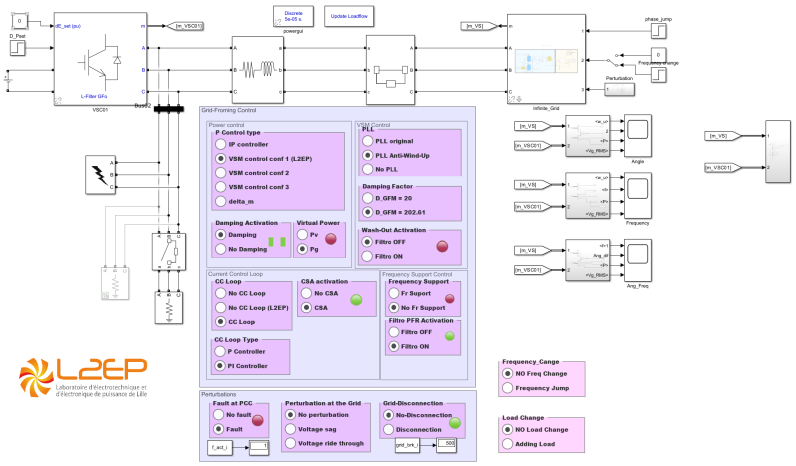

Figure 3.2: GFM-VSC power converter simulink model

where it is maintained, is the fault duration. When faults are short, the system is able to regain synchronism with the grid, but if a fault is too long, it is unable, and synchronism is lost. A good indicator of how good the transient behaviour of a GFM-VSC power converter is its Critical Clearing Time (CCT). This is the longest time a fault can be cleared in before synchronism is lost.

An example for the analysis of the behaviour of the GFM-VSC power converter against faults will be the case of a power converter with a PLL (phase locked loop) estimating the frequency of the PCC and equipped with a CL (Current Limiter) and a current control algorithm known as CSA (Current Saturation Algorithm). This example, known as GFM-VSC-PLL-CL-CSA will be the reference example explored, and in further chapters, other cases will be analysed and compared to this first case.

Table 3.1: Transitory variables analysed

Name of variable	Symbol of representation	Units
Angle difference between the GFM-VSC power converter and the grid	$\delta - \delta_e$	deg (°) or rad
Frequency of the GFM-VSC power converter compared to the grid's	ω_{GFM} & ω_e	Hz or pu (50Hz base)
Active and Reactive power injected into the grid by GFM-VSC power converter	P_g & Q_g	MW or pu (100MVA base)
Modulated voltage and voltage of the terminal	e_m & v_g	pu (400kV AC & 640kV DC bases)
Current injection by the GFM-VSC power converter	i_s & i_s	pu (bases of 100MVA & 400kV)
Critical Clearing Time	CCT	ms

For the analysis of transient stability, the variables presented in table **??** will be analysed by observing their transitory behaviour over different short circuit fault durations (except for the CCT which will be treated on its own for each case of GFM-VSC power converter model used): These variables will be represented in different graphs along time. These include δ-t, P_g & Q_g-t, ω-t, e_m & v_g-t, v_g & i_g-t and i_s-t graphs and the P-δ curves.

3.4 P-δ curves and EAC in GFM-VSC power converters

In the same way as in SM (Synchronous Machines), it is common to use P-δ curves to analyse transient stability in GFM-VSC power converters. The concept may be different, as the angle of the GFM-VSC power converter does not represent a physical angle, as could be the angle of the rotor of a SM, but, the transient sequence of the angle and power follows a similar procedure, and therefore the P-δ curves and the EAC can be used similarly.

In this case, due to the implementation of the CSA (current saturation algorithm) to the GFM-VSC power converter, the shape of the P-δ curve changes. At first, it follows the usual sinusoidal shape, starting in the origin, until the current is limited by the CSA. Then it follows a different curve where the current output is the current limit. The equations are the following:

$$P_g = \begin{cases} \frac{e_m^0 v_e}{x_{tot}} sin\delta, \text{if } \delta < \delta_a \\ \frac{e_m^0 v_e sin\delta}{\sqrt{(e_m^0)^2+(v_e)^2-2e_m^0 v_e cos(\delta)}} i_g^{max}, \text{if } \delta \geq \delta_a \end{cases} \tag{3.1}$$

The equation 3.1 form the curve seen in figure

The sequence when a fault occurs in the GFM-VSC VSM-PLL-CL-CSA is shown in figure 3.3

The pre-fault moment, labelled a) has coordinates (δ_0,Pg_0). The point labelled b) represents the instant the fault occurs and has coordinates (δ_0,0). Then, c) represents the moment right before the fault is cleared, with coordinates (δ_{cl},0). The point labelled d) shows the moment where the fault is cleared, and the power generation returns to the curve coordinates (δ_{cl},Pg_d). Then, the maximum angle, labelled max) represents the greatest angle of the sequence and has coordinates (δ_{max}, Pg_{max}), before, if possible, it returns to the initial point of equilibrium (δ_0,Pg_0). If synchronism is lost, like in figure (loss of synch fig), the maximum angle point is the final point, with coordinates (δ_{final}, Pg_0).

From this sequence, the EAC can be applied to find the critical clearing angle, which is associated to a CCT, as explained in chapter 1, which can then be compared to the CCT obtained via the simulation model. The EAC works in the same way as the case without the CSA, and a general case and the critical clearing angle are shown in figures 3.4 & 3.5:

In the case of GFM-VSC power converters, as the damping coefficient D_{GFM} is so large (202.6pu), it does have a great effect in the transitory of a fault (as shown by the swing equation). Therefore, it is expected that the CCT calculated by the EAC is lower than the CCT obtained by the simulation model, as damping has a positive effect on transient stability.

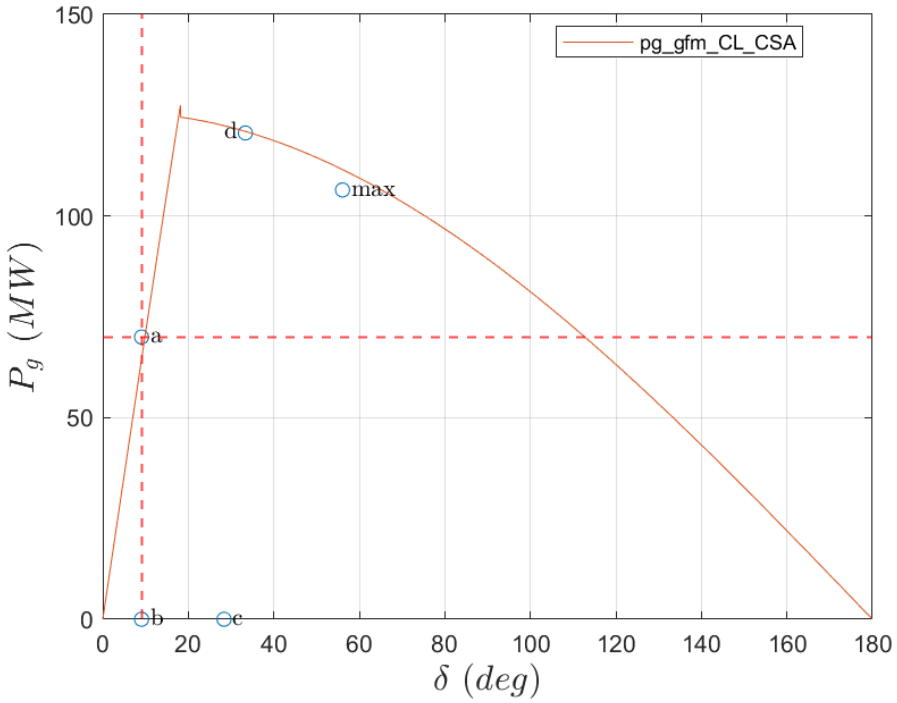

Figure 3.3: GFM-VSC WITH CL-CSA: P-δ curve

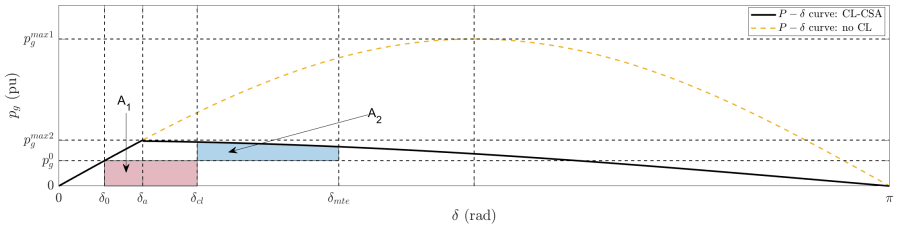

Figure 3.4: EAC WITH CL-CSA: generic angle

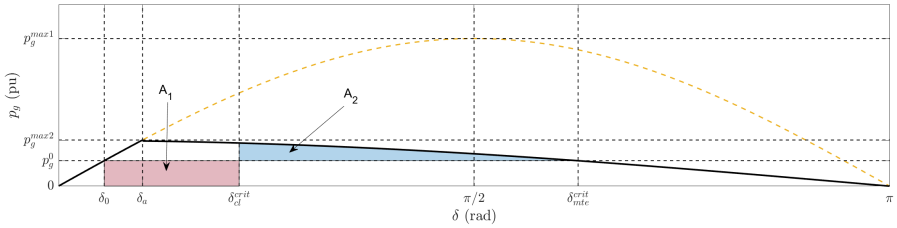

Figure 3.5: EAC WITH CL-CSA: critical angle

3.5 Fault simulation and results

Before comparing the CCT's obtained by both ways, a short and long fault's simulation will be presented to observe the different variables with time and the P-δ curves of both faults:

Short faults of 300ms, 800ms and 1600ms will be presented. The objective of these faults is to observe the case of faults where synchronism will not be lost. The last one is close to the CCT, and therefore, the GFM-VSC power converter barely maintains synchronism. Next to them, a fault of 2000ms will be presented. Here synchronism is expected to be lost. Please note that this is not a real example and due to the characteristics and simplicity of the model, faults as long as these will be analysed with a more qualitative approach rather than a quantitative applicable approach to real world systems. In reality, it is expected for protections against sub-voltage, super-voltage, sub-frequency, super-frequency and against loss of synchronism to act long before this clearing time can occur.

First, some of the graphs of the individual faults will be shown. Here, the focus will be the angle and power against time, and then the P-δ curve for each fault clearing time, showing the points a), b), c), d) and max) mentioned previously, and starting with the shortest fault clearing time:

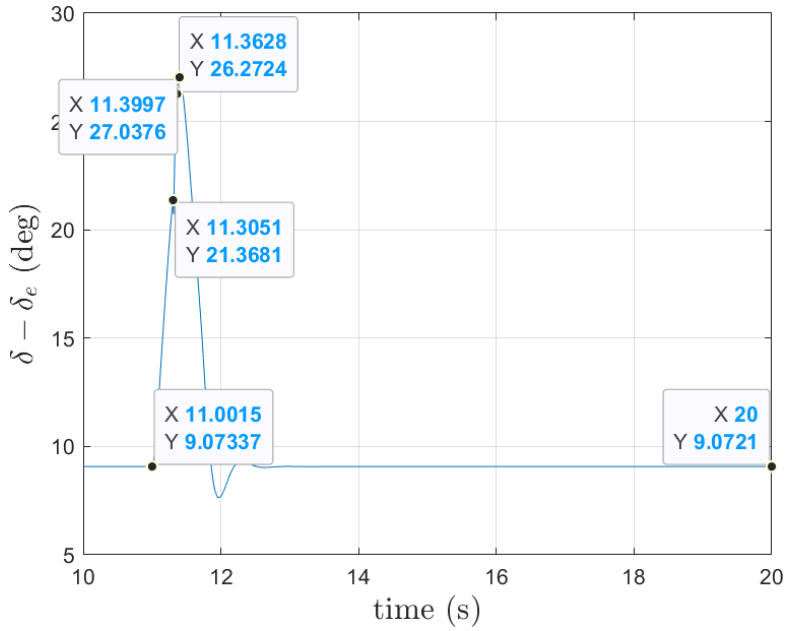

Figure 3.6: δ-t curve for a clearing time of 300ms

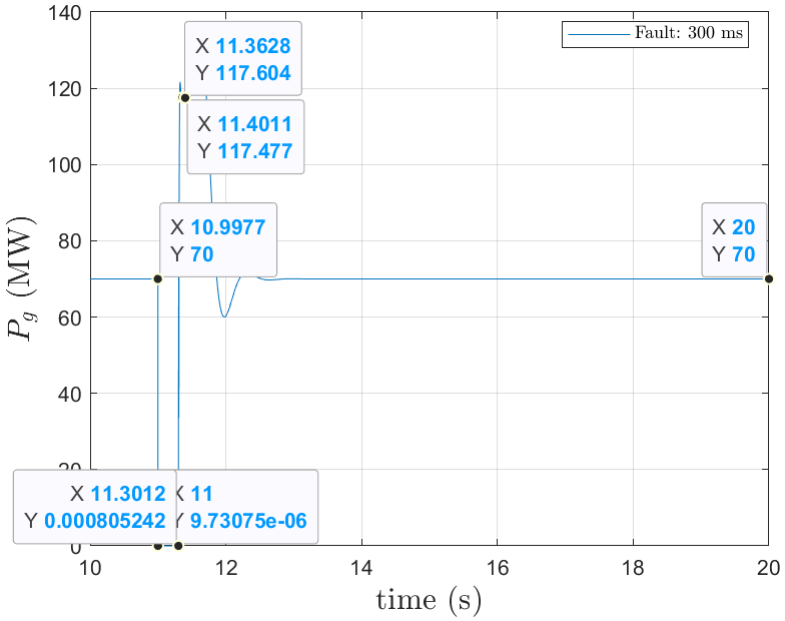

Figure 3.7: P-t curve for a clearing time of 300ms

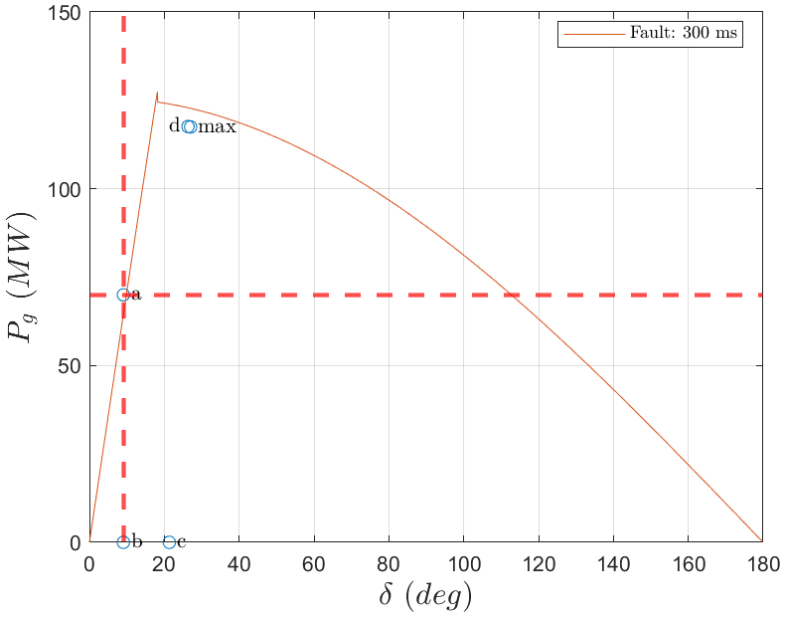

Figure 3.8: P-δ curve for a clearing time of 300ms

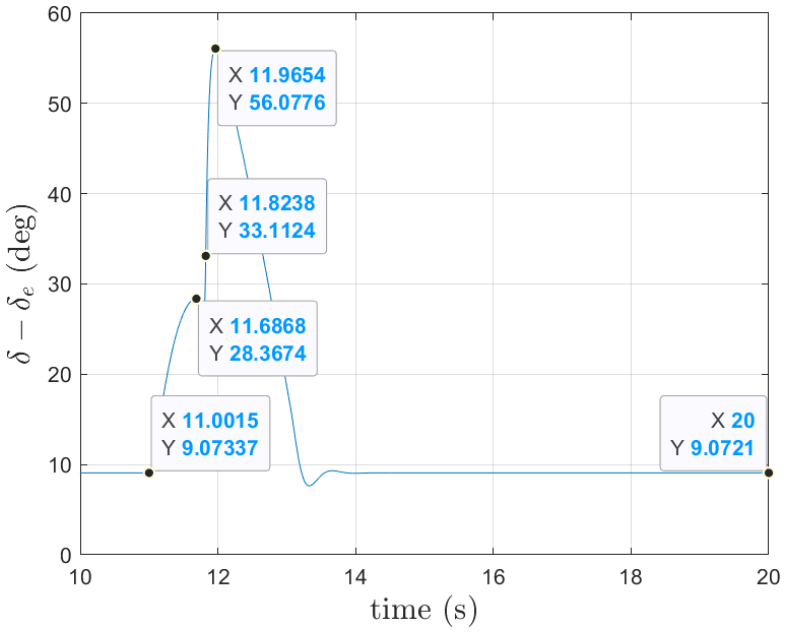

Figure 3.9: δ-t curve for a clearing time of 800ms

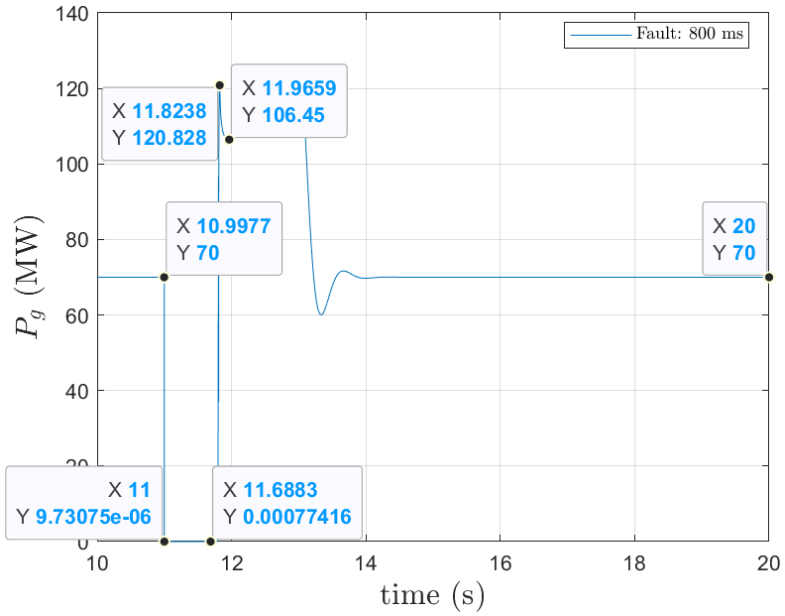

Figure 3.10: P-t curve for a clearing time of 800ms

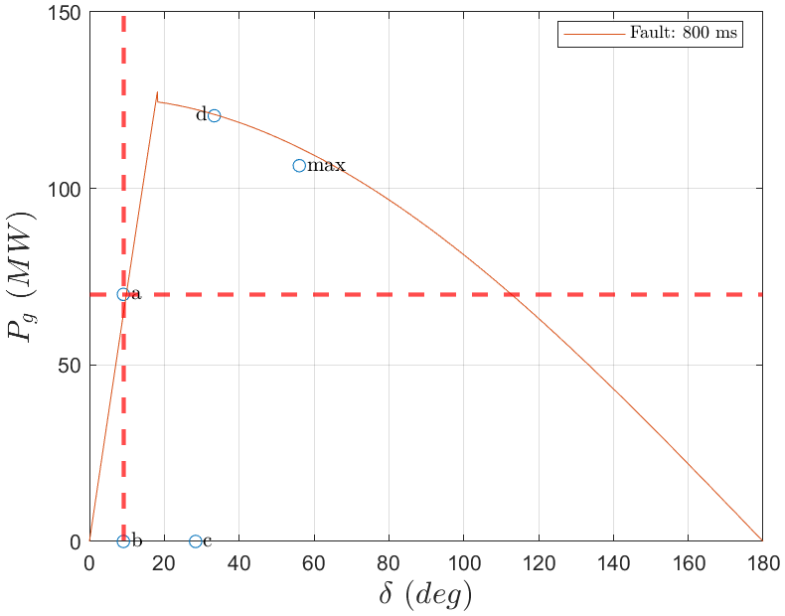

Figure 3.11: P-δ curve for a clearing time of 800ms

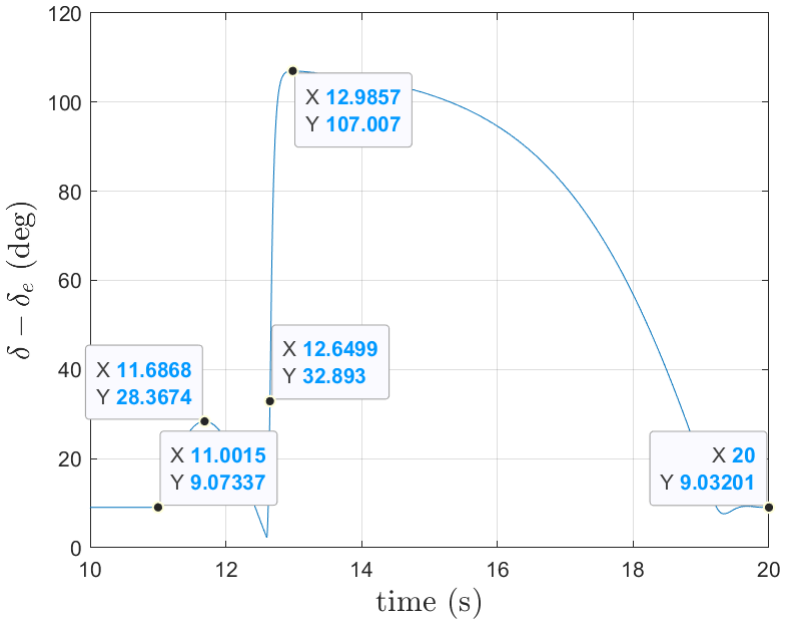

Figure 3.12: δ-t curve for a clearing time of 1600ms

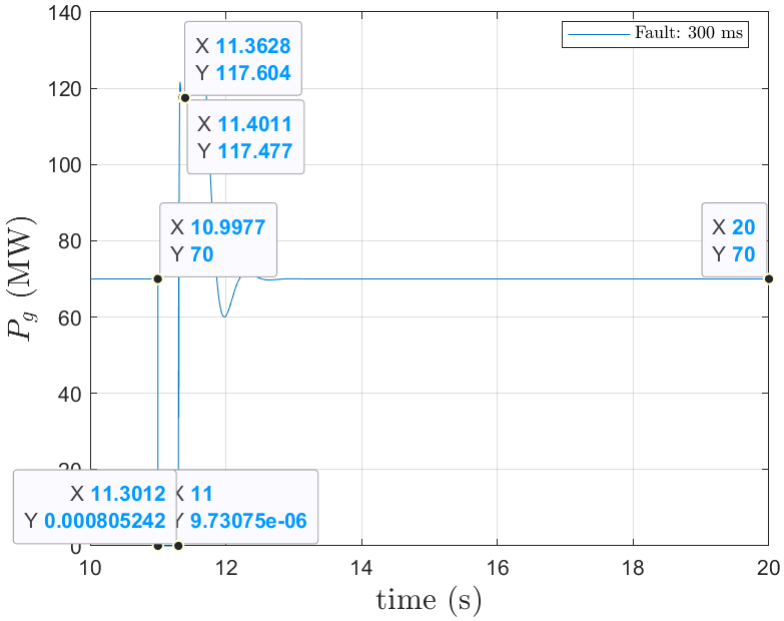

Figure 3.13: P-t curve for a clearing time of 1600ms

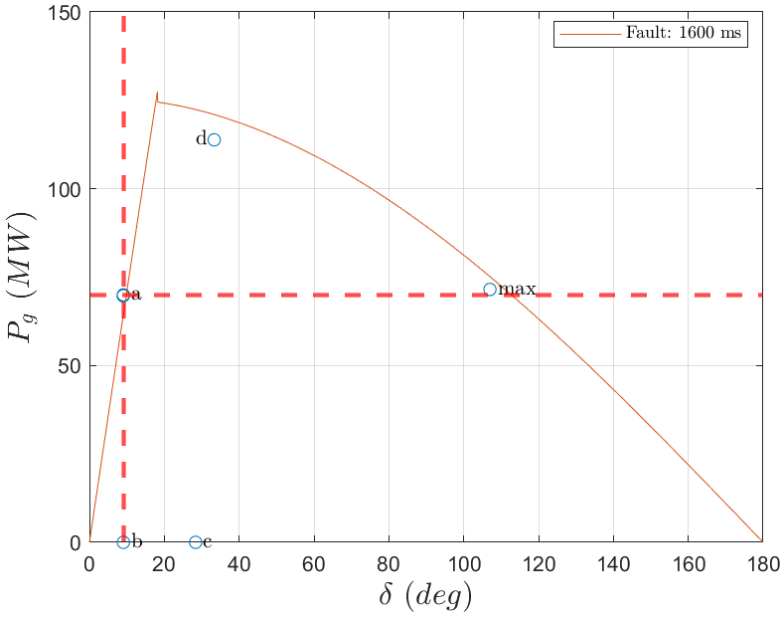

Figure 3.14: P-δ curve for a clearing time of 1600ms

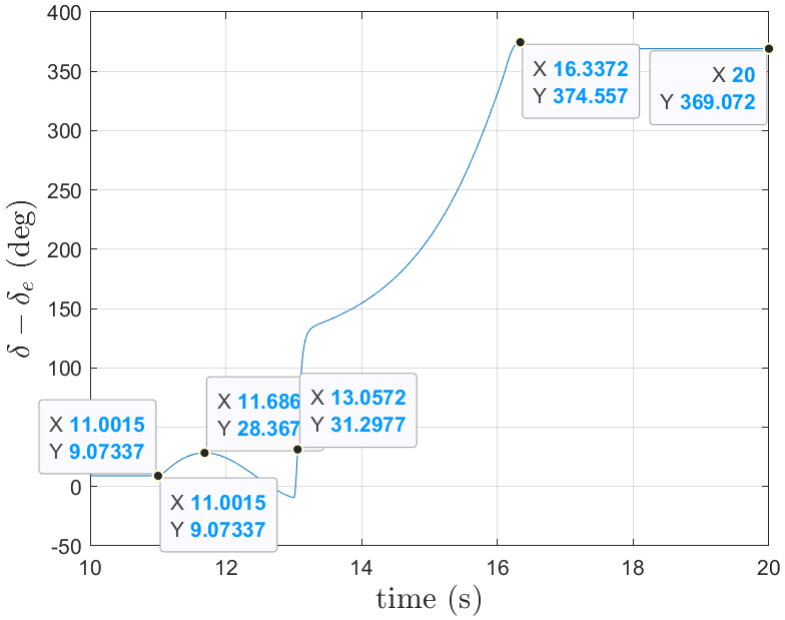

Figure 3.15: δ-t curve for a clearing time of 2000ms

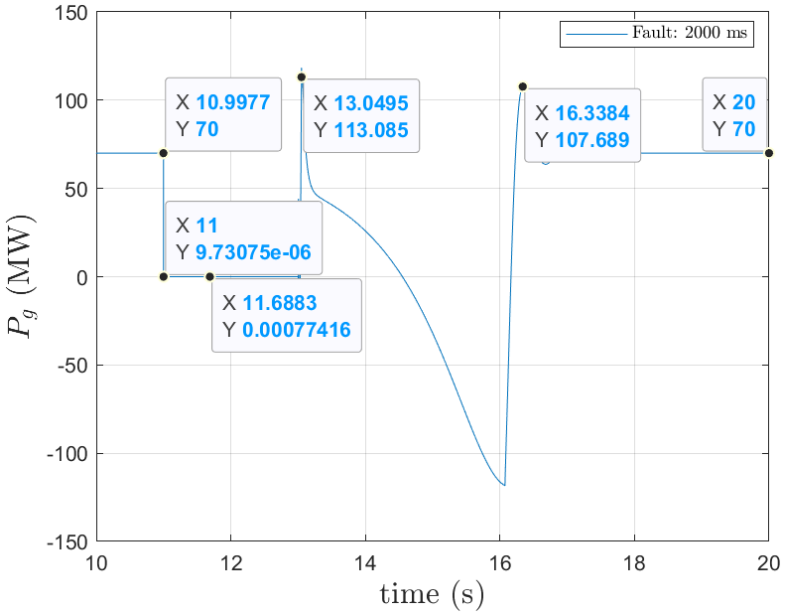

Figure 3.16: P-t curve for a clearing time of 2000ms

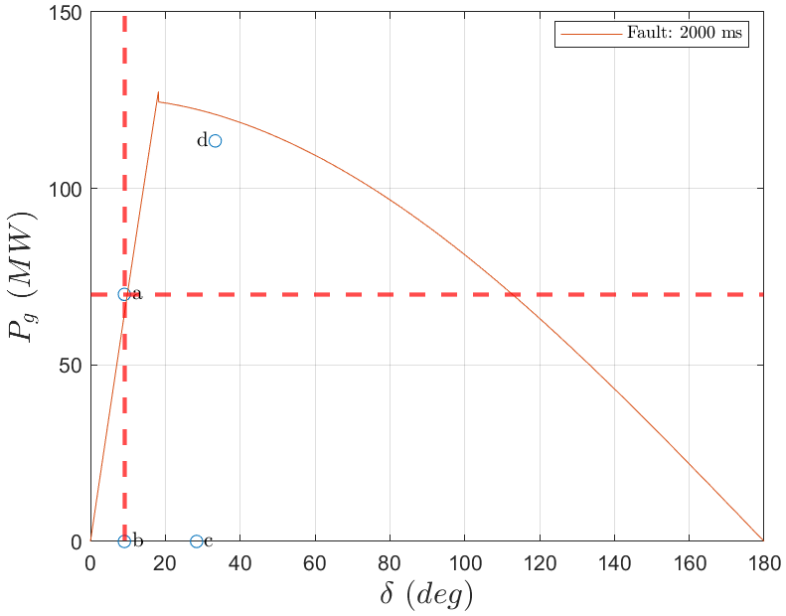

Figure 3.17: P-δ curve for a clearing time of 2000ms

The pre-fault situation is always the same, as this does not depend on the time the fault clears. Therefore, the moment the fault occurs, the variables are also equal in all examples. From this point onward, as the faults clear in different times, the angle of clearance is not the same, and should be greater as the fault gets longer. There is an unknown behaviour, as before the fault is cleared, the GFM-VSC power converter seems to start to decelerate, as it can be observed that the angle has a tendency to reduce. This is more notable in the longer faults, where in some cases it drops below the initial angle situation like in 3.12 & 3.15. Meanwhile, the power is still 0 until the fault is cleared. Then, the power and angle follow a similar shape, with a sudden peak of power, which then starts to reduce, and then slightly increases to the value of the peak, to finally return to the pre-fault power injection in the cases of no loss of synchronism. In the longer fault, the power never stops reducing, and the angular velocity seems to start to reduce, until a point, where it accelerates. This is seen in 3.15 in the point where the gradient changes after the fault is cleared. Even though it seems to return to the pre-fault situation in steady state in both power and angle (+360°), this is not true and represents an error in the model. This is not important, as it is a clear loss of synchronism, and therefore its final steady state will never be taken into account. This loss of synchronism can also be observed in 3.17, as the point max) cannot be seen in the curve. This happens because the angle continues to grow indefinitely.

To compare the examples, include more important variables and explain further the strange angle drop, more graphs will be included:

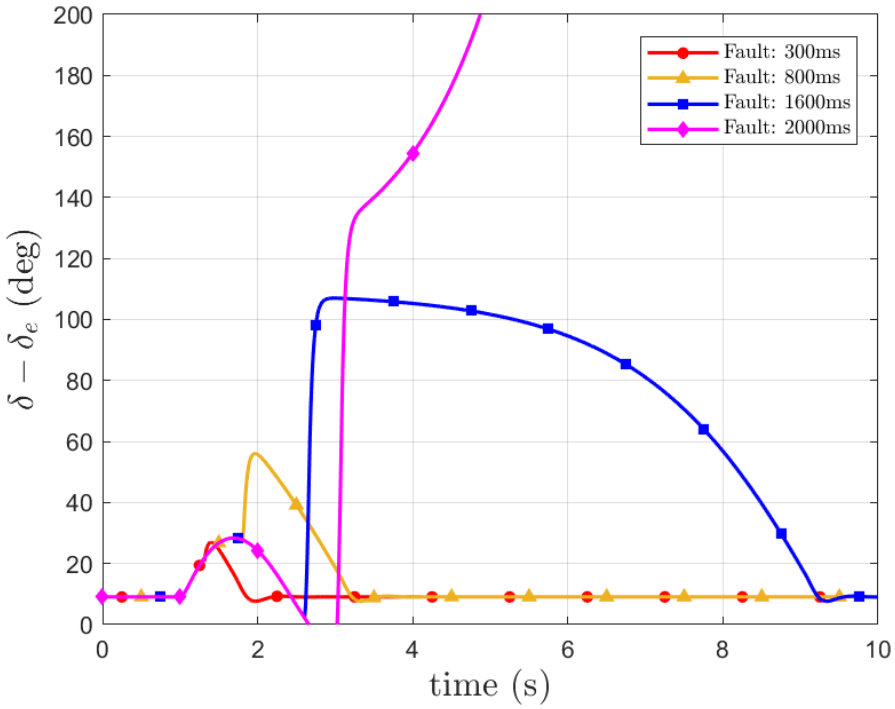

Figure 3.18: δ-t curves for previous fault clearing times

The active power and angle graphs 3.19 & 3.18 have already been explained with the previous graphs and are shown only for a more visual comparison. The graph that shows the reactive power injected along time 3.19 shows that the pre-fault situation is 0, and during the fault, as the line is open, the injection remains 0. When the fault is cleared, there is a peak, also seen in v_g, e_m and i_s. This power peak happens to return v_g and to 1pu and keep e_m close to 1pu too. The reason the P-δ curves do not follow the exact expected shape is that the e_m is not always exactly 1pu. Also, it can be observed that the longer it takes to clear the fault, the longer there is injection of Q. In the case of the loss of synchronism, it seems to take a shorter time than the shorter fault of 1600ms, but again, it is an error of the model, and therefore, from the moment synchronism is lost, this graph should not be taken into account. The frequency graph is also very important, and helps explain the tendency of the angle to reduce before the fault is cleared. As can be observed in 3.20, the estimation of the PLL for the frequency is as if it were lower than 50Hz. This is not a correct estimation, as if the GFM-VSC power converter behaved as a SM, it would accelerate, and therefore, its frequency would increase

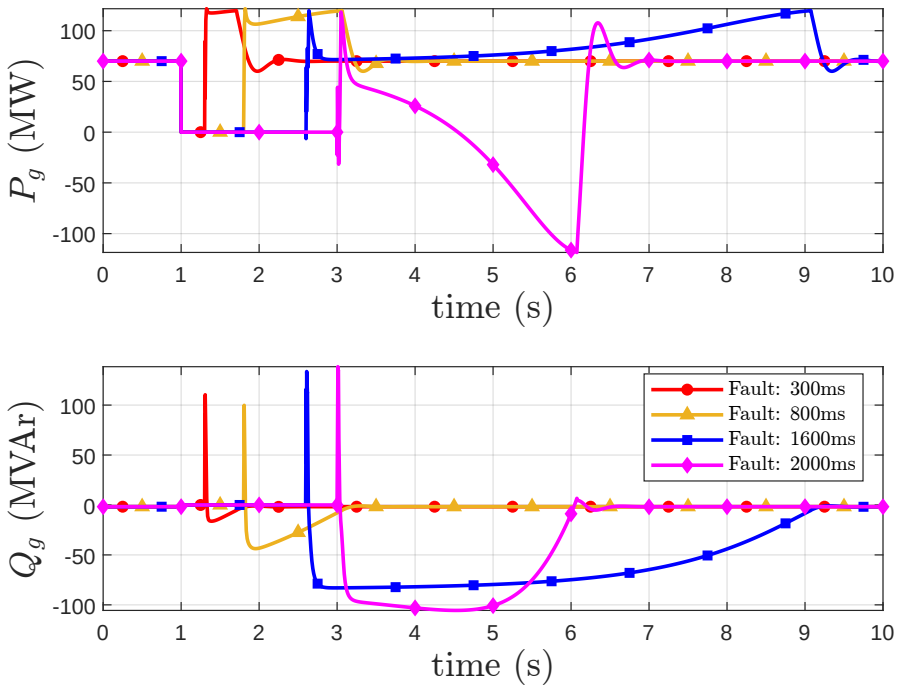

Figure 3.19: P_g & Q_g-t curves for previous fault clearing times

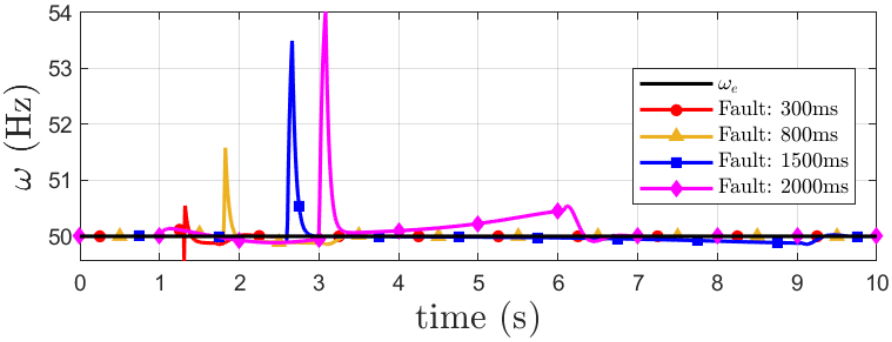

Figure 3.20: ω-t curves for previous fault clearing times

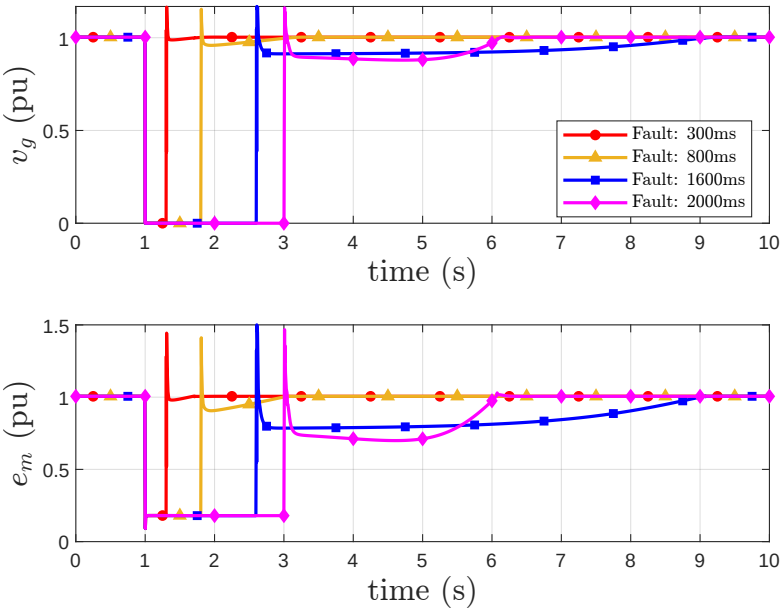

Figure 3.21: v_g & e_m-t curves for previous fault clearing times

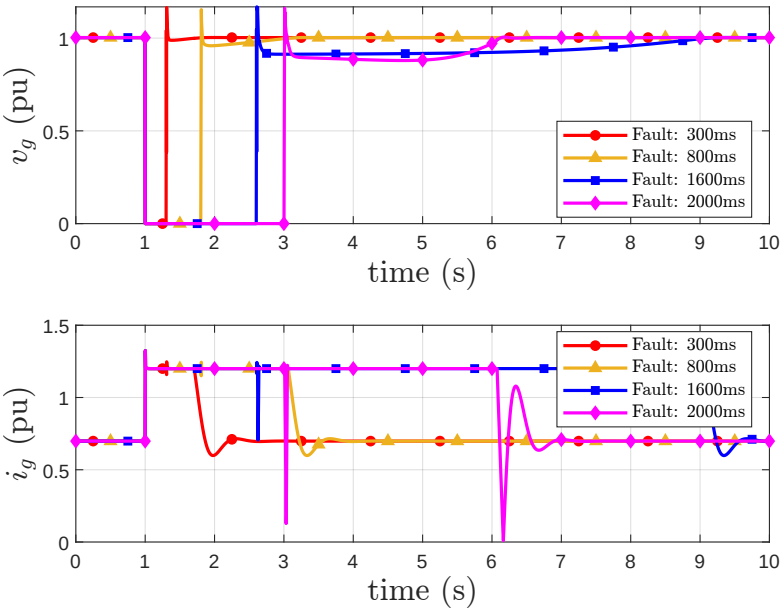

Figure 3.22: v_g & i_g-t curves for previous fault clearing times

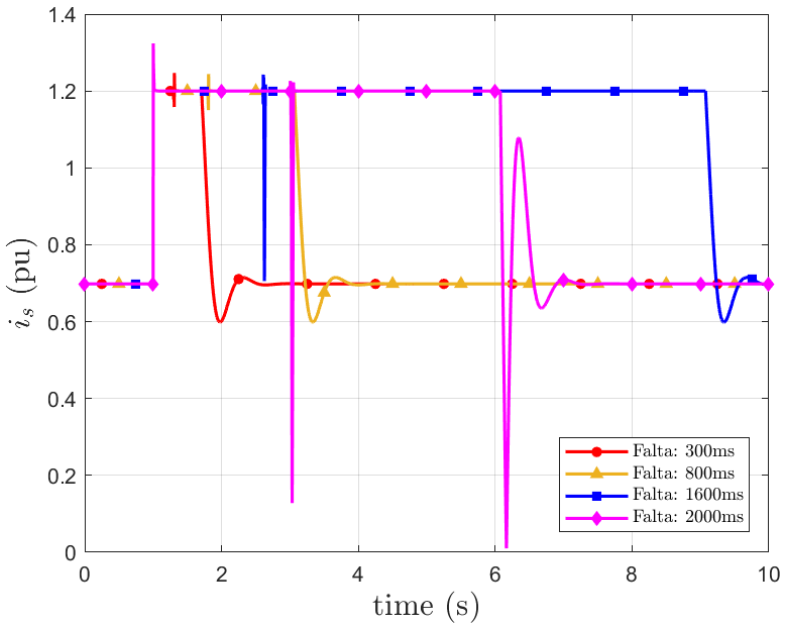

Figure 3.23: i_s-t curves for previous fault clearing times

over 50Hz. Even if this is a strange event, it causes the angle to reduce before the fault is cleared. In this manner, the angle can reach values lower than the pre-fault value. When the fault is cleared, the frequency has a peak much over 50Hz, which explains the quick jump in the angle, and starts to steadily reduce to its steady state of 50Hz if possible. This is why the angle reaches a maximum angle, and then returns to the initial value as seen in 3.18. Figure 3.22 shows both v_g and i_g . As can be seen in this graph, the changes of v_g causes perturbations in the graph of i_g . It also makes sense that when the fault is happening, the value of the injected current is not 0, as it drops through the PCC (where the fault occurs). This current is also shown by its own in 3.23, and the peaks when the faults are cleared are more obvious. Again, in the fault that is cleared in 2000ms, the current seems to go down quicker than for the one cleared in 1600ms, but as mentioned previously, this would not happen in reality.

3.6 CCT calculation and comparison

Using the EAC method, the critical angle obtained is $\delta_{cl}^{crit} = 39,133°$. From here, we can obtain a CCT of 690ms. By running the CCT simulation script for this case, we obtain a simulated CCT of 1620ms. There is a great difference between these two values, and therefore, for this case, the EAC is not applicable. This difference

may be caused by the effect that the damping coefficient has on transient stability, or by the effect the estimation of the PLL has on the frequency, causing the angle to fall before the fault is cleared. Table 3.2 shows the CCTs calculated via the EAC method and the one obtained by the CCT calculation script of the GFM-VSC VSM-PLL-CL-CSA. After every chapter, the new cases will be added to this table.

Table 3.2: CCT table GFM-VSC VSM-PLL-CL-CSA

Case	Method used to obtain	CCT (ms)
GFM-VSC VSM-PLL-CL-CSA $D_{GFM} = 202,61pu$	EAC	690
GFM-VSC VSM-PLL-CL-CSA $D_{GFM} = 202,61pu$	CCT algorithm	1620

3.7 Summary & Conclusions

In this chapter, the following points have been tackled:

- Introduction of the model and scheme of the GFM-VSC power converter connected to an infinite grid. The model used is GFM-VSC VSM-PLL-CL-CSA with $D_{GFM} = 202,61pu$
- Introduction of the important variables and how they will be represented and analysed
- How EAC can be applied, how it works with CL-CSA
- A series of simulations of different fault clearing times and representation of the variables with comparison between the different clearing times simulated
- Calculation of the CCT via the EAC and the simulation of the CCT for the case GFM-VSC VSM-PLL-CL-CSA with $D_{GFM} = 202,61pu$

The following conclusions have been reached:

- Even if the angle difference between the GFM-VSC power converter and the grid (δ) stabilises at $360° + \delta_0$, synchronism is considered to be lost
- Due to fluctuations in v_g & e_m, the P-δ curve does not develop perfectly on top of the P-δ curve for CL-CSA
- The strange behaviour of the PLL causes the angle difference between the GFM-VSC power converter and the grid (δ) to have a different shape to expected before the fault is cleared

- The simulated CCT for the GFM-VSC VSM-PLL-CL-CSA model is much greater than the CCT obtained via the EAC

Chapter 4

Analysis of the PLL of GFM-VSCs on Transient Stability

4.1 Introduction

In this chapter, the scheme of the PLL used will be shown, and a new model will be introduced and explained to habilitate a better understanding of the phenomenon. This model will be named GFM-VSC VSM-PLL-Freeze-CL-CSA. Then a series of fault clearing times for the new model will be simulated, and the variables will be shown and compared to the previous model of the GFM-VSC VSM-PLL-CL-CSA. Then, the simulated CCT of the GFM-VSC VSM-PLL-Freeze-CL-CSA will be obtained and compared to the CCT calculated via the EAC and the simulated CCT of the GFM-VSC VSM-PLL-CL-CSA.

4.2 Frozen PLL model design

As introduced in the previous chapter, one of the reasons that the CCT of the simulation is so different to the one calculated via the EAC is the PLL frequency estimation. To further understand how the PLL works, the block diagram of the PLL is shown in figure 4.1, obtained from [7]. The "mistaken" or peculiar estimation of the PLL seems to make the GFM-VSC power converter have a larger CCT, which translates into a more positive transitive behaviour. But, as the reason the frequency is estimated as seen in figure 4.2, is unknown, it is not wise for the analysis of transient stability of GFM-VSCs to base the complete analysis on this sole example. That is why a new case has been developed to understand the phenomenon more deeply. This case, known as GFM-VSC VSM-PLL-Freeze-CL-CSA during the period of fault, freezes the PLL's estimation during the fault duration. In this case, the PLL frequency remains the prefault estimation, or,

in other words, 1pu. In this manner, the angle follows a more similar trajectory than how it would in a SM. In figure 4.3, eventhough the PLL still estimates a sub-nominal frequency, it's estimation is disabled, as can be seen, the GFM-VSC power converter's frequency does not reduce as it does without the Freeze feature. In this

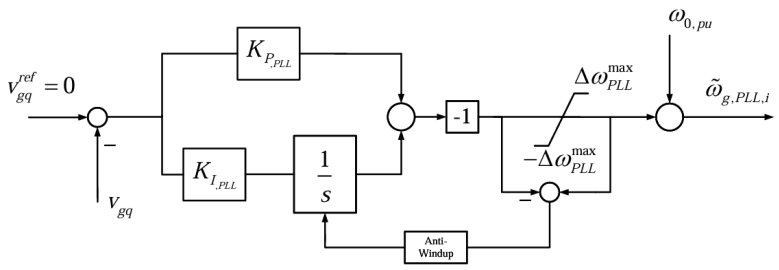

Figure 4.1: PLL block diagram equipped with an anti-windup

chapter, the behaviour of the new frozen PLL will be compared to the behaviour of the basic PLL model. The comparison will be made by using the different variables against time, the P-delta curves and both the simulated CCTs and the CCTs obtained via the EAC. The goal is to understand how each system behaves against faults (both short and long), and to observe if the empirical calculation of the CCT via the EAC of the GFM-VSC-PLL-Freeze-CL-CSA is closer to the simulated CCT. Due to the difference in transient stability, the faults compared will have different clearing times, as the system without the frozen PLL will have a greater CCT.

4.3 P-δ curves and EAC for Frozen PLL

As the case GFM-VSC VSM-PLL-Freeze-CL-CSA still includes the CL and the CSA, the P-δ curve is the same as the case where the PLL was not frozen during the fault duration. This means the CCT calculated via the EAC method is the same as the CCT of the GFM-VSC VSM-PLL-CL-CSA case, and remains 690ms.

4.4 Fault simulation and results

In this case, as it is very similar to the case attacked in the previous chapter, first a series of short and long faults will be analysed individually for the new case introduced, to observe the behaviour of the angle δ and the power injection P_g

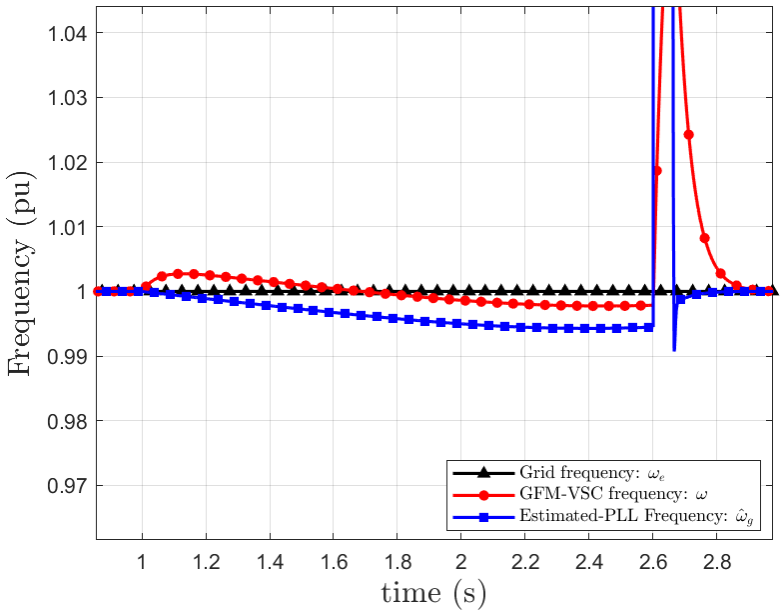

Figure 4.2: PLL estimated frequency compared to GFM-VSC frequency before fault clears (No Freeze)

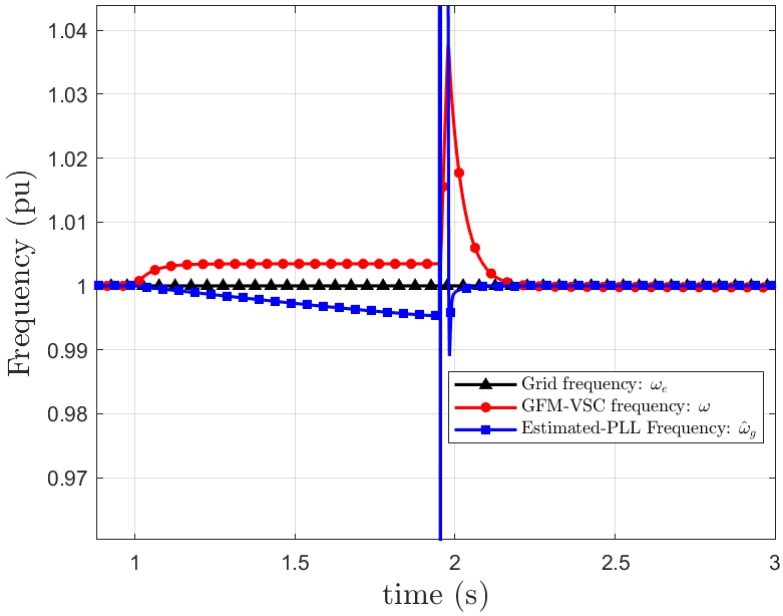

Figure 4.3: PLL estimated frequency compared to GFM-VSC frequency before fault clears (Freeze)

with time, and then in a P-δ graph. Here, the drop of δ is not expected to be as notable as in the GFM-VSC VSM-PLL-CL-CSA case.

After this has been analysed, both cases will be compared, by comparing faults that are cleared in the same times.

For continuity and coherence, the analysed fault clearing times will be 300ms, 800ms, 950ms for the "short" clearing times, and 1500ms for the "long one". The important comparison between these cases is not the magnitude of the clearing time, but the shape of the cases For the direct comparison with the previous case, the 300ms and 950ms clearing times will be discarded, as, with the other faults, and the δ-t and P_g-t shown in figures: (delta t y pg t de 300ms y 1600ms freeze) of these clearing times they bring enough information without occupying the extra space of adding too many figures.

As in the previous chapter, first, some graphs of the individual clearing times will be shown and explained. Then, a comparison of the important variables will be made by including together the transitory behaviour of the variables in the cases with and without the frozen PLL feature.

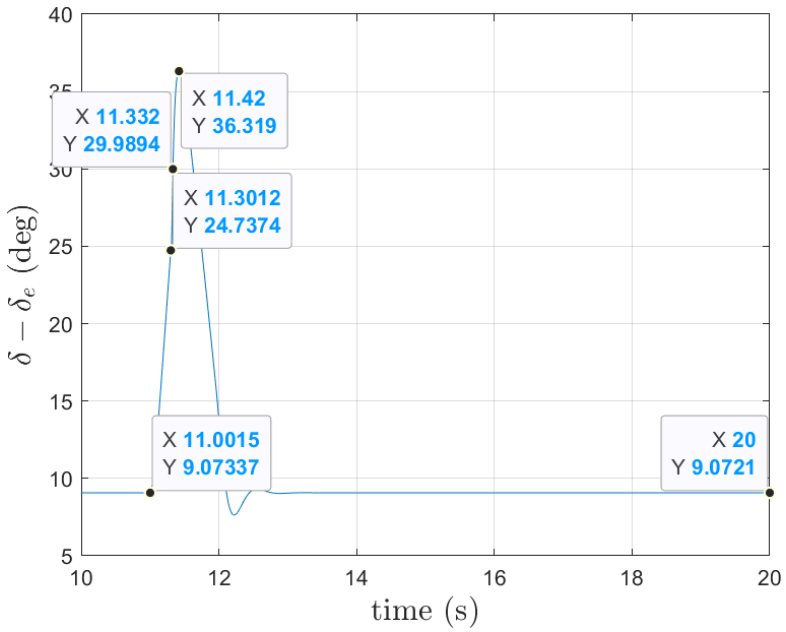

Figure 4.4: δ-t curve for a clearing time of 300ms

As can be seen in figures 4.4, 4.7, 4.10 & 4.13, the angle no longer starts to drop before the fault is cleared. It is also true that, as expected, this affects transient stability negatively, as the PLL's estimation helped it maintain synchronism for longer clearing times. The power develops very similarly as in the case without

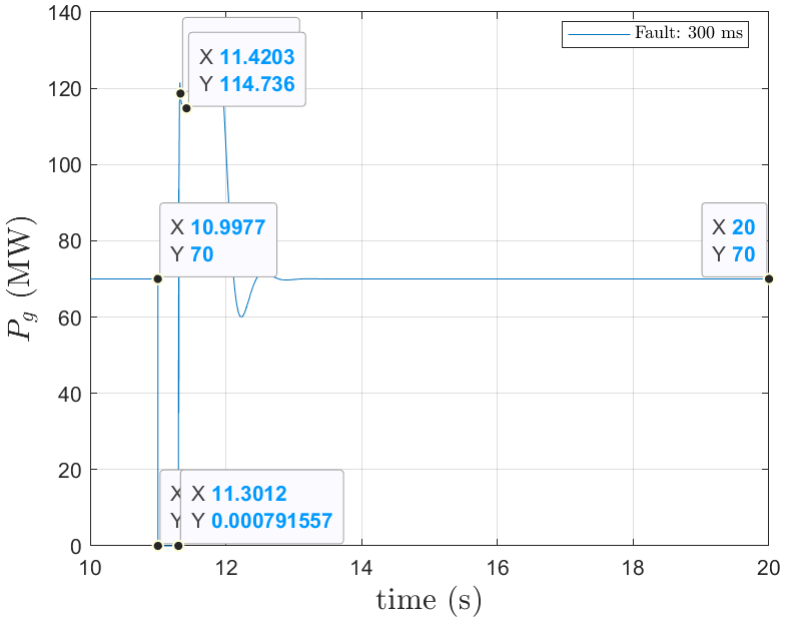

Figure 4.5: P-t curve for a clearing time of 300ms

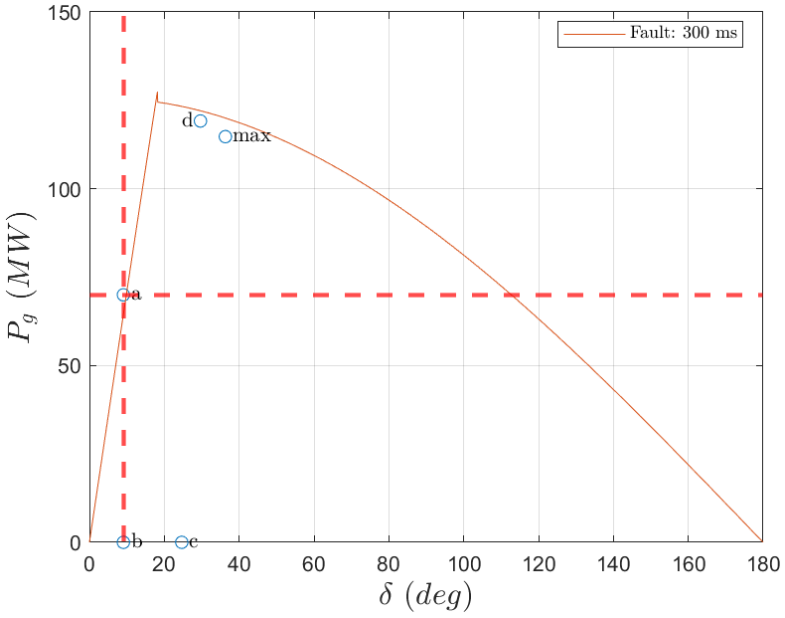

Figure 4.6: P-δ curve for a clearing time of 300ms

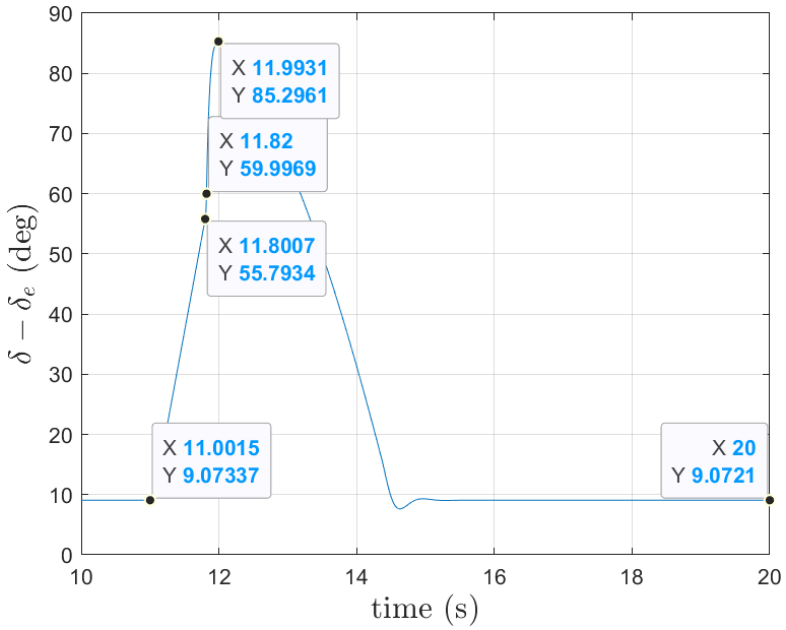

Figure 4.7: δ-t curve for a clearing time of 800ms

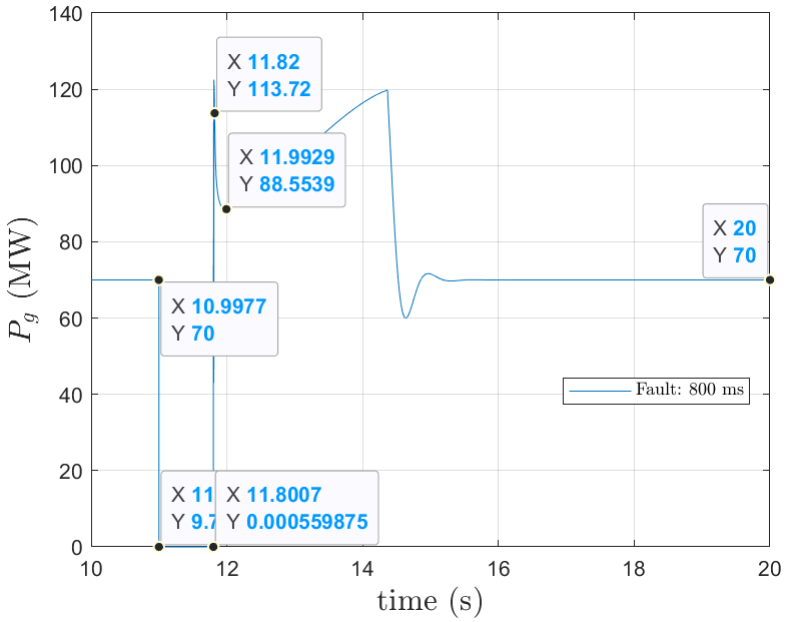

Figure 4.8: P-t curve for a clearing time of 800ms

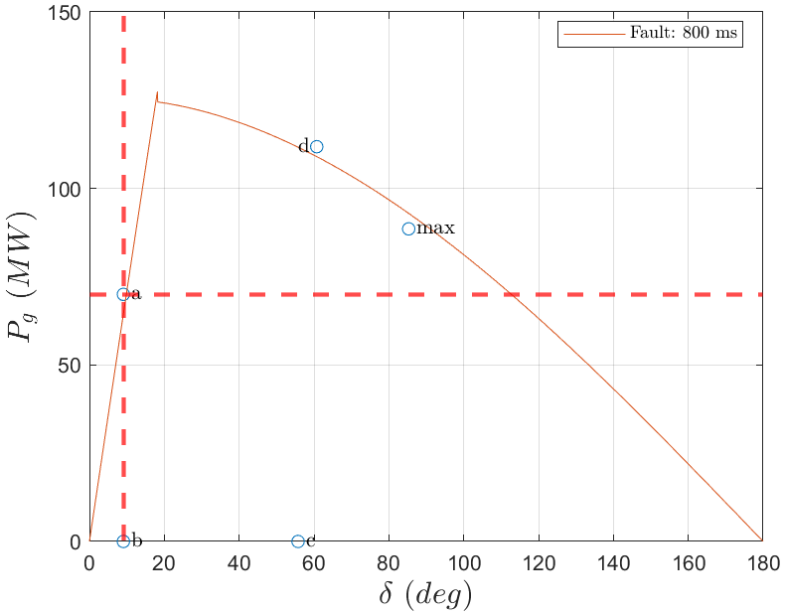

Figure 4.9: P-δ curve for a clearing time of 800ms

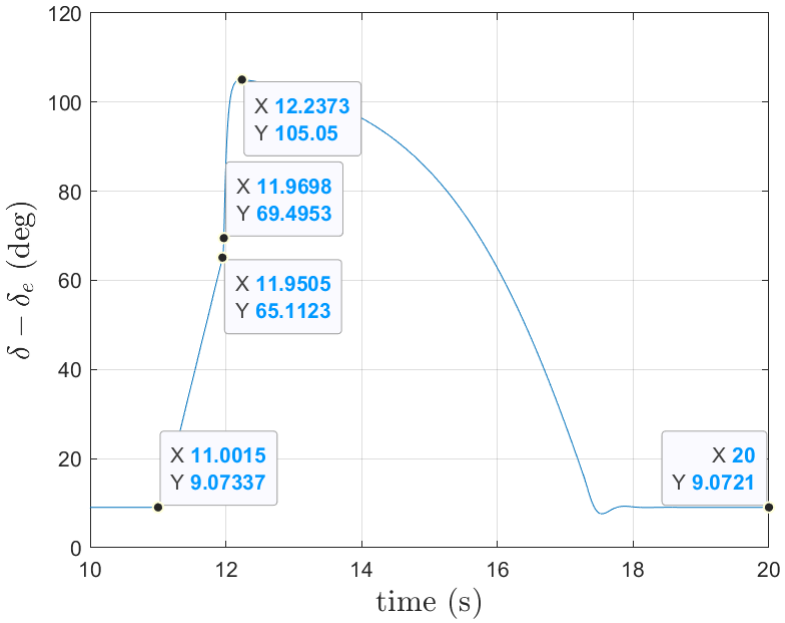

Figure 4.10: δ-t curve for a clearing time of 950ms

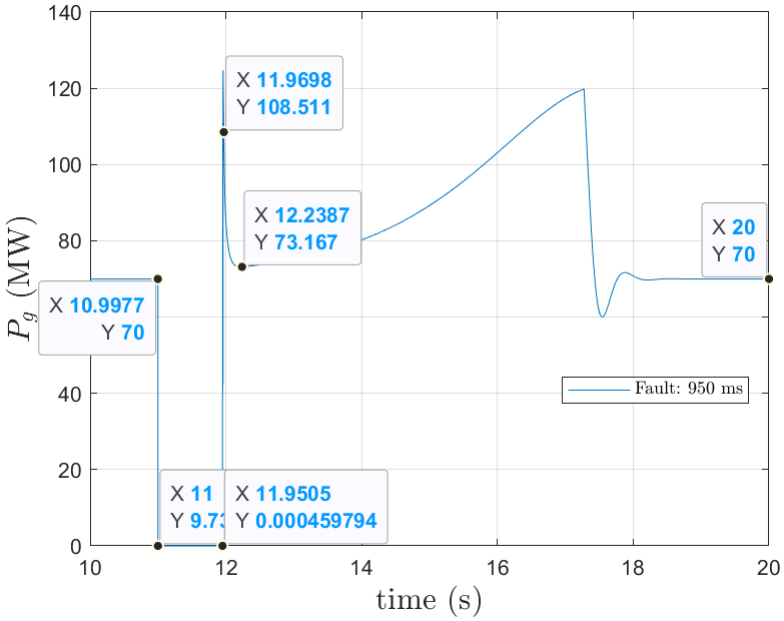

Figure 4.11: P-t curve for a clearing time of 950ms

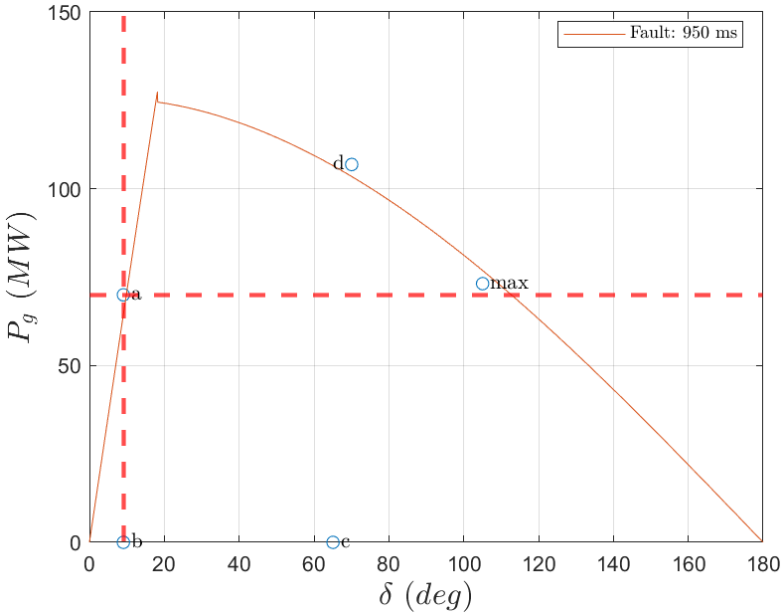

Figure 4.12: P-δ curve for a clearing time of 950ms

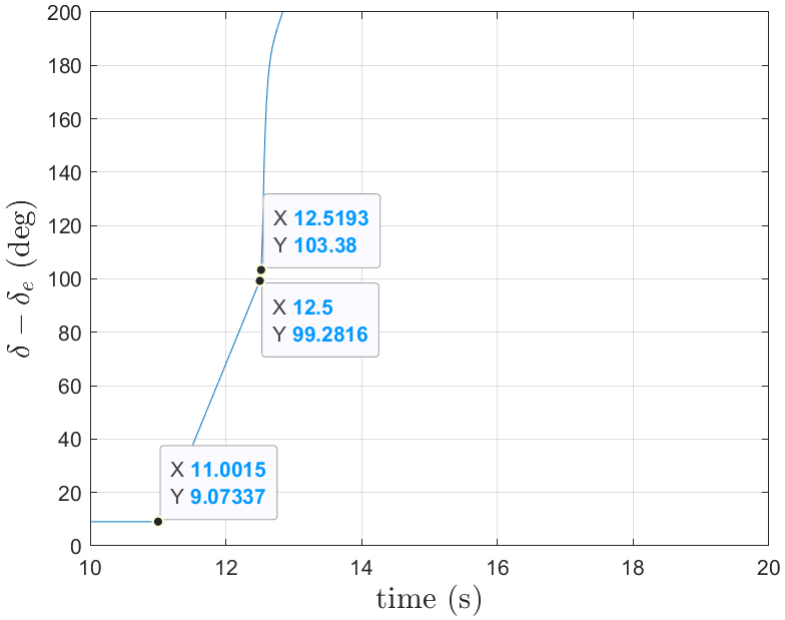

Figure 4.13: δ-t curve for a clearing time of 1500ms

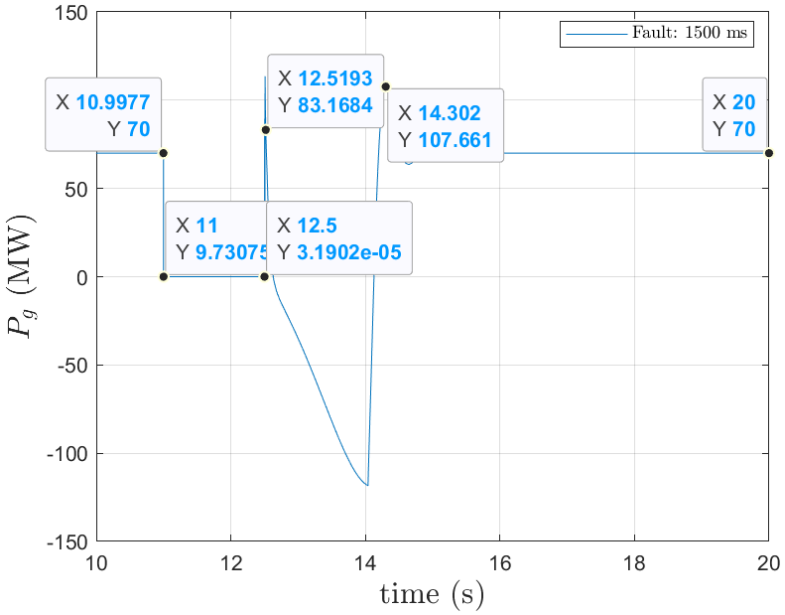

Figure 4.14: P-t curve for a clearing time of 1500ms

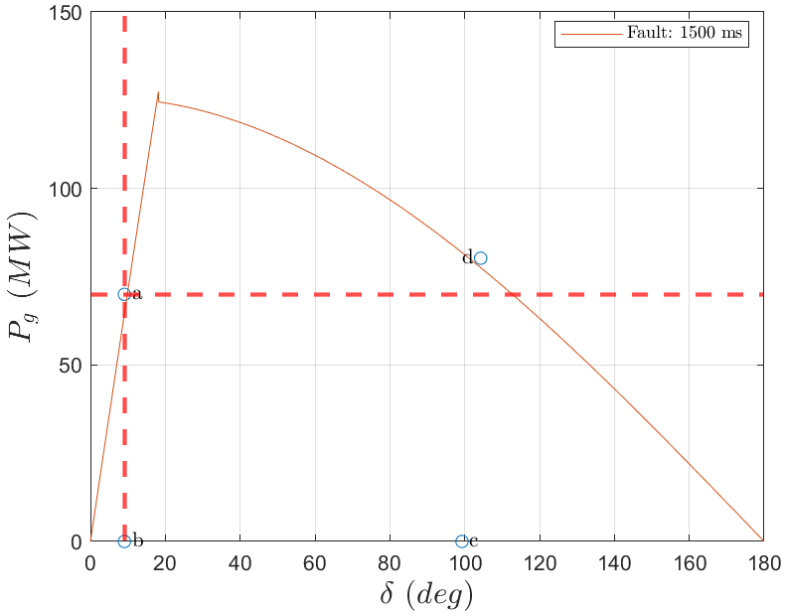

Figure 4.15: P-δ curve for a clearing time of 1500ms

the frozen PLL, and is seen in figures 4.5, 4.8, 4.11 & 4.14. The P-δ curves for the clearing times simulated are shown in figures 4.6, 4.9, 4.12 & 4.15, and, due to the change of behaviour with the angle, the points a), b), c), d) and max) follow the curve better. Again, as synchronism is lost in the fault where the clearing time was 1500ms, the final angle is the initial one plus one full cycle (+360°), and the point max) does not show in the P-δ curve. For the comparison of the cases with and without the frozen PLL, short clearing times of 800ms will be compared, and a clearing time of 1500ms for the frozen PLL will be compared to one of 2000ms for the unfrozen PLL for the long clearing times. In figure 4.16, as mentioned before, the PLL freeze case does not have the angle drop, and its increase follows a straight line until the fault is cleared. After the fault is cleared, behaviour is similar. The straight increase makes sense when observing figure 4.18, as the frequency in the GFM-VSC power converter before the fault is cleared reaches a constant value. When comparing the power curves seen in figure 4.17, the curves have a similar shape, but in the case of the frozen PLL, P_g has to be injected into the grid for longer, and more Q_g needs to be injected into the GFM-VSC power converter in order for it to maintain synchronism with the grid. The voltages, as seen in figure 4.19 follow almost identical curves as the PLL without the frozen feature, but it takes for them to reach the final values. This makes sense when contrasting this with the need of injection of Q_g into the GFM-VSC power converter, as this is related to the Q/V control. Also, during this time, i_g is injected, as shown in figure

4.20 together with v_g, and by its own in figure 4.21. In the frozen PLL model, the spike that happens when the fault is cleared is somewhat smaller, but otherwise, follows a similar shape with the difference that the injection time has to be longer, as mentioned for the power and voltage.

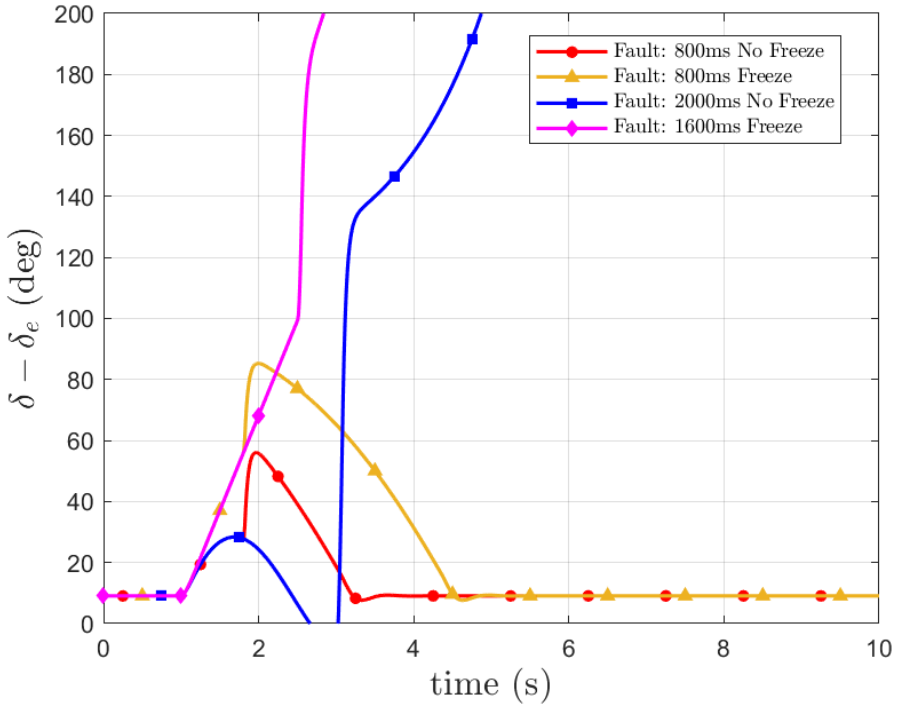

Figure 4.16: δ-t curves for PLL-Freeze vs PLL-NoFreeze

4.5 CCT calculation and comparison

As mentioned previously, the EAC calculated CCT will still be 690ms. The simulated CCT has been 970ms, and as expected, it is lower than the CCT simulated in the case with the unfrozen PLL, and, as also predicted, also closer to the EAC calculated CCT. Table 4.1 shows a summary of the CCTs obtained for both cases analysed.

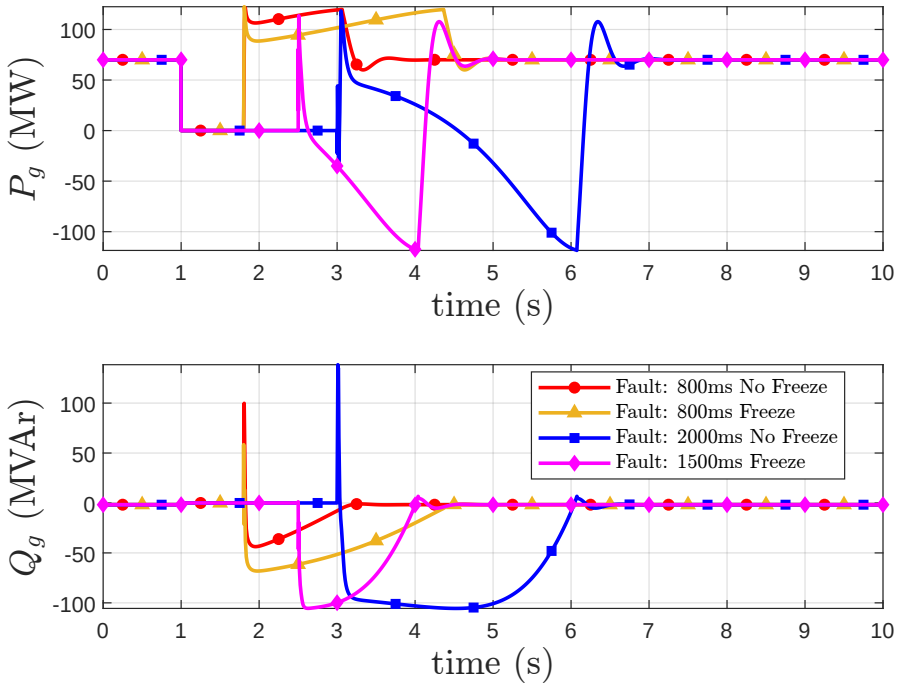

Figure 4.17: P_g & Q_g-t curves for PLL-Freeze vs PLL-NoFreeze

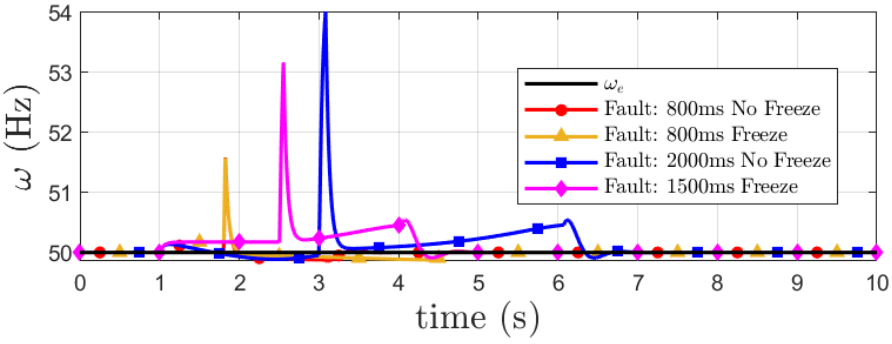

Figure 4.18: ω-t curves for PLL-Freeze vs PLL-NoFreeze

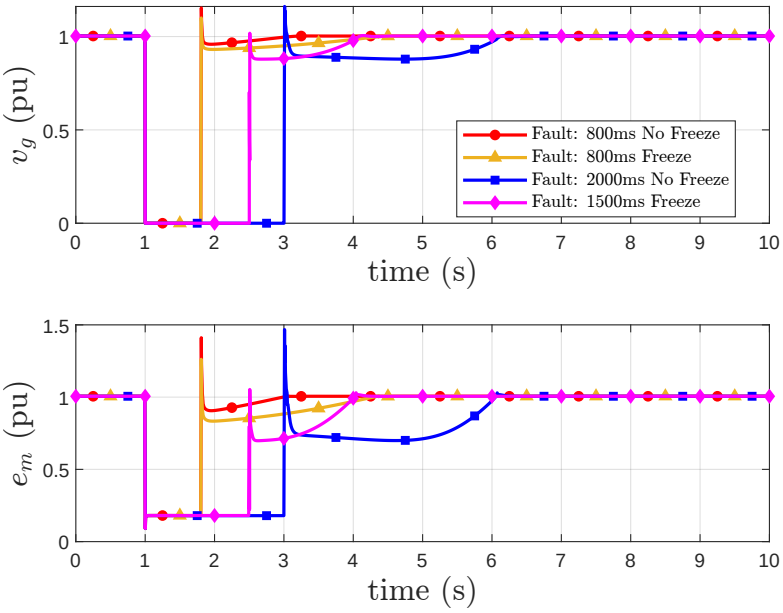

Figure 4.19: v_g & e_m-t curves for PLL-Freeze vs PLL-NoFreeze

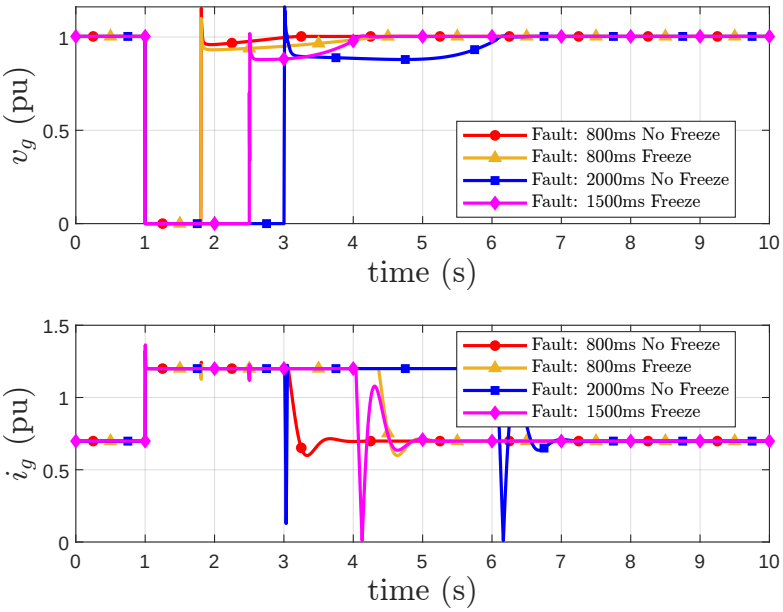

Figure 4.20: v_g & i_g-t curves for PLL-Freeze vs PLL-NoFreeze

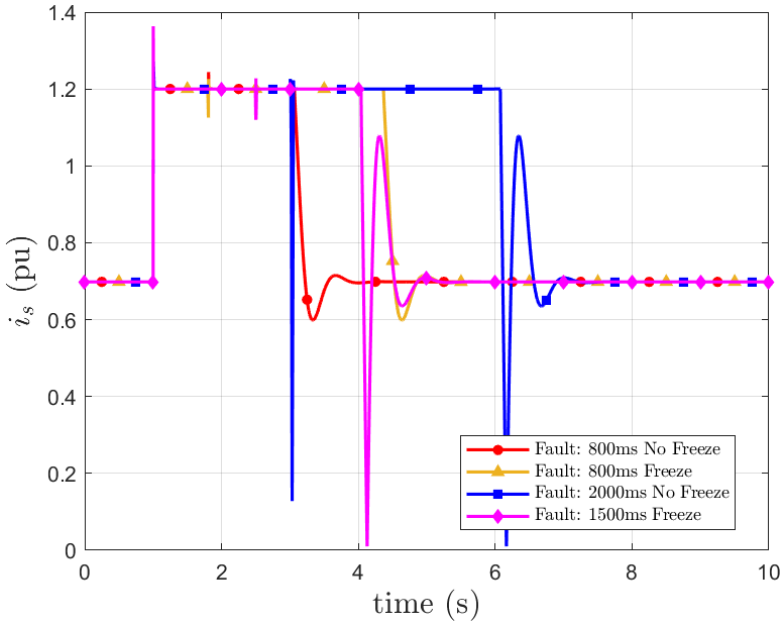

Figure 4.21: i_s-t curves for PLL-Freeze vs PLL-NoFreeze

Table 4.1: CCT table GFM-VSC VSM-PLL-Freeze-CL-CSA

Case	Method used to obtain	CCT (ms)
GFM-VSC VSM-PLL-CL-CSA $D_{GFM} = 202,61pu$	EAC	690
GFM-VSC VSM-PLL-CL-CSA $D_{GFM} = 202,61pu$	CCT algorithm	1620
GFM-VSC VSM-PLL-Freeze-CL-CSA	CCT algorithm	970

4.6 Summary & Conclusions

In this chapter, the following points have been tackled:

- Introduction of the block diagram of the PLL used
- Design of the GFM-VSC VSM-PLL-Freeze-CL-CSA model
- A series of simulations for the new model of different fault clearing times and representation of the variables with comparison between the different clearing times and the clearing times simulated in the previous chapter
- Simulation to obtain the simulated CCT of the GFM-VSC VSM-PLL-Freeze-CL-CSA model and comparison with the simulated CCT of the GFM-VSC

VSM-PLL-CL-CSA model (both with $D_{GFM} = 202,61pu$ and the CCT obtained via the EAC.

The following conclusions have been reached:

- The frozen feature introduced into the PLL does help the angle difference between the GFM-VSC power converter and the grid develop normally
- This feature does not affect any other variable besides the angle difference (and therefore the GFM-VSC power converter's frequency)
- The strange behaviour in the PLL before the frozen feature was introduced into the PLL makes the model have a larger CCT (even if the reason for this behaviour is not known)
- The CCT of the GFM-VSC VSM-PLL-Freeze-CL-CSA is closer to the CCT obtained via the EAC, but still higher

Chapter 5

Effect of Damping in GFM-VSCs on Transient Stability

5.1 Introduction

From this chapter onward, the case used as the reference case, and from which the comparisons will be made is the case of the GFM-VSC VSM-PLL-Freeze-CL-CSA with a damping coefficient $D_{GFM} = 202.61pu$. From here, the effect of the damping coefficient with and without the CL & the CSA will be studied. This effect will be analysed via the simulation and presentation of the different variables with different fault clearing times and the CCTs obtained for each individual case using the methods presented in the previous chapters. The case of no damping causes the model to be completely unstable, and therefore, some damping is required for the simulations to run without error. For the cases of no damping, $D_{GFM} = 20pu$ will be used to compare magnitudes of damping of a SM and to the model of GFM-VSC NoPLL, which is designed with $D_{GFM} = 20pu$. It is expected that the CCT obtained by simulation for both cases with "no damping" is close to the CCT obtained via the EAC, as in these cases the damping coefficient D_{GFM} does not have much effect, and it's term in the swing equation is small compared to the other terms (which is one of the suppositions made in the EAC).

5.2 P-δ curves and EAC

In this chapter, some of the examples to analyse do not include the CL & the CSA, and therefore, the shape of the P-δ curve is not the same as in the previous chapters. In these examples, the current is not limited by any value, and can develop normally. An example of the shape, and sequence labelled with the key points a), b), c), d) and max) (implying synchronism is not lost in this case) is

shown in figure 5.1.

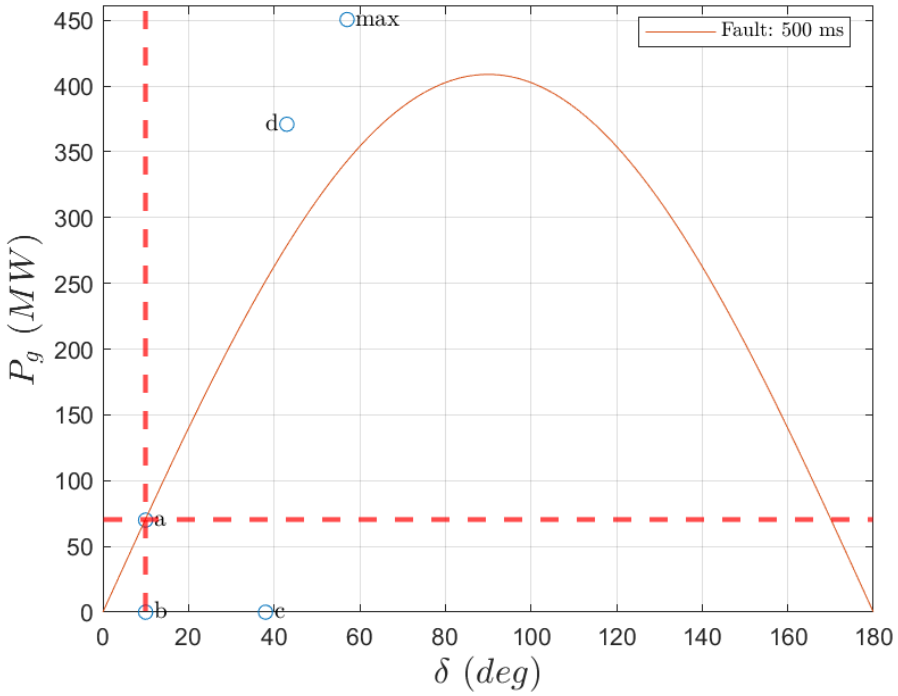

Figure 5.1: GFM-VSC VSM-PLL No CL: P-δ curve

5.3 Fault simulation and results

In this section, two separate experiments will be shown to observe the effect of damping. The first will observe how damping affects the behaviour of the GFM-VSC power converter against different clearing times, and its respective CCTs for the case of GFM-VSC VSM-PLL-Freeze-CL-CSA with a high damping coefficient $D_{GFM} = 202,61pu$ and with a low damping coefficient $D_{GFM} = 1pu$. The second experiment will go to a more simple case of GFM-VSC VSM-PLL-Freeze-NoCL to explore and understand the effects of changing the damping coefficient D_{GFM}. The high damping coefficient will still be $D_{GFM} = 202,61pu$, and the low one $D_{GFM} = 20pu$. It is important to note that the cases with low damping, due to this feature, the variables will be oscillatory, and the cases where synchronism is lost is when the angles either increase suddenly and indefinitely or, if the oscillations become greater after each period. In this chapter, angle stability under small disturbances also plays a role, but it will not be analysed, as it is not the goal of this bachelor thesis.

5.3.1 Effect of damping with CL & CSA

The case of $D_{GFM} = 202,61pu$ is the same as the case presented in the last chapter, including the feature of the frozen PLL when the fault is still active. Therefore, to maintain coherence, in this section, two different fault clearing times will be shown, and these will be examples of a short and a long fault clearing times for comparison to determine the effect the damping coefficient has on the transient stability of the GFM-VSC power converter compared to the highly damped clearing times of 800ms and 1500ms. The short and long faults for the cases with low damping coefficient will be 100ms and 300ms. Also the CCTs of both examples will be compared to test the hypothesis that states that a high damping coefficient has a positive effect for the GFM-VSC power converter's transient stability.

Similarly to the previous chapters, first some variables will be shown of each clearing time individually, to then compare them together, and be able to analyse correctly the effect of damping. Due to the oscillations, the figures will be very different to the highly damped figures.

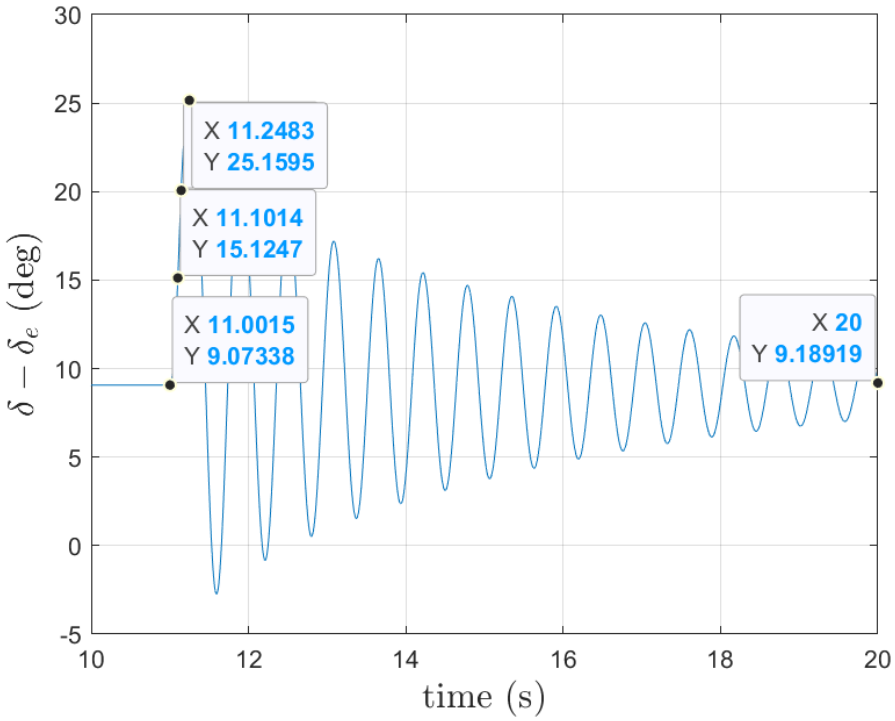

Figure 5.2: δ-t curve for a clearing time of 100ms with $D_{GFM} = 20pu$ and CL-CSA

Figures 5.2 & 5.5 show how the angle behaves. The case of the first one shows an oscillation around the initial value (δ_0), that is continuously damped,

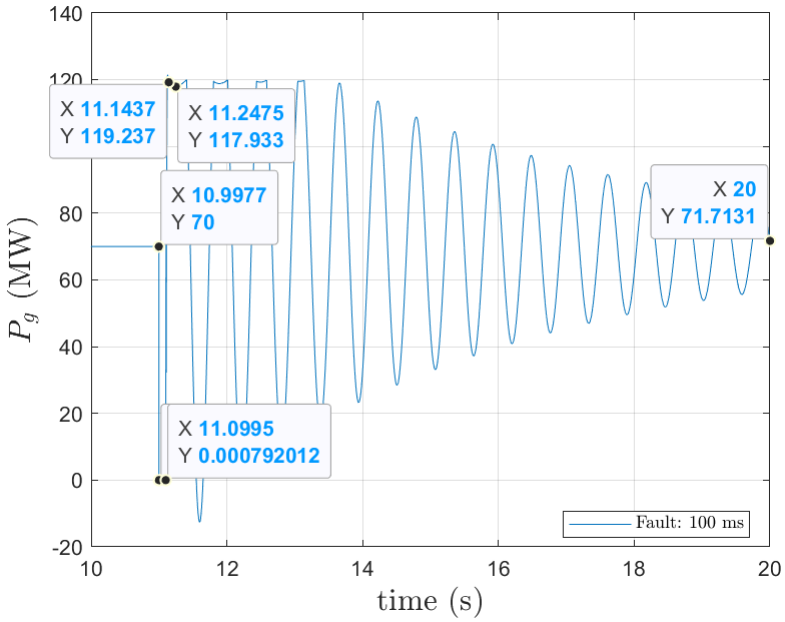

Figure 5.3: P-t curve for a clearing time of 100ms with $D_{GFM} = 20pu$ and CL-CSA

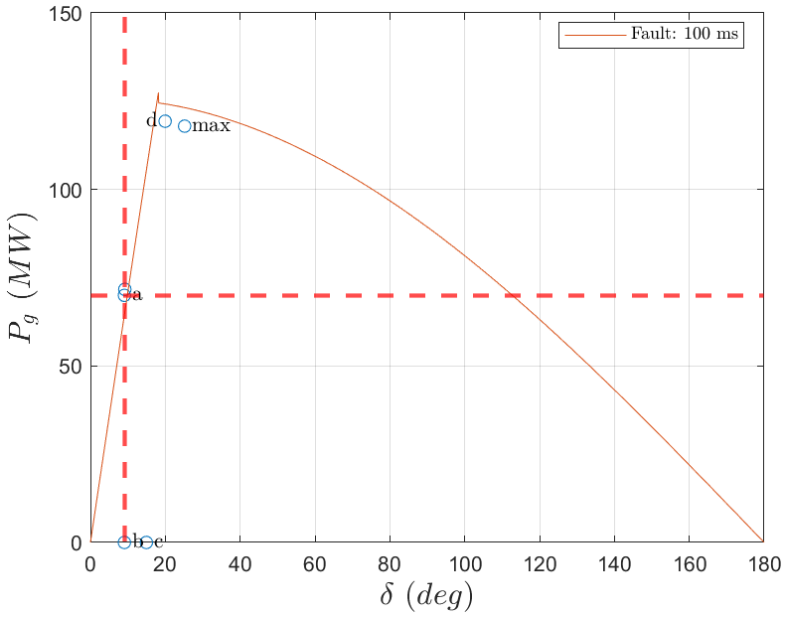

Figure 5.4: P-δ curve for a clearing time of 100ms with $D_{GFM} = 20pu$ and CL-CSA

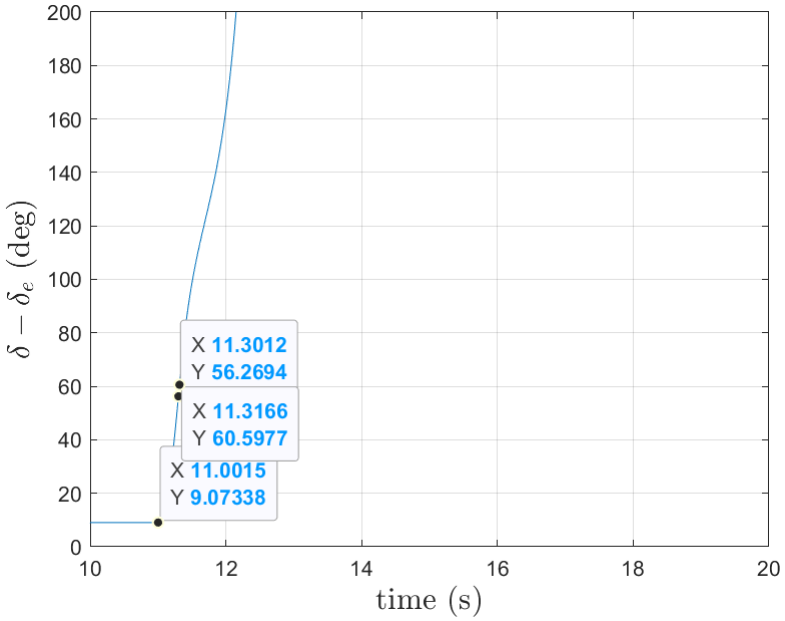

Figure 5.5: δ-t curve for a clearing time of 300ms with $D_{GFM} = 20pu$ and CL-CSA

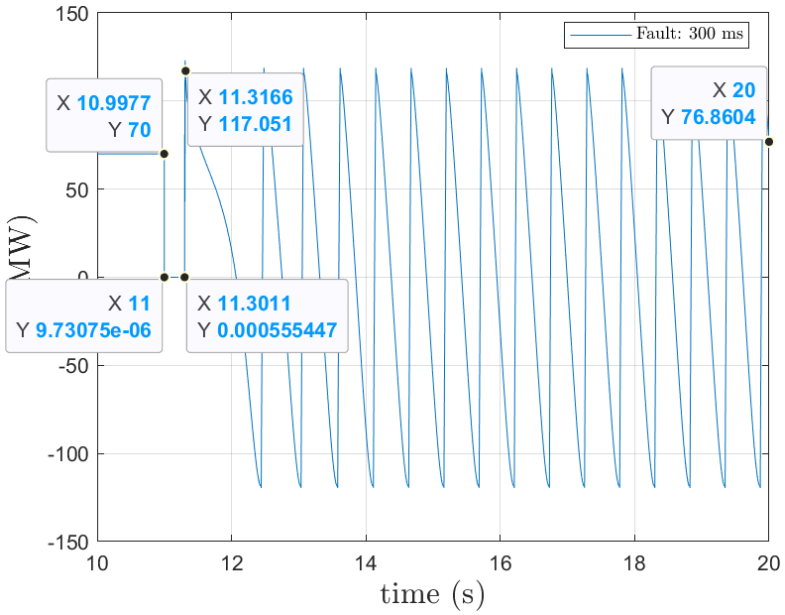

Figure 5.6: P-t curve for a clearing time of 300ms with $D_{GFM} = 20pu$ and CL-CSA

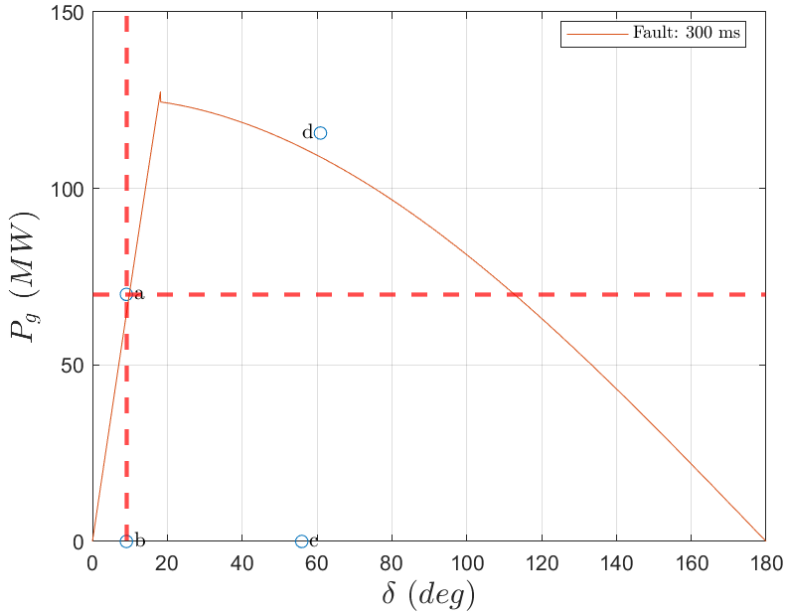

Figure 5.7: P-δ curve for a clearing time of 300ms with $D_{GFM} = 20pu$ and CL-CSA

and, finally in steady state, tends to δ_0, and therefore, synchronism is regained. In the case of the second figure, synchronism is lost as soon as the fault is cleared, the angle increases greatly, and never stops (in reality protections would act to stop this from happening). I this steep increase, some small oscillations can be observed due to the low damping coefficient. The power curve shown in figure 5.3 shows another damped oscillation that starts once the fault is cleared, and returns to P_{g0} in steady state. Here, the power limit can also be observed, as in the first oscillations, the top of the sine curve is cut at a constant value. Figure 5.6 shows a completely different case, as it no longer is as sinusoidal, and is no longer damped. It looks more like a "saw teeth" shape that revolves around a minimum value of 0 MW. This is another clear sign of loss of synchronism. Finally, figures 5.4 & 5.7 show the P-δ curves. Even though the P-t and δ-t curves are not similar to the ones with higher damping, the P-δ curves is similar, and can be used similarly to see if synchronism is lost or not. In the first case, the point of maximum angle max) appears in the curve. This indicates that the GFM-VSC power converter is able to decelerate and return the angle to δ_0. In the case of the fault cleared in 300ms, the same thing cannot be said, as, when the fault is cleared, the angle (δ_d) is too big for the converter to be able to regain synchronism.

As the δ-t curves have been somewhat explained already, figure 5.8 will be explained quickly. In this figure, it is clear that only the faults cleared in 800ms

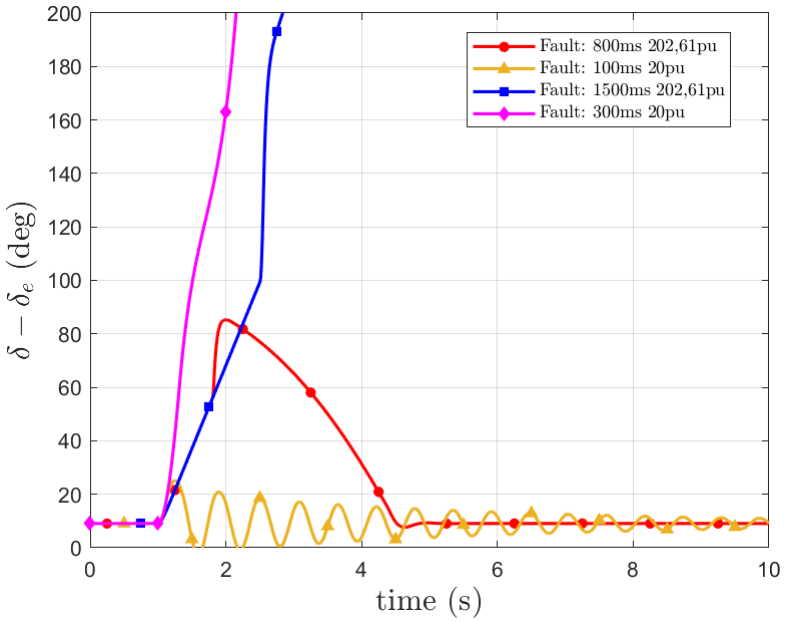

Figure 5.8: δ-t curves for $D_{GFM} = 20pu$ vs $D_{GFM} = 202,61pu$ with CL-CSA

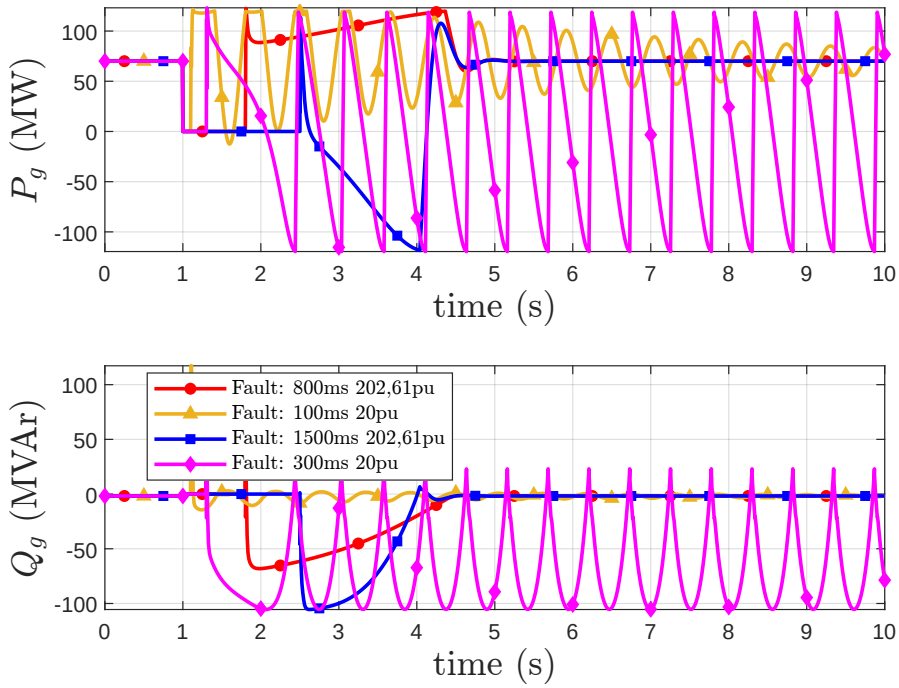

Figure 5.9: P_g & Q_g-t curves for $D_{GFM} = 20pu$ vs $D_{GFM} = 202,61pu$ with CL-CSA

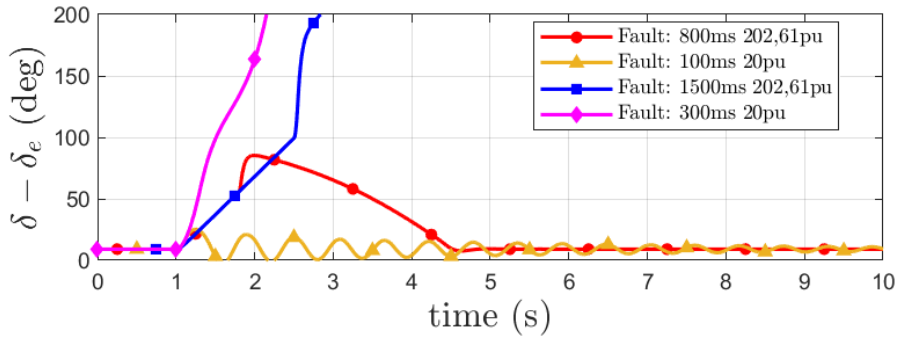

Figure 5.10: ω-t curves for $D_{GFM} = 20pu$ vs $D_{GFM} = 202,61pu$ with CL-CSA

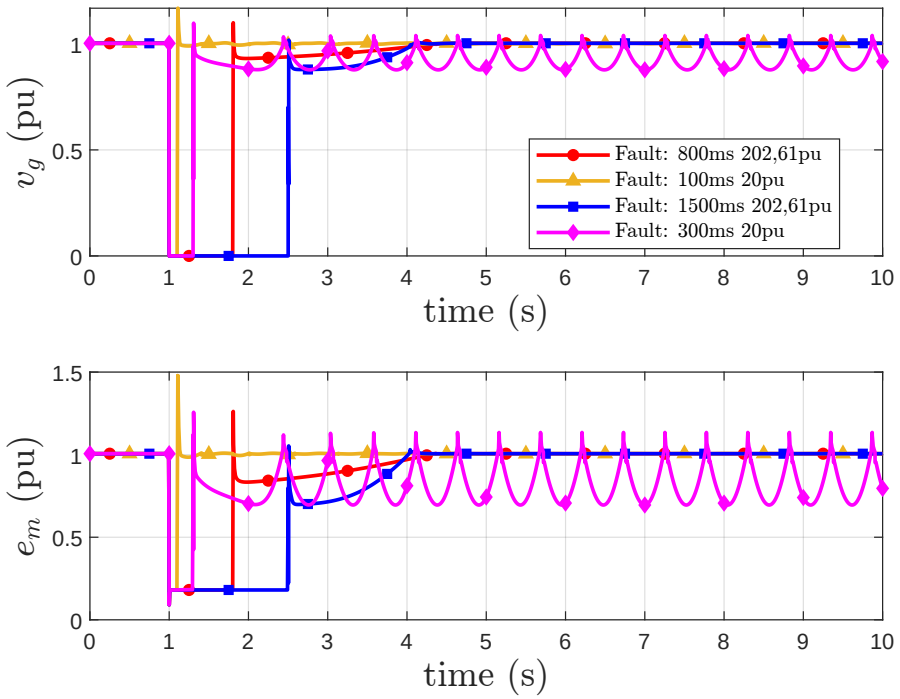

Figure 5.11: v_g & e_m-t curves for $D_{GFM} = 20pu$ vs $D_{GFM} = 202,61pu$ with CL-CSA

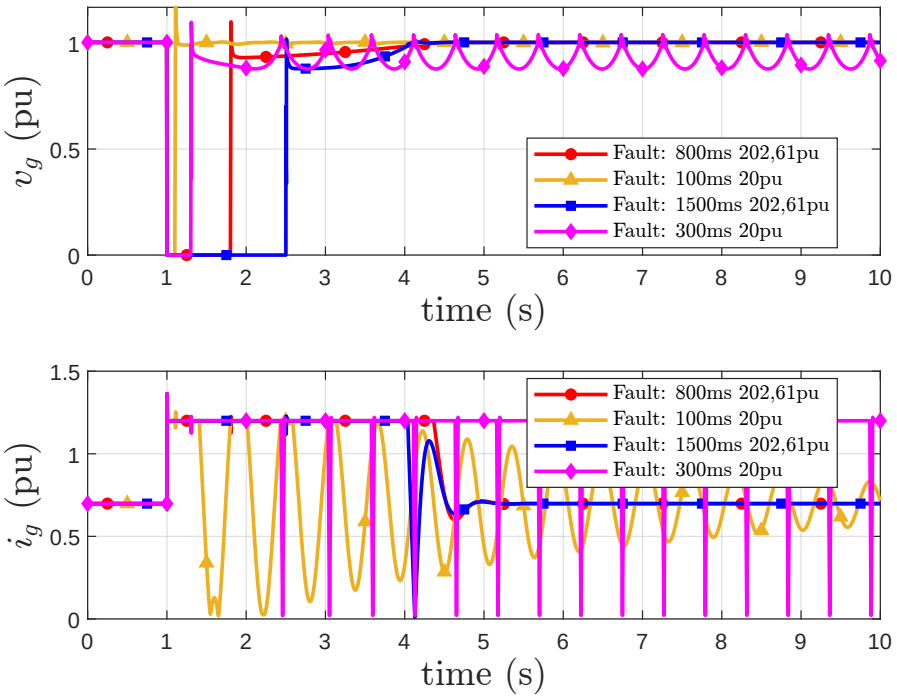

Figure 5.12: v_g & i_g-t curves for $D_{GFM} = 20pu$ vs $D_{GFM} = 202,61pu$ with CL-CSA

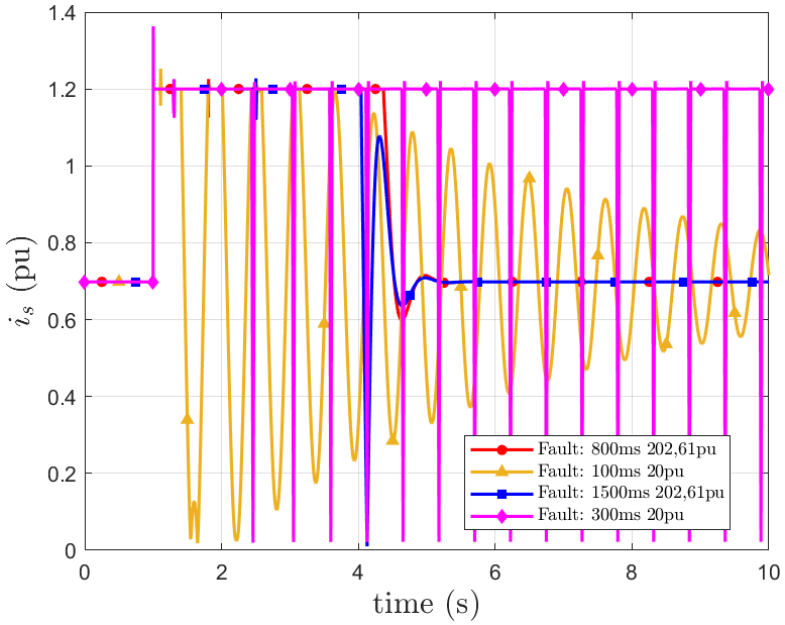

Figure 5.13: i_s-t curves for $D_{GFM} = 20pu$ vs $D_{GFM} = 202,61pu$ with CL-CSA

($D_{GFM} = 202,61pu$) and in 100ms ($D_{GFM} = 20pu$) are able to regain synchronism. Evidently, due to its duration, the second case reaches an average of δ_0 before. The other two faults lose synchronism, and the case of the fault cleared in 300ms ($D_{GFM} = 20pu$), the GFM-VSC accelerates quicker than in the case of the fault cleared in 1500ms ($D_{GFM} = 202,61pu$). Then, figure 5.9 shows the power curves along time. The cases of low damping behave completely differently to the cases with a high damping coefficient. The active power curves have already been discussed previously, but the reactive power curves have not. In both cases (long & short clearing times for low damping), Q_g has an oscillatory behaviour, but, for the short clearing time, it revolves around 0 Mvar with a more sinusoidal shape. For the long clearing time, the shape has more spikes, and has a mean value very much below 0 Mvar. This means the GFM-VSC power converter receives Q from the grid. Figure 5.10 shows the frequency of the GFM-VSC power converter in each case. Both cases of low damping have oscillatory behaviour again. This makes sense, due to the P_g's behaviour, which is also oscillatory. Anyway, the fault with the longer clearing time (300ms), has a steep acceleration, whilst the shorter one just revolves around 50Hz. The behaviour of the longer fault after it is cleared makes no sense, as the oscillation is around 52Hz, and this would never happen. Figure 5.11 shows the comparison of the highly damped and the less damped cases. This comparison makes more sense, as in this case, the behaviour is very similar.

In all curves, the voltages fall when the faults occur, and once they are cleared, they have a peak, which then falls (this makes sense, as there is a positive peak in Q_g to lower the voltage). Also, in synch with the reactive power curve along time, the GFM-VSC power converter wants to have $e_m = v_g = 1pu$, and, as they have an average value below 1pu (in the case of $D_{GFM} = 20pu$), the grid injects Q_g in average. The oscillations of the fault that is cleared in a longer time are not damped, as in Q_g. Figures 5.12 & 5.13 show the current injected to the grid (the first figure also includes v_g for comparison). Again, visual comparison with the cases with a high damping is useful, as the shapes are similar. The fault cleared in less time shows an oscillatory behaviour once the fault is cleared, with a limit of 1,2 pu (the limit imposed by the CSA), that tends to i_{g0}. The longer one remains at the maximum value of 1,2 pu, with sudden peaks every time the converter injects power into the grid.

5.3.2 Effect of damping with No CL

In a similar way to the previous section, short and long fault clearing times will be simulated (again 800ms & 2000ms), to observe the effect the damping coefficient has on transient stability in a more simple model (without the CL & CSA). This time, the EAC CCT calculated is different, as the P-δ curve is not the same. Also, the simulated CCTs will be compared between each other, and finally to the EAC CCT.

As in the previous section (and of course, as in the previous chapters), first the important variables will be shown of each clearing time individually, to then compare them together, and be able to analyse correctly the effect of damping when there is no CL or CSA. Again, the order will be by clearing time rather than by damping coefficient characteristic.

As this is the first case where there is no CL, first, the case of $D_{GFM} = 202,61pu$ examples will be shown. The fault clearing times shown will be those of 800ms & 3000ms for a short and a long clearing times. Then, for the case of $D_{GFM} = 20pu$, clearing times of 500ms & 600ms will be simulated.

Figures 5.14 & 5.17 show the δ-t curves for the highly damped examples for a short and a long clearing time (800ms & 3000ms respectively). This is similar to the curves with CL-CSA, as the moment the fault is cleared is where there is a change in gradient, and, if synchronism is regained, the angle returns to δ_0. The power curves shown in figures 5.15 & 5.18 have a higher peak once the fault is cleared with respect to the curves with CL-CSA, as there is no current limit. In this case, when synchronism is lost, the angle gets so large that, power is injected into the GFM-VSC power converter. This is explained by the location of c) and d) in figure 5.19 (they are in the next part of the curve, where power injected into the grid would be negative). Figure 5.16 shows the P-δ curve of the shortly cleared

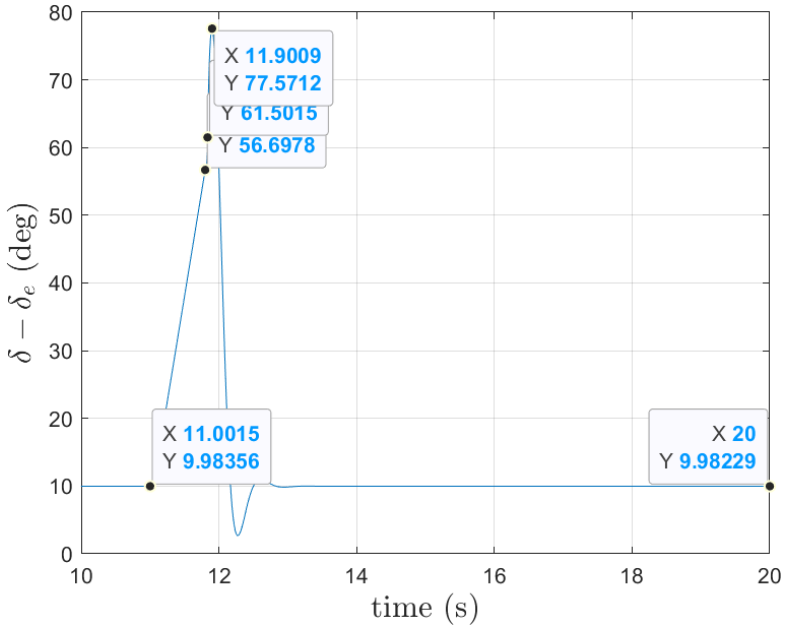

Figure 5.14: δ-t curve for a clearing time of 800ms with $D_{GFM} = 202,61pu$ and No CL

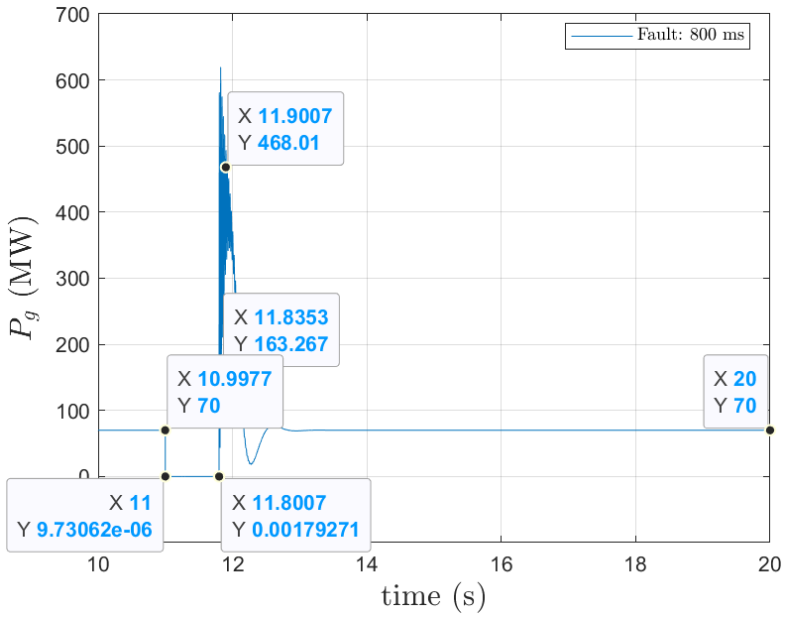

Figure 5.15: P-t curve for a clearing time of 800ms with $D_{GFM} = 202,61pu$ and No CL

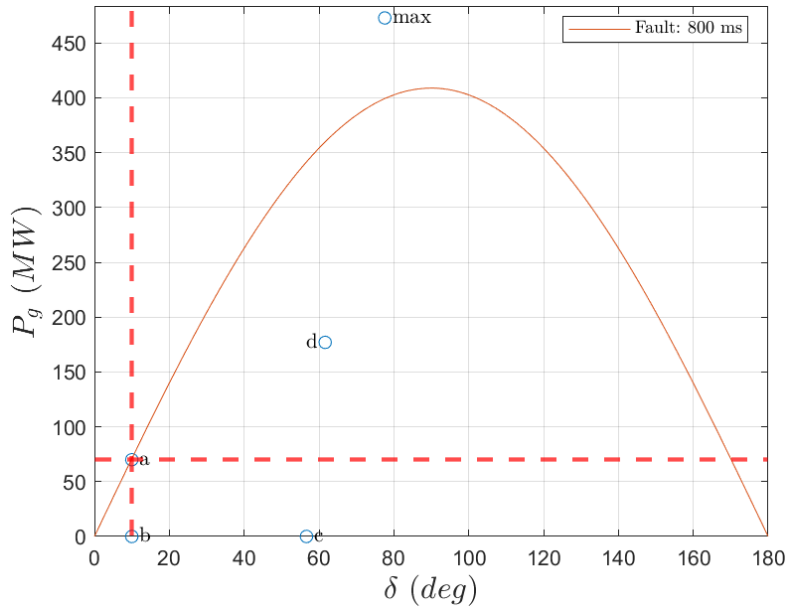

Figure 5.16: P-δ curve for a clearing time of 800ms with $D_{GFM} = 202,61pu$ and No CL

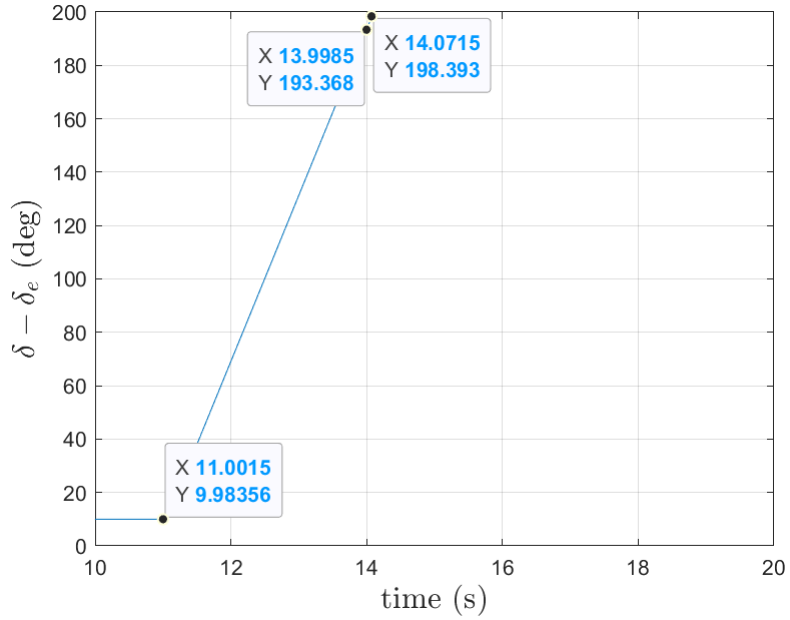

Figure 5.17: δ-t curve for a clearing time of 3000ms with $D_{GFM} = 202,61pu$ and No CL

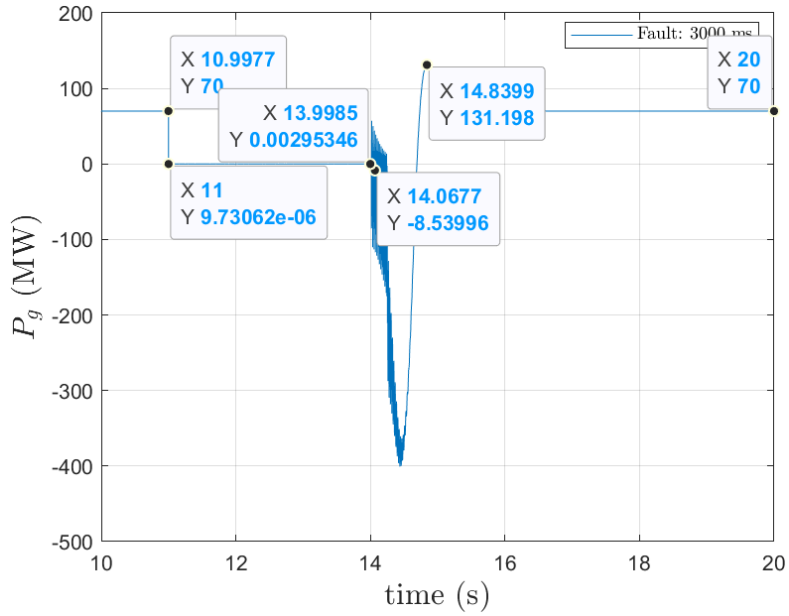

Figure 5.18: P-t curve for a clearing time of 3000ms with $D_{GFM} = 202,61pu$ and No CL

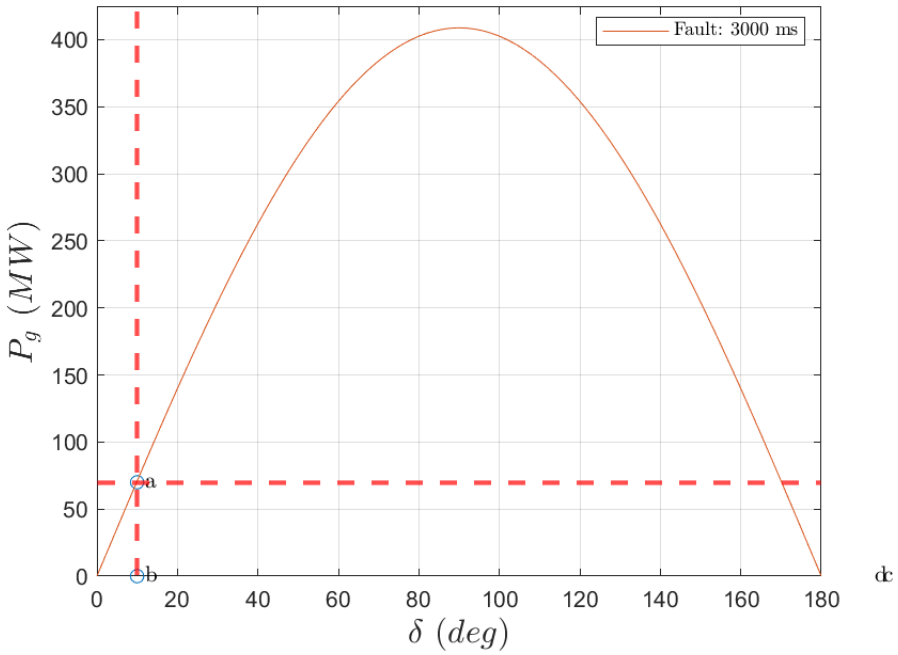

Figure 5.19: P-δ curve for a clearing time of 3000ms with $D_{GFM} = 202,61pu$ and No CL

fault. The location of the points is not directly in the curve due to the values of v_g & e_m, which are not exactly 1pu in those moments. This will be seen and discussed later, when the graphs are shown.

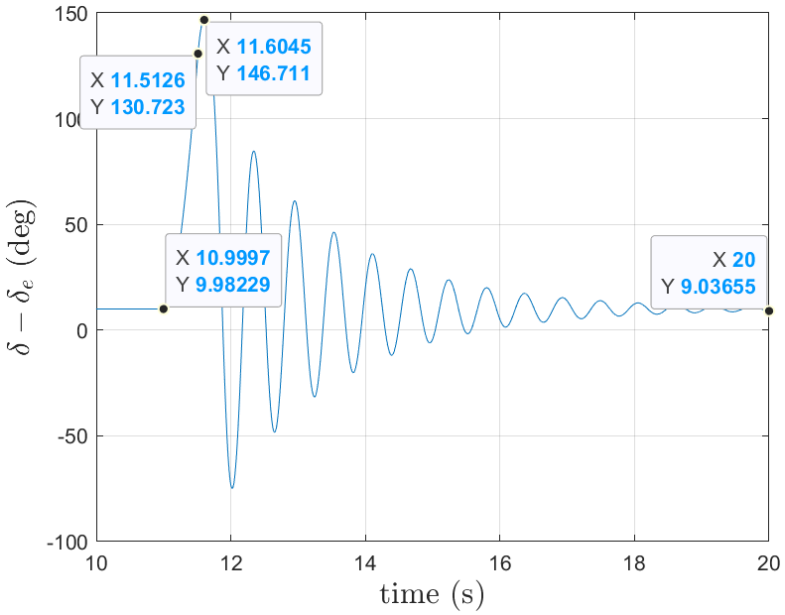

Figure 5.20: δ-t curve for a clearing time of 500ms with $D_{GFM} = 20pu$ and No CL

Figures 5.20 & 5.23 show the δ-t curves for the examples with No CL and $D_{GFM} = 20pu$. Before the fault is cleared, the curves are very similar to the ones with a higher damping, but once they are cleared, as in the case of the ones with low damping and CL-CSA, they oscillate. In the case of the shortly cleared fault (500ms), the mean value is δ_0, and in the case of the fault cleared in a longer time (600ms), the mean and final value is $360° + \delta_0$. This is a clear case of loss of synchronism, different to the one in the previous section, where the angle grew indefinitely. Again, the P_g-t curves shown in figures 5.21 & 5.24 have a similar behaviour to the ones with a higher damping before the fault is cleared, but once they are cleared, as in the case of the ones with low damping and CL-CSA, they oscillate. In this case, the oscillations both in the δ-t & P_g-t curves are damped. The P-δ curves shown in figures 5.22 & 5.25 again show a case of loss and no loss of synchronism. The behaviour, again is similar. As mentioned before, the points do not fall perfectly on the curves, as will be seen later v_g & e_m are not exactly 1pu during the full transitory.

Figure 5.26 shows the δ-t curves of the distinct clearing time durations of the cases of No CL for the higher and lower damping coefficients. As they have been

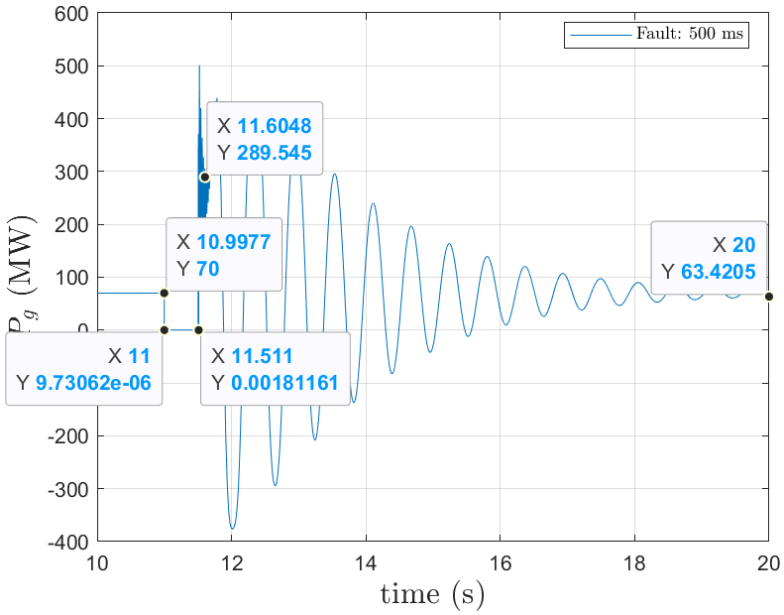

Figure 5.21: P-t curve for a clearing time of 500ms with $D_{GFM} = 20pu$ and No CL

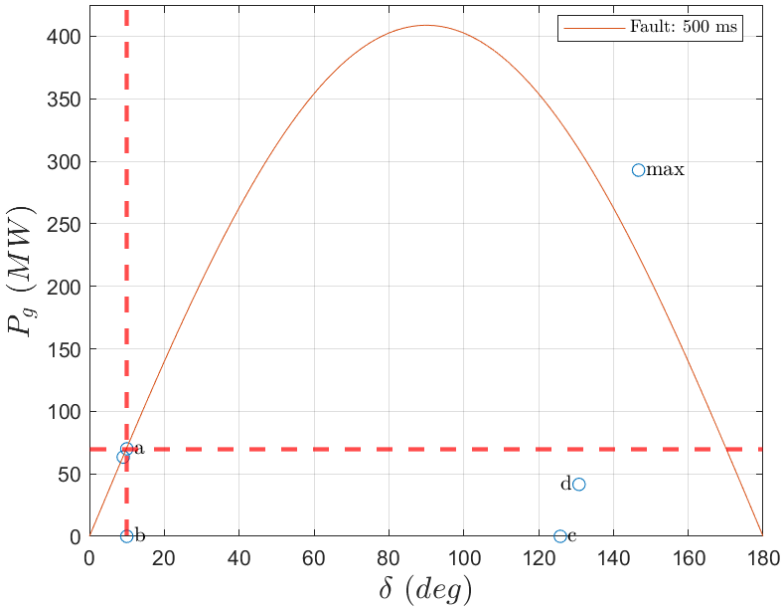

Figure 5.22: P-δ curve for a clearing time of 500ms with $D_{GFM} = 20pu$ and No CL

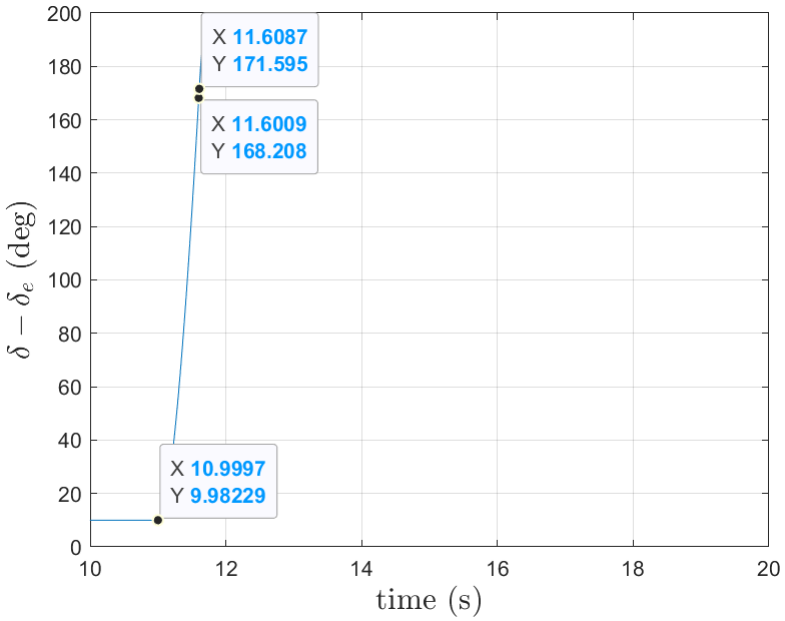

Figure 5.23: δ-t curve for a clearing time of 600ms with $D_{GFM} = 20pu$ and No CL

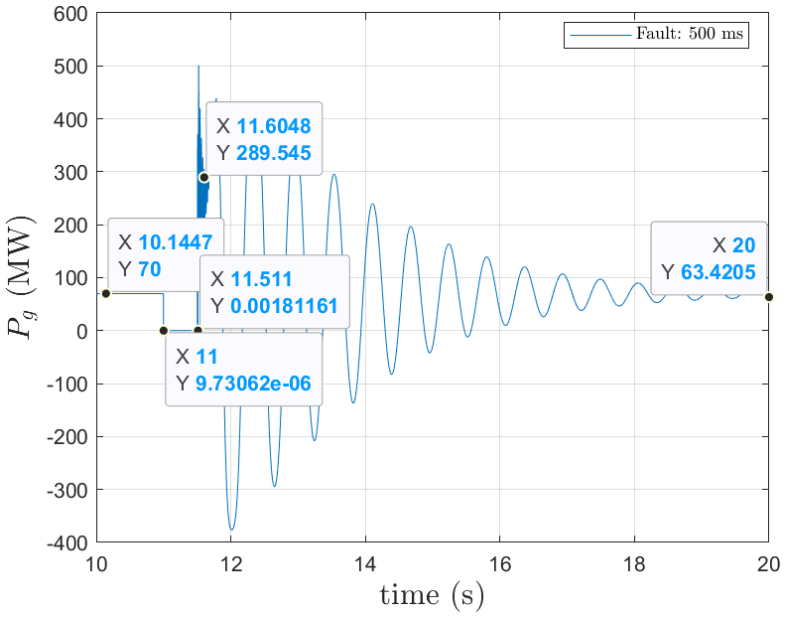

Figure 5.24: P-t curve for a clearing time of 600ms with $D_{GFM} = 20pu$ and No CL

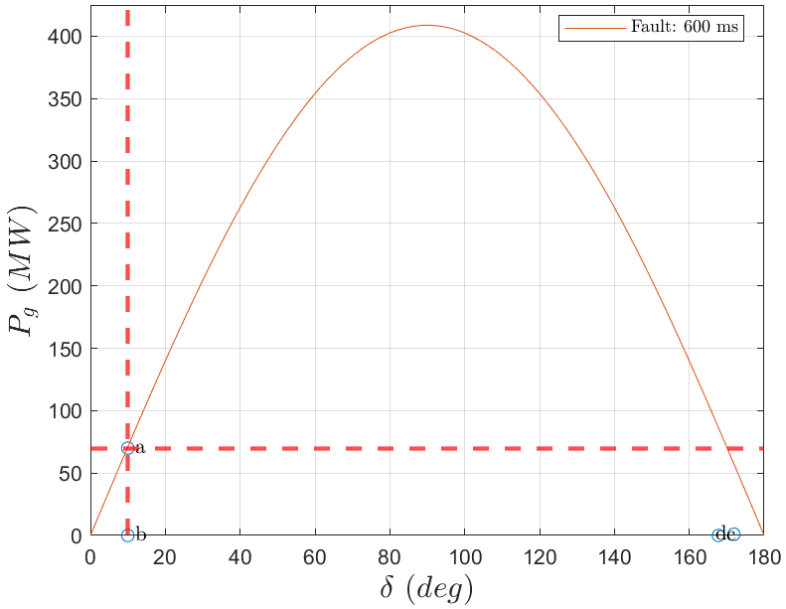

Figure 5.25: P-δ curve for a clearing time of 600ms with $D_{GFM} = 20pu$ and No CL

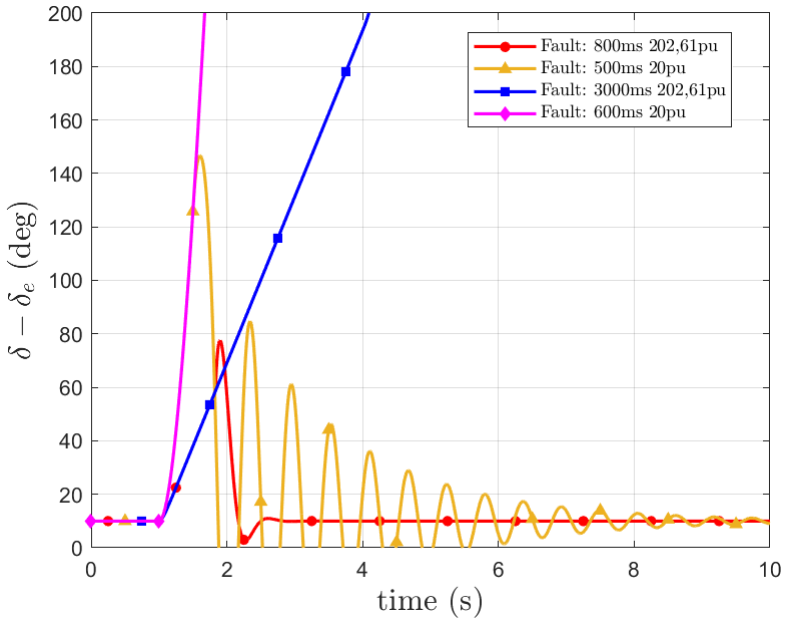

Figure 5.26: δ-t curves for $D_{GFM} = 20pu$ vs $D_{GFM} = 202,61pu$ No CL

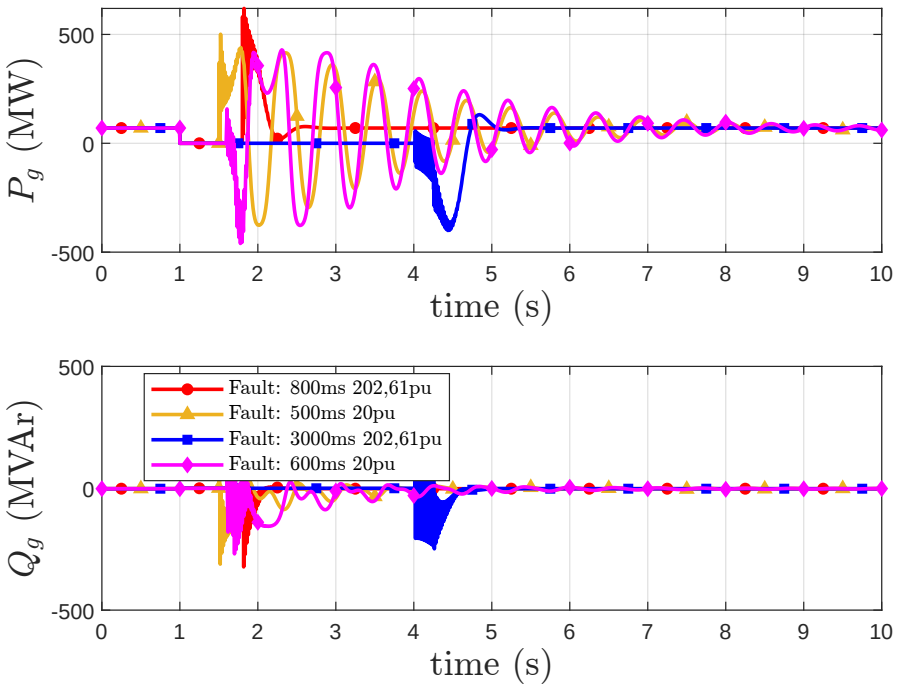

Figure 5.27: P_g & Q_g-t curves for $D_{GFM} = 20pu$ vs $D_{GFM} = 202,61pu$ No CL

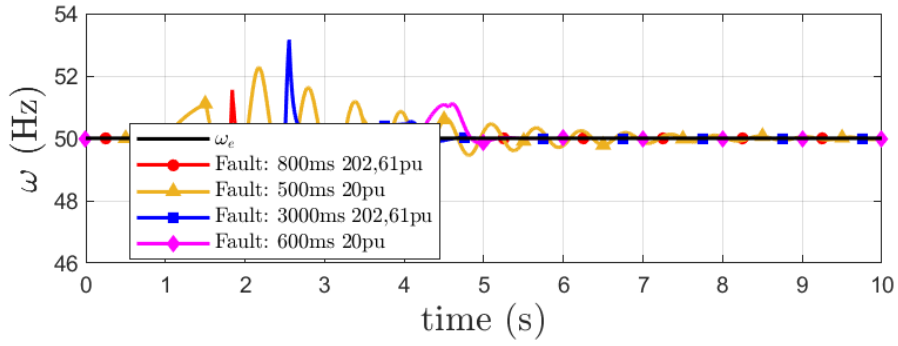

Figure 5.28: ω-t curves for $D_{GFM} = 20pu$ vs $D_{GFM} = 202,61pu$ No CL

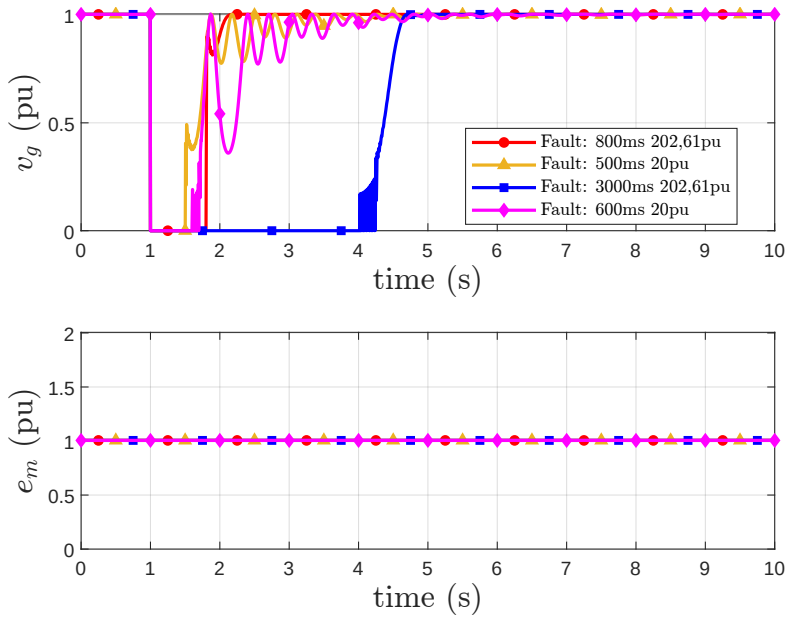

Figure 5.29: v_g & e_m-t curves for $D_{GFM} = 20pu$ vs $D_{GFM} = 202,61pu$ No CL

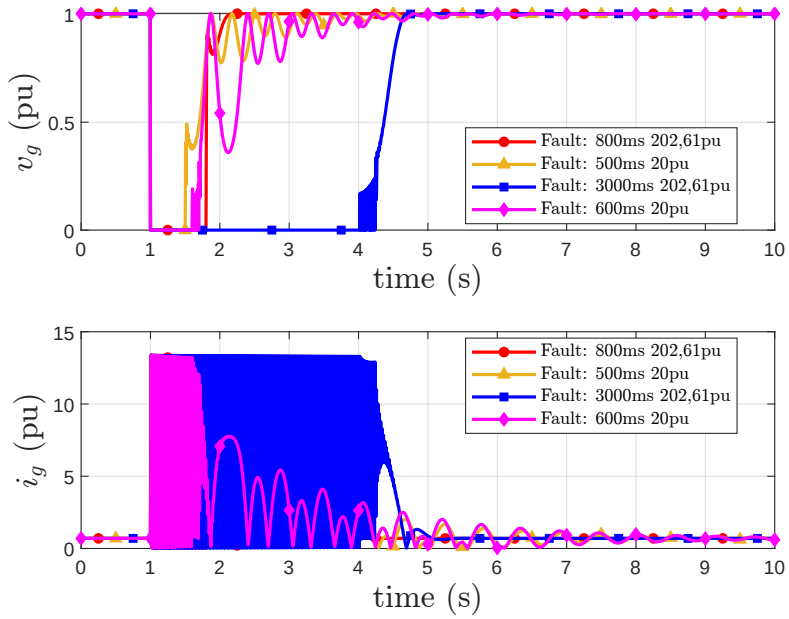

Figure 5.30: v_g & i_g-t curves for $D_{GFM} = 20pu$ vs $D_{GFM} = 202,61pu$ No CL

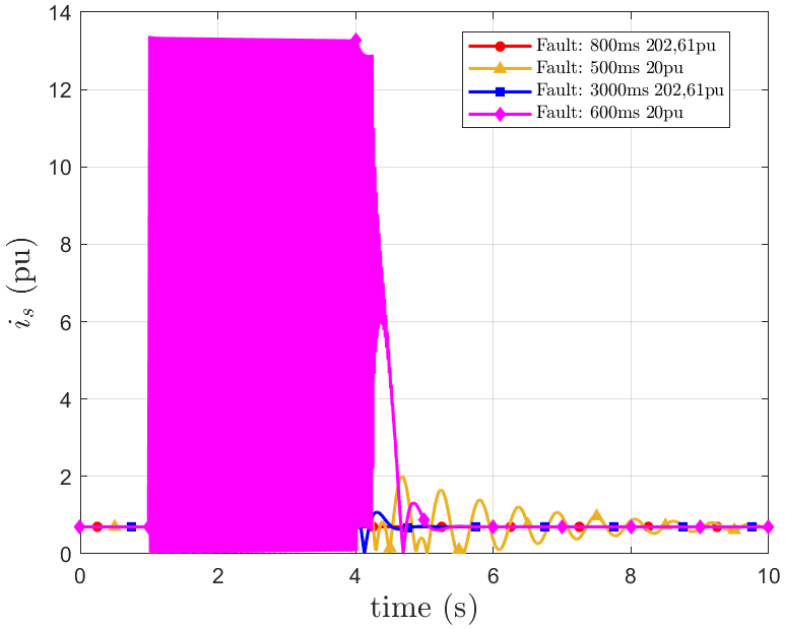

Figure 5.31: i_s-t curves for $D_{GFM} = 20pu$ vs $D_{GFM} = 202,61pu$ No CL

discussed above, this figure will be left for visual comparison. The same applies for the P_g-t curves in figure 5.27. In the case of Q_g, the highly damped cases reach steady state easily, and, the cases with lower damping oscillate for a longer time before reaching steady state. Figure 5.28 shows the frequency of each case. As expected, the cases with high damping follow similar shapes as the ones shown previously, and the cases with less damping oscillate around 50Hz. The voltage curves v_g & e_m-t shown in figure 5.29 show that, as expected, for the low damped examples, v_g oscillates greatly before reaching steady state. This is compatible with the shape of Q_g. Figures 5.30 & 5.31 both show i_g. The ones with high damping will not be deeply analysed, as they follow a similar shape as the ones shown previously, with the difference that there is no limit. The short clearing time with low damping's current oscillates around the final value until it reaches it. Finally, in the case where synchronism is lost, there are heavy fluctuations in the current, reaching values of over 13pu. Then it steadies to the final value.

5.4 CCT calculation and comparison

As the EAC already assumes a negligible damping effect, the critical angle obtained via the EAC does not depend on D_{GFM}, and is the same for the high and low damping coefficients. This also means, the CCT obtained via the equation

that states the relationship $f(\delta_{cl}^{crit}) = CCT$ is the same if the control strategy is the same. The EAC calculated CCT for the cases with CL & CSA is the same one as in both previous chapters amd has a value of: . For the case of the GFM-VSC VSM-PLL-Freeze-NoCL, the critical angle $\delta_{cl}^{crit} = 120,3211°$. From this angle, the CCT obtained is: 1320ms. As mentioned before, as the EAC method assumes $D_{GFM} = 0$, it is expected for the simulated CCTs for the cases with low damping coefficients to be closer to the CCTs obtained via the EAC. In this case, as the GFM-VSC power converter is not identical to a SM, its behaviour with low damping is not the one that was expected. The effect of the oscillations in angle and power cause the system to lose synchronism with shorter clearing times than expected, and therefore, the CCTs are very much smaller to what was expected. The CCTs obtained by simulation for $D_{GFM} = 20pu$, GFM-VSC VSM-PLL-Freeze-CL-CSA & GFM-VSC VSM-PLL-Freeze-NoCL are 270ms and 530ms respectively. Table 5.1 shows a summary of the CCTs obtained until this point. This is the final table of the thesis and includes all of the cases and examples discussed in this bachelor thesis.

Table 5.1: CCT table GFM-VSC VSM-PLL-Freeze effect of damping coefficient

Case	Method used to obtain	CCT (ms)
GFM-VSC VSM-PLL-CL-CSA $D_{GFM} = 202,61pu$	EAC	690
GFM-VSC VSM-PLL-CL-CSA $D_{GFM} = 202,61pu$	CCT algorithm	1620
GFM-VSC VSM-PLL-Freeze-CL-CSA $D_{GFM} = 202,61pu$	CCT algorithm	970
GFM-VSC VSM-PLL-Freeze-CL-CSA $D_{GFM} = 20pu$	CCT algorithm	270
GFM-VSC VSM-PLL-Freeze-NoCL $D_{GFM} = 202,61pu$	EAC	1320
GFM-VSC VSM-PLL-Freeze-NoCL $D_{GFM} = 202,61pu$	CCT algorithm	2600
GFM-VSC VSM-PLL-Freeze-NoCL $D_{GFM} = 20pu$	CCT algorithm	530

5.5 Summary & Conclusions

In this chapter, the following points have been tackled:

- P-δ curves for cases with no CL
- Fault simulation of different clearing times for GFM-VSC VSM-PLL-Freeze-CL-CSA with low damping ($D_{GFM} = 20pu$)
- Comparison of different fault clearing times to observe the effect of damping in GFM-VSC VSM-PLL-Freeze-CL-CSA ($D_{GFM} = 20pu$ vs $D_{GFM} = 202,61pu$)

- Fault simulation of different clearing times for GFM-VSC VSM-PLL-Freeze-NoCL with high damping ($D_{GFM} = 202,61pu$)
- Fault simulation of different clearing times for GFM-VSC VSM-PLL-Freeze-NoCL with low damping ($D_{GFM} = 20pu$)
- Comparison of different fault clearing times to observe the effect of damping in GFM-VSC VSM-PLL-Freeze-NoCL ($D_{GFM} = 20pu$ vs $D_{GFM} = 202,61pu$)
- Simulation to obtain the simulated CCT of the GFM-VSC VSM-PLL-Freeze-CL- CSA $D_{GFM} = 20pu$ model and comparison with the simulated CCT of the GFM-VSC VSM-PLL-Freeze- CL-CSA $D_{GFM} = 202,61pu$ model and the CCT obtained via the EAC for CL-CSA
- Simulation to obtain the simulated CCT of the GFM-VSC VSM-PLL-Freeze-NoCL- $D_{GFM} = 202,61pu$ model, the CCT of the GFM-VSC VSM-PLL-Freeze-NoCL- $D_{GFM} = 20pu$ model and calculation of the CCT obtained via the EAC for no CL.

The following conclusions have been reached:

- The CCTs obtained via simulation for the models with low damping ($D_{GFM} = 20pu$) are lower than the CCTs obtained via the EAC, and not similar, as would have been expected
- The points do not fall directly as expected in the P-δ curves (less so in the case with no CL)
- This means it is not a good estimation for these cases
- The EAC is not directly applicable, as the behaviour of GFM-VSC power converters, even if it tries to emulate the behaviour of SM, is not the same.

Chapter 6

Conclusions

6.1 General conclusions

In this final chapter, the summaries and conclusions reached in each chapter will be presented and developed individually and then presented and summarised in a general conclusion.

6.1.1 Model without the frozen PLL

With respect to this point the following ideas have been developed:

- Introduction of the model and scheme of the GFM-VSC power converter connected to an infinite grid. The model used is GFM-VSC PLL-CL-CSA with $D_{GFM} = 202,61pu$
- Introduction of the important variables and how they will be represented and analysed
- How EAC can be applied, how it works with CL-CSA
- A series of simulations of different fault clearing times and representation of the variables with comparison between the different clearing times simulated
- Calculation of the CCT via the EAC and the simulation of the CCT for the case GFM-VSC PLL-CL-CSA with $D_{GFM} = 202,61pu$

From these ideas, the following conclusions have been reached:

- The strange behaviour of the PLL causes the angle difference between the GFM-VSC power converter and the grid (δ) to have a different shape to expected before the fault is cleared

- The simulated CCT for the GFM-VSC PLL-CL-CSA model is much greater than the CCT obtained via the EAC

6.1.2 Effect of the frozen PLL

With respect to this point the following ideas have been developed:

- Introduction of the block diagram of the PLL used
- Design of the GFM-VSC PLL-Freeze-CL-CSA model
- A series of simulations for the new model of different fault clearing times and representation of the variables with comparison between the different clearing times and the clearing times simulated in the previous chapter
- Simulation to obtain the simulated CCT of the GFM-VSC PLL-Freeze-CL-CSA model and comparison with the simulated CCT of the GFM-VSC PLL-CL-CSA model (both with $D_{GFM} = 202,61pu$ and the CCT obtained via the EAC.

From these ideas, the following conclusions have been reached:

- The frozen feature introduced into the PLL does help the angle difference between the GFM-VSC power converter and the grid develop normally
- This feature does not affect any other variable besides the angle difference (and therefore the GFM-VSC power converter's frequency)
- The strange behaviour in the PLL before the frozen feature was introduced into the PLL makes the model have a larger CCT
- The CCT of the GFM-VSC PLL-Freeze-CL-CSA is closer to the CCT obtained via the EAC, but still higher

6.1.3 Effect of damping

With respect to this point the following ideas have been developed:

- P-δ curves for cases with no CL
- Fault simulation of different clearing times for GFM-VSC PLL-Freeze-CL-CSA with low damping ($D_{GFM} = 20pu$)
- Comparison of different fault clearing times to observe the effect of damping in GFM-VSC PLL-Freeze-CL-CSA ($D_{GFM} = 20pu$ vs $D_{GFM} = 202,61pu$)

- Fault simulation of different clearing times for GFM-VSC PLL-Freeze-NoCL with high damping ($D_{GFM} = 202,61pu$)
- Fault simulation of different clearing times for GFM-VSC PLL-Freeze-NoCL with low damping ($D_{GFM} = 20pu$)
- Comparison of different fault clearing times to observe the effect of damping in GFM-VSC PLL-Freeze-NoCL ($D_{GFM} = 20pu$ vs $D_{GFM} = 202,61pu$)
- Simulation to obtain the simulated CCT of the GFM-VSC PLL-Freeze-CL-CSA $D_{GFM} = 20pu$ model and comparison with the simulated CCT of the GFM-VSC PLL-Freeze- CL-CSA $D_{GFM} = 202,61pu$ model and the CCT obtained via the EAC for CL-CSA
- Simulation to obtain the simulated CCT of the GFM-VSC PLL-Freeze-NoCL- $D_{GFM} = 202,61pu$ model, the CCT of the GFM-VSC PLL-Freeze-NoCL- $D_{GFM} = 20pu$ model and calculation of the CCT obtained via the EAC for no CL.

From these ideas, the following conclusions have been reached:

- The CCTs obtained via simulation for the models with low damping ($D_{GFM} = 20pu$) are lower than the CCTs obtained via the EAC, and not similar, as would have been expected
- The points do not fall directly as expected in the P-δ curves (less so in the case with no CL)
- This means it is not a good estimation for these cases
- The EAC is not directly applicable, as the behaviour of GFM-VSC power converters, even if it tries to emulate the behaviour of SM, is not the same.

6.1.4 Final conclusions

To sum up, general conclusions obtained in this bachelor thesis can be summarized as follows:

- Transient stability (angle stability under large disturbances) is also present in grid-forming power converters (GFM-VSC).
- Equal Area Criterion (EAC), a theoretical method often used to assess transient stability margin in synchronous machines, cannot be applied directly to assess transient stability in GFM-VSCs, mainly due to the fact that GFM-VSCs have a high damping coefficient.

- This work has analyzed GFM-VSC control strategies based on VSM-PLL scheme; and this work has investigated the use of a freezing strategy in the PLL during faults (frozen PLL, for short). This scheme allows to understand better transient stability behaviour of GFM-VSCs.

6.2 Future work

The EAC, one of the best methods to determine the CCT of a system (for all types of generators), works best when applied to cases with a low damping coefficient, as one of the assumptions of this method is that the damping coefficient's term in the swing equation is negligible compared to the other terms of the equation. In this bachelor thesis, the applicability of the EAC for GFM-VSC power converters has been studied, with various cases.

One of the advantages of GFM-VSC power converters is that, the damping coefficient D_{GFM} can be designed with a high value (in the case of this thesis to a value of $D_{GFM} = 202,61pu$) for better transient stability. Also, due to the PLL estimation of frequency, when a fault occurs, the frequency of the GFM-VSC power converter sometimes falls unexpectedly below the nominal frequency, when it is expected to accelerate well over it. Even if these features or behaviours show a positive behaviour of the GFM-VSC power converter, it means the EAC is not applicable and the CCT obtained by it is considered not useful, as it can differ greatly, and can mean an overly safe calculation (as it is much lower than the real simulated CCT).

A line of possible future work could be the development of a similar method to the EAC to calculate the CCT via an empirical method so long simulations could be avoided.

Another possible line of future work could be to understand the reason for which the PLL estimates a frequency below the nominal frequency when a fault occurs, and figure out if it applies always, as it is a great behaviour for transient stability.

Other lines of work that could be useful for the full understanding of GFM-VSC power converters could be the study of other phenomena of stability such as resonance stability, voltage stability, frequency stability, or staying inside angle stability, and studying small disturbance angle stability within GFM-VSC power converters.

Appendix A

Economic analysis

An economic analysis is not the focus of this bachelor thesis, but an exploration of the possible ways the energy sector could receive economic benefits from the insertion of GFM-VSC converters could be useful. This bachelor thesis has the intention of analysing an important behaviour of GFM-VSC power converters when faults occur, and tries to make their implementation a little bit easier, so the economic analysis will not be directly of this project, but it will assess the economic benefits of adding GFM-VSC power converters once their behaviour is fully known and it is viable to insert them into a power system. As this chapter is not meant to be a crucial part of this work, and will not be included as part of the final conclusions, the analysis will be purely qualitative.

Moreover, this analysis will not dive deeply into the economic benefits that the use of some of the models and control techniques seen in this bachelor thesis can cause, as they may be too specific to be applied in the future at a great scale. This economic analysis will give a general overview of how having an energy system with a higher amount of GFM-VSC power converters can be beneficial to the economy.

First of all, it is obvious that GFM-VSC power converters connected to sources of energy such as photovoltaic power plants are less harmful to the environment than other sources of energy such as combined cycle power plants, and eventhough, this is not directly related to money, the environment is a precious good and should be taken care of and taken more into account.

Following the previous point, many countries in the world are making their systems more reliant on renewable energy sources, some of which follow a strategy control of GFL. If these systems are too reliant on energy sources that do not give enough support to the grid (as is the case of generators with GFL strategies), the system becomes very sensitive to faults, and full systems may even collapse when they should not. This can be a great problem, as if the system is not robust enough, a more systematic renewal of materials would be needed, and more maintenance of the machinery and electric instruments would be required.

In cases that are not as extreme as full system blackouts, sometimes the grid operators choose not to use some of the energy given by sources such as photovoltaic or wind powered plants, as the grid could be too fragile to support the energy provided by these sources. This activity is known as "Curtailment". With GFM-VSC power converters, the excess energy "thrown away", that can be considered a cost ceases to exist as curtailment, as now this injection of power is able to support the grid's frequency and voltage. This helps many power plants be idle a smaller amount of time, and therefore is a great economic benefit.

To conclude this chapter, the insertion of GFM-VSC power converters can have a great positive impact economically on any power system, and can simultaneously create the possibility to reach the so-wanted 100% converter based system with great robustness and reliability.

Appendix B

Budget for the replication of the project

As this is a thesis with a focus on the investigation of the Transient Stability Phenomenon in Grid-Forming Power Converters, it is important to include a general budget for a company, organism or investigator to replicate the experiment. This budget will include the cost of the essential materials and the cost of the work, which include the work of engineering and the cost of supervision for the completion of the project. These subdivisions include also the cost of some of the tools required or recommended, and not just the direct cost of having an engineer carrying out the job, or a supervisor checking in on how the project develops. The total duration of the project was of 9 months approximately, starting in November 2025 and stretching until July 2026.

B.1 Material costs

For the completion of the project, a computer is needed, as well as a Matlab+Simulink license and the use of AI (Artificial Intelligence) for help in the development of some of the scripts used for the experiments. In this case the AI license used was Google Gemini. Finally, a Microsoft Office 365 license is also required for use of Microsoft Teams for meetings, and use of the other applications like Microsoft Excel or Microsoft Powerpoint to prepare presentations along the project. All of this is resumed in Table B.1:

Table B.1: Material Costs

Element	Units	Quantity (units)	Unitary Cost (€/unit)	Total Cost (€)
Computer	units	1	1000	1000
Matlab+Simulink License	units	1	500	500
Gemini	months	9	20	180
Office 365 License	months	9	10	90
Total Material Costs	-	-	-	1770

B.2 Labour costs

The labour costs include the work of engineering and the supervision of the project. The work of engineering includes the realisation of the some of the scripts used, the simulations realised, the research dedicated time and the memory writing. It is to note that to complete the project, previous work was already done, including Simulink models, Matlab scripts and some formulation. Therefore, this synthesis of the engineering work represents the expansion of an already existing base project. The supervision of this project was completed by two individuals, and therefore, the amount of hours dedicated to supervision will be doubled, as if one person had been a single supervisor. The work of supervision take into account meetings, time to work on the models and scripts and corrections made in the memory and presentations. Table B.2 resumes the cost of labour of this project:

Table B.2: Labour Costs

Element	Units	Quantity (units)	Unitary Cost (€/h)	Total Cost (€)
Engineering Cost	hours	400	50	20000
Supervision Cost	hours	2x100	100	20000
Total Labour Costs	-	-	-	40000

B.3 Total costs

Table B.3 shows a summary of the total cost to be expected if replicating this experiment:

Table B.3: Labour Costs

Element	Total Cost (€)
Cost of materials	1770
Cost of labour	40000
Total Costs	41770

Appendix C

Bisection Method Algorithm

The algorithm used to determine the simulated CCTs of each case runs a number of simulations until it determines the CCT by a method of trial and error called the Bisection Method. In the case of this thesis, by observing the graph δ-t of each test, the algorithm is able to determine whether or not synchronism is lost in an individual iteration. A positive test represents the case where synchronism is recovered, and a negative one represents the case where the GFM-VSC power converter loses synchronism with the grid. This method needs a chosen initial value. In the first iteration, it runs the test. If it tests positive, it means the CCT is equal or higher to the tested value, so the algorithm tries a higher value for the CCT. If not, it tests a lower value, as the CCT is necessarily lower to the tested clearing time. Depending on the result of the second iteration, again it can try a value outside of the range tested, or if the wanted value is within the range tested, the algorithm tries the midpoint of this range. In this manner, the wanted value is narrowed down, until a same value tests positive twice. This means it is the highest value to test positive, and therefore the CCT. An example of the logic for the running of the algorithm is shown in table C.1 and the CCT for this case is 1620ms. This example represents the case of the GFM-VSC power converter with PLL, no freezing and CL-CSA. The script used to run this algorithm has a tolerance of 5ms. In other words, the values the algorithm works with are rounded to the nearest 10ms, as working in the scale of 1ms would increase the number of iterations greatly without providing any extra quality.

Table C.1: Bisection Method Algorithm

Iteration nº	Fault Clearing Time (ms)	Loss of synchronism? (Y/N)	Bisection (ms)
1	2500	Y	1250
2	1250	N	1880
3	1880	Y	1570
4	1570	N	1730
5	1730	Y	1650
6	1650	Y	1610
7	1610	N	1630
8	1630	Y	1620
9	1620	N	1630
10	1630	Y	1620
11	1620	N	End

Appendix D

P-δ script

This chapter of the appendix includes the code to obtain the graphs for the individual fault clearing time simulations. It creates the following graphs for a chosen clearing time, and automatically labels the points a), b), c), d) & max) mentioned in the bachelor thesis:

- δ-t
- P_g-t
- P-δ

The code is made for Matlab 2022b and is shown in the next figures:

```
close all

j = sqrt(-1);

CL_NoCL = 0; % 1 CL-CSA 0 No CL

t_fault = 0.5; % fault duration

data_CaseA =↙
'data_GFMIB_NoPFR_VSM1_Dvsc202p61_PLLAWU_Freeze_FaultPCC500msNoCCLoop__v1'; %fault↙
type

Sn_MVA = 100;

ve = 1;
delta_e = 0;

pg_0 = 0.7;
qe_0 = 0;

rc = 0;
xc = 0.15;

xe = 0.1;
re = xe/10;

x_tot = xe+xc;

pe_0 = pg_0;
se_0_vec = pe_0 + j*qe_0;
ve_phasor = ve*exp(j*delta_e);

ig_0_phasor = (se_0_vec/ve_phasor)';
zc = rc + j*xc;
ze = re + j*xe;
vg_0_phasor = ve_phasor+ze*ig_0_phasor;
em_0_phasor = vg_0_phasor + zc*ig_0_phasor;
em_0 = abs(em_0_phasor);

b_delta = 0.001;
delta_curvas = [0:b_delta:pi]';
delta_curvas_deg = delta_curvas*180/pi;

% GFM-VSC - No CL

pg_gfm_no_CL = Sn_MVA*em_0*ve*sin(delta_curvas)/x_tot;

% GFM-VSC - CL-CSA

ig_max = 1.25;
se_max = ve*ig_max;

delta_ig_0 = angle(ig_0_phasor);
```


Figure D.1: Matlab script for producing P-δ curves page no. 1

```
ig_d_max = ig_max*cos(delta_ig_0);
pg_lim = em_0*ig_d_max;

delta_CL_CSA = asin(pg_lim*x_tot/em_0/ve);

i_ind_a1 = find(delta_curvas<=delta_CL_CSA);
i_ind_a2 = find(delta_curvas>delta_CL_CSA);

pg_gfm_CL_CSA = 0*pg_gfm_no_CL;
pg_gfm_CL_CSA(i_ind_a1) = Sn_MVA*em_0*ve*sin(delta_curvas(i_ind_a1))/x_tot;
pg_gfm_CL_CSA(i_ind_a2) = Sn_MVA*(em_0*ve*sin(delta_curvas(i_ind_a2)))./(sqrt ↙
(em_0^2+ve^2-2*em_0*ve*cos(delta_curvas(i_ind_a2))))*ig_max;

load(data_CaseA);

Pg_MW = [Pg_MW.Data]*1e-6;
delta_E_VSC_g = [delta_E_VSC.Data];
theta_f_deg = [theta_m_deg.Data theta_e_deg.Data];
theta_f13_deg = theta_m_deg.Data - theta_e_deg.Data;
t = [theta_m_deg.Time];

t_a = 11;
Pg_a = Pg_MW(1+(11/Time_Step)); %tiempo inicial
delta_a = theta_f13_deg(1+11/Time_Step);

t_b = 11+Time_Step;
Pg_b = Pg_MW(2+(11/Time_Step));
delta_b = theta_f13_deg(2+(11/Time_Step));

for i=(1+fix((11)/Time_Step)):(1+(11+t_fault)/Time_Step)
    if theta_f13_deg(i)>theta_f13_deg(i-1)
        t_c=i*Time_Step;
    end
end

Pg_c = Pg_MW(fix(t_c/Time_Step));
delta_c = theta_f13_deg(fix(t_c/Time_Step));

t_max = 1;

for i=(1+fix((11+t_fault)/Time_Step)):(1+20/Time_Step)
    if theta_f13_deg(i)>theta_f13_deg(1+fix(t_max/Time_Step))
        t_max=i*Time_Step;
    end
end

for i=(1+fix((11+t_fault)/Time_Step)):t_max/Time_Step
    if theta_f13_deg(i)-delta_c<5 && Pg_MW(i)>0
        t_d=i*Time_Step;
    end
end

Pg_d = Pg_MW(fix(t_d/Time_Step));
delta_d = theta_f13_deg(fix(t_d/Time_Step));
```


Figure D.2: Matlab script for producing P-δ curves page no. 2

```
Pg_max = Pg_MW(fix(t_max/Time_Step));
delta_max = theta_f13_deg(fix(t_max/Time_Step));

Pg_final = Pg_MW(1+20/Time_Step);
delta_final = theta_f13_deg(1+20/Time_Step);

Pg = [Pg_a Pg_b Pg_c Pg_d Pg_max Pg_final];
delta = [delta_a delta_b delta_c delta_d delta_max delta_final];

% Calculo de áreas


area_ace = Pg_a*(delta_c-delta_a)*pi/180;
area_dec = 0;

pg_gfm = zeros(1,180/b_delta);

for i = fix(delta_c/b_delta):fix((180-delta_a)/b_delta)
        if CL_NoCL == 0 || i*pi/180*b_delta<=delta_CL_CSA
        pg_gfm(i) = Sn_MVA*em_0*ve*sin(i*b_delta*pi/180)/x_tot;
    else
        pg_gfm(i) = Sn_MVA*(em_0*ve*sin(i*b_delta*pi/180))./(sqrt(em_0^2+ve^2-↙
2*em_0*ve*cos(i*b_delta*pi/180)))*ig_max;
    end
    area_dec = area_dec + (pg_gfm(i)-Pg_a)*b_delta;
end

title_cases = {sprintf('Fault: %d ms', t_fault*1000)};
Fontsize_leg = 8.5;

figure
h1 = plot(t,Pg_MW);
hold on

xlabel('time (s)','FontSize',15,'interpreter','latex')
ylabel('$P_{g}$ (MW)','FontSize',15,'interpreter','latex')
xlim([10 20]);
hold on

grid
LEG = legend(h1,title_cases,'FontSize',↙
Fontsize_leg,'interpreter','latex','location','best');
hold on
datatip(h1, t_a, Pg_a)
datatip(h1, t_b, Pg_b)
datatip(h1, t_c, Pg_c)
datatip(h1, t_d, Pg_d)
datatip(h1, t_max, Pg_max)
datatip(h1, t_final, Pg_final)

figure
h2 = plot(t,theta_f13_deg);
hold on
```


Figure D.3: Matlab script for producing P-δ curves page no. 3

```
xlabel('time (s)','FontSize',15,'interpreter','latex')
ylabel('$\delta-\delta_{e}$ (deg)','FontSize',15,'interpreter','latex')
xlim([10 20])
hold on

grid
LEG = legend(h1,title_cases,'FontSize',↙
Fontsize_leg,'interpreter','latex','location','best');
hold on

datatip(h2, t_a, delta_a)
datatip(h2, t_b, delta_b)
datatip(h2, t_c, delta_c)
datatip(h2, t_d, delta_d)
datatip(h2, t_max, delta_max)
datatip(h2, t_final, delta_final)

figure
h3 = plot(delta,Pg,'o');
hold on

grid
LEG = legend(h3,title_cases,'FontSize',↙
Fontsize_leg,'interpreter','latex','location','best');

xlabel('$\delta$ ($deg$)','FontSize',15,'interpreter','latex')

ylabel('$P_{g}$ ($MW$)','FontSize',15,'interpreter','latex')

xlim([0 180])

hold on
if CL_NoCL == 1
    h4 = plot(delta_curvas_deg, pg_gfm_CL_CSA);
    ylim([0 150])
else
    h4 = plot(delta_curvas_deg, pg_gfm_no_CL);
    ylim([0 max(Pg_max+10, 3*sqrt(2)*Sn_MVA)])
end

hold on
% datatip(h1, delta_a, Pg_a)
text(delta_a+2, Pg_a, 'a','interpreter','latex');

% datatip(h1, delta_b, Pg_b)
text(delta_b+2, Pg_b, 'b', 'interpreter','latex');

% datatip(h1, delta_c, Pg_c)
text(delta_c+2, Pg_c, 'c', 'interpreter','latex');

% datatip(h1, delta_max, Pg_max)
text(delta_max+2, Pg_max, 'max', 'interpreter','latex');
```


Figure D.4: Matlab script for producing P-δ curves page no. 4

5/07/26 17:24 C:\Users\nicoh\OneDriv...\PuntosPdelta.m 5 of 5

```
% datatip(h1, delta_d, Pg_d)
text(delta_d-5, Pg_d, 'd','interpreter','latex');

if delta_final-delta_a>1
%     datatip(h1, delta_final, Pg_final)
    text(delta_final+2, Pg_final, 'final', 'interpreter','latex');
end

hold on

yline(Pg_a, '--r', 'LineWidth', 2);
% xline(delta_c,'--r', 'LineWidth', 2);
xline(delta_a,'--r', 'LineWidth', 2);

LEG = legend(h4,title_cases,'FontSize',↙
Fontsize_leg,'interpreter','latex','location','best');
```


Figure D.5: Matlab script for producing P-δ curves page no. 5

Appendix E

Alignment with the Sustainable Development Goals

The Sustainable Development Goals (SDG) are a combination of crucial plans of action to help the present and later generations of living creatures (including human beings) to enjoy a better planet earth. They were proposed by the UN, and they intend to minimise our impact, and improve the conditions for less developed countries, so we can all have good quality lives without destroying our planet. Figure E.1 shows all of the SDGs.



Figure E.1: Sustainable Development Goals

The goal of this bachelor thesis is greatly aligned with the SDGs. The introduction of GFM-VSCs into power systems around the world has benefits in many aspects analysed in the SDGs, like helping make better energy, improving the in-

dustry and helping countries to tackle climate change directly. The SDGs tackled by this thesis directly are: SDG $n°7$, SDG $n°9$ and SDG $n°13$.

E.1 SDG $n°7$: Affordable & Clean Energy

The purpose of the implementation of GFM-VSC power converters is to help to increase the percentage of renewable energy source's generation. All research on this topic leads to a situation where energy is cleaner and more affordable.

E.2 SDG $n°9$: Industry, Innovation & Infrastructure

Any research on GFM-VSC, no matter how theoretical it may be, helps innovation on energy systems, and, therefore, will cause future infrastructure development to apply efficiency enhancements discovered theoretically. Therefore, knowing the behaviour of GFM-VSC power converters is crucial for the future.

E.3 SDG $n°13$: Climate Action

This research, far from only helping increase the number renewable energy source plants, will also help to reduce the number of non-renewable sources of energy, and produce the opportunity for great scale systems to evaluate whether to go 100% renewable, knowing well about the limitations and risks of making this decision.

Bibliography

[1] N Hatziargyriou et al. "Definition and classification of power system stability - revisited and extended". In: *IEEE Transactions on Power Systems* 36.4 (2021), pp. 3271–3281.

[2] Régulo E. Ávila-Martínez et al. "Revisiting angle stability in power systems with grid-forming power converters". In: *IEEE Transactions on Energy Conversion* doi: 10.1109/TPWRS.2026.3703616 (2026), pp. 1–4.

[3] A Gómez-Expósito, A J Conejo, and C A Canizares (Coordinators). *Electric energy systems: analysis and operation*. CRC press, Taylor & Francis Group, Boca Raton, FL, USA, 2018.

[4] Olve Mo, Salvatore D'Arco, and Jon Are Suul. "Evaluation of Virtual Synchronous Machines With Dynamic or Quasi-Stationary Machine Models". en. In: *IEEE Transactions on Industrial Electronics* 64.7 (July 2017), pp. 5952–5962. ISSN: 0278-0046, 1557-9948. DOI: 10.1109/TIE.2016.2638810.

[5] Kanakesh Vatta Kkuni et al. "Comparative assessment of typical control realizations of grid forming converters based on their voltage source behaviour". en. In: *Energy Reports* 9 (Dec. 2023), pp. 6042–6062. ISSN: 23524847. DOI: 10.1016/j.egyr.2023.05.073.

[6] Yorgo Laba et al. "Virtual Power-Based Technique for Enhancing the Large Voltage Disturbance Stability of HV Grid-Forming Converters". en. In: *2023 25th European Conference on Power Electronics and Applications (EPE'23 ECCE Europe)*. Aalborg, Denmark: IEEE, Sept. 2023, pp. 1–8. ISBN: 978-90-75815-41-2. DOI: 10.23919/EPE23ECCEEurope58414.2023.10264486.

[7] R E Ávila-Martínez et al. "Impact on transient stability of self-synchronisation control strategies in grid-forming power converters". In: *International Journal of Electrical Power & Energy Systems* 174.111540 (2026), pp. 1–18. DOI: 10.1016/j.ijepes.2025.111540.

[8] L2EP-LILLE. "VSC_Lib: Grid forming models for Matlab/SimPowerSystem". In: https://github.com/l2ep-epmlab/ (accessed 08-07-2020) (2020).

[9] T Qoria et al. "Tuning of cascaded controllers for robust grid-forming Voltage Source Converter". In: *Proc. Power systems computation conference (PSCC), dublin, ireland*. 2018, pp. 1–8.

[10] T Qoria et al. "Inertia effect and load sharing capability of grid forming converters connected to a transmission grid". In: *15th IET int. Conf. on AC and DC power transmission (ACDC), coventry, UK*. 2019, pp. 1–6.